ERDC/EL TR-08-17

US Army Corps
of Engineers®
Engineer Research and
Development Center

Investigations of Controlling Factors for Air Emissions Associated with the Dredging of Indiana Harbor and Canal (IHC) and CDF Operations

Louis J. Thibodeaux, Kalliat T. Valsaraj,
Raghunathan Ravikrishna, Kenneth Fountain,
and Cynthia L. Price

April 2008

Environmental Laboratory

ERDC/EL TR-08-17
April 2008

Investigations of Controlling Factors for Air Emissions Associated with the Dredging of Indiana Harbor and Canal (IHC) and CDF Operations

Louis J. Thibodeaux, Kalliat T. Valsaraj, Raghunathan Ravikrishna, and Kenneth Fountain

Louisiana State University
Department of Chemical Engineering
Baton Rouge, LA 70803

Cynthia L. Price

Environmental Laboratory
U.S. Army Engineer Research and Development Center
3909 Halls Ferry Road
Vicksburg, MS 39180-6199

Final report

Prepared for U.S. Army Engineer District, Chicago
Chicago, IL

Abstract: This report describes a series of investigations conducted examining a number of specific factors that control air emissions associated with the dredging of Indiana Harbor and Canal (IHC) and associated IHC Confined Disposal Facility (CDF) operations. Three primary objectives were addressed: (1) measurement of Henry's Law constants and sediment-water desorption constants for various chemicals in the IHC sediment, (2) measurement of volatile emissions from IHC sediments exposed to air, and (3) reformulation of models for air emissions from dredging of contaminated sediment and handling of dredged materials.

Equilibrium sediment-water partition constants for PAHs and PCBs in IHC sediments were measured in laboratory investigations. These values are presented and compared to literature values. Laboratory experiments measuring the water-air partition constant (Henry's Law constant) were conducted using IHC pore water. Experimentally determined Henry's constants for PAHs and PCBs are presented and compared to literature values. Investigations from wind tunnel studies measuring semi-volatile emissions from IHC sediments are summarized. A model for estimating emissions from mechanical or hydraulic delivery of dredged IHC sediments is presented. Chemical volatilization models for emissions from dredging operations associated with IHC sediment and site conditions are discussed.

Contents

Figures and Tables

Figures

Tables

Preface

The Environmental Laboratory (EL) of the U.S. Army Engineer Research and Development Center (ERDC) conducted this work. The U.S. Army Corps of Engineers (USACE) Chicago District funded ERDC under Project Order W81G6631268752. The initial project manager was Bill White and the current project manager is Joanne Milo of the USACE Chicago District.

This report was written by Drs. Louis J. Thibodeaux, Kalliat T. Valsaraj, Ragunathan Ravikrishna, and Kenneth Fountain of Louisiana State University, Department of Chemical Engineering, and Cynthia L. Price, Environmental Processes Branch (EP-P), Environmental Processes and Engineering Division (EPED), EL. Internal reviewers for USACE Chicago District were Jay Semmler and Le Thai.

This study was conducted under the direct supervision of Dr. Richard E. Price, Chief, EPED, and under the general supervision of Dr. Beth Fleming, Director, EL.

COL Richard B. Jenkins was Commander and Executive Director of ERDC. Dr. James R. Houston was Director.

Introduction

Project background

Indiana Harbor and Canal (IHC) is an authorized Federal navigation project located in East Chicago, IN. Sediments in the IHC are contaminated and have been determined to be suitable only for upland confined disposal. As a result of studies undertaken by the U.S. Army Corps of Engineers (USACE) Chicago District to address disposal issues, dredging is to be undertaken throughout the IHC Federal navigation project to authorized project depths and widths. A confined disposal facility (CDF) is to be constructed on a former petroleum refinery site owned by Energy Cooperative Industries (ECI). Due to the proximity of the ECI site to area business and residential properties, volatile emissions from dredged material after disposal are a concern.

The USACE Chicago District requested assistance with assessment of various volatile chemical emissions locales associated with the IHC project. A literature review investigating volatilization rates from dredged materials and soils for the Chicago District was previously conducted (Thibodeaux et al. 2002). A diffusion-controlled model (Thibodeaux and Hwang 1982) was recommended as the best available approach to estimating the volatilization of contaminants from a CDF containing dredged material; specifically one that contains IHC sediments. A comparison of the model versus measured fluxes was performed revealing that the diffusion controlled algorithm tends to over-predict volatile and semi-volatile emissions. A critical review and analysis of the available data representative of the IHC and the appropriateness of its use in making calibrated predictions of volatilization to air from a CDF was performed (Thibodeaux et al. 2002). Results of model formulations and review indicated a lack of sufficient data upon which to attempt a calibration of the existing theoretical air emission model for the IHC site. Additional efforts are required to complete the emissions model being developed due to the lack of correlation between theoretically modeled volatile and semi-volatile compound emissions estimates and actual emissions.

Objectives

The objectives of this research were to investigate some specific factors that control air emissions associated with the dredging of IHC sediments and associated CDF operations. Three primary objectives were proposed. The first objective involved measurements of Henry's Law constants and sediment-water desorption constants for various chemicals from IHC sediments. The second involved measurement of volatile emissions from IHC sediments exposed to air. The third addressed the reformulation of models developed for air emissions from dredging contaminated sediment and handling of dredged materials. Investigations to address these objectives were conducted under three separate research tasks.

The purpose of this report is to describe the results of investigations conducted under each Research Task. Three separate reports were produced during the course of these investigations and are compiled into one document.

Research Task 1: K_d's and H's

Sediment-water partition coefficients (K_d's) and air-water partition constants (Henry's Law (H)) are two key parameters in the volatilization flux algorithms used to estimate polyaromatic hydrocarbons (PAHs) and other volatile and semi-volatile chemicals. Literature-derived values are generally appropriate for screening purposes, but not for site-specific applications. Values can vary by one or more orders of magnitude. Since literature-derived values of K_d commonly reflect only adsorption conditions, measurements of partition constants using actual IHC sediment under desorption conditions are needed to simulate the conditions and operations at the site.

Estimates of H in the literature vary widely due to the different methods of estimation. The primary obstacle to determination of H for semi-volatile compounds such as PAHs and polychlorinated biphenyls (PCBs), is the low vapor pressure of some of these chemicals. The majority of reported values for H are for exchange between air and distilled and/or deionized (DI) water. The pore water in the IHC dredged material has an increased dissolved organic carbon content, which may have an effect on the air-water equilibrium partition constants. Measurements of Henry's Law constants using IHC pore water are needed for input into the flux algorithms used for estimation of emissions from IHC sediments.

Research Task 2: IHC Volatile Emissions

Much of the chemical emissions data (flux to air) from sediments and soils is based upon laboratory experiments (Thibodeaux et al. 2002). The equipment used for these experiments typically uses a small mass of material with small evaporative surface areas. Large-scale lysimeter/wind tunnel experiments appear to be the best compromise between conducting laboratory-scale simulations and field-scale measurements. The lysimeter system will allow for controlled simulations of the drying, consolidation, and cracking of dredged materials that occur in the field. The use of IHC dredged material in this type of system will provide needed data for use in estimating emissions exposure at the IHC site.

Research Task 3: Reformulated Volatilization Model

Thibodeaux (1989) assessed the available theoretical models for the estimation of volatile chemical emissions to air during the process of dredged material disposal in a CDF. An objective of this research was to identify the primary vapor phase transport mechanisms for various CDF designs and stages of filling. This work provided the theoretical basis for assessing relative volatilization rates. A second object reviewed available laboratory and field procedures for obtaining the information needed to measure volatile losses. Four VOC emissions locales were identified: (1) the sediment relocation locale, (2) the exposed sediment locale, (3) the ponded sediment locale, and (4) vegetation-covered sediment locale. These locales were designated as specific areas within a CDF that exhibit common operational characteristics that result in the release/generation of VOCs to air. The thermodynamic basis of chemical vapor equilibrium and contaminated sediment is discussed, and rate equations are presented and reviewed. These equations represent the quantitative results of the models of emission mechanisms from each of the four locales.

Some of the information given in Thibodeaux (1989) needs to be updated and focused to the particular needs of the CELRC with regard to modeling chemical vapor emissions to air at the IHC CDF site. An updated literature review and reformulated model equations are needed to more accurately access volatile emissions from the various locales associated with dredging and disposal of the IHC sediments.

References

Thibodeaux, L. J., and S. T. Hwang. 1982. Landfarming of Petroleum Waste – Modeling the Air Emission Problem. *Environmental Progress* 3(1): 42.

Thibodeaux, L. J. 1989. Theoretical Models for Evaluation of Volatile Emissions to Air During Dredged Material Disposal with Applications to New Bedford Harbor, Massachusetts. Miscellaneous paper EL-89-3, U.S. Army Engineer Waterways Experiment Station, Vicksburg, MS.

Thibodeaux, L. J., R. Ravikrishna, and K. T. Valsaraj. 2002. Volatilization Rates from Dredged Material and Soils – A Literature Review. Final Report. USACE, Chicago District. Vicksburg, MS: U.S. Army Engineer Research and Development Center.

1 Measurement of Sediment-Water and Air-Water (Henry's Law Constant) Partition Constants for PAHs/PCBs of Concern in Indiana Harbor and Canal Dredged Material

Sediment-Water Partition Constant, K_d

Project scope and objectives

This project is aimed at obtaining measurements of sediment-water equilibrium partition constant for polyaromatic hydrocarbons (PAHs) and polychlorinated biphenyls (PCBs). The sediment-water equilibrium partition constant, K_d, facilitates estimation of pore water concentration of a chemical in equilibrium with dredged material (DM) solids from the measured concentration of the chemical in the DM solids. This parameter approximates the thermodynamic limit of the availability of the chemical in the pore water as a result of desorption from the dredged solids. The value of K_d typically correlates strongly with the organic carbon-water partition constant, K_{OC}, and the fractional organic carbon content. In the absence of site-specific measurements of the sediment-water equilibrium partition, the K_d is estimated from the measured fractional organic carbon and the K_{OC}. Values of K_{OC} reported in the literature vary considerably and are dependent on the types of organic carbon that exist in sediments. The most reliable approach is to measure the K_d for use as a parameter in the mathematical models that attempt to predict chemical release from sediment or DM solids.

The project objective was to quantify the equilibrium sediment-water partition constants of PAHs and PCBs present in Indiana Harbor and Canal (IHC) DM by direct measurement of water and solid phase concentrations after equilibration and separation. The general experimental method was to equilibrate a small amount of DM with a known volume of water and measure the concentrations in each phase after separation by centrifuge. The water phase was replaced and re-equilibrated with the solids for the next stage of desorption. This process was conducted for four stages of desorption for the PAHs and three stages of desorption for the PCBs. At

the end of the final stage of desorption, the chemical concentration on sediment was measured by solvent extraction. The direct ratio of the chemical concentrations in the sediment and water were calculated to be the K_d.

Experimental methods

K_d measurement

The experiments designed to measure the sediment-water equilibrium partition constants were based on the American Society for Testing and Materials (ASTM) method (ASTM E1195-01, 2002) for the measurement of the sorption constant and on the method described by Kommalapati et al. (2002). Separate sets of experiments were performed for the PAHs and the PCBs. These experiments were based on measurement of the water phase and the solid phase concentration of the chemicals after equilibration and phase separation. All experiments were conducted with a 1 Kg sub-sample of the IHC DM received from U.S. Army Engineer Research and Development center (ERDC), Vicksburg, MS. The DM was obtained from a location identified as Reach 5. The subsample was stored at 4°C. Approximately 5 g of wet IHC DM were measured into a 50 mL round-bottomed Pyrex centrifuge bottle. A 50 mL measure of electrolyte solution containing sodium azide, sodium chloride, and calcium chloride were added to the bottle containing the DM to prevent biodegradation. The electrolyte facilitated good separation of the solids and liquids phases during the centrifuge and also adjusted the pH and conductivity of the deionized water to a value closer to that of the IHC pore water.

The 5 g IHC DM sample and the 50 mL electrolyte mixture were shaken manually to ensure the breakage of solid clumps. The bottle caps were lined with Teflon and aluminum foil to minimize adsorption and sealed with parafilm. In each batch of this experiment, 12 replicates were used. The bottles were packed into a plastic jar set to equilibrate in a tumbling machine equipped with rollers. Equilibration time varied between 15 and 35 days. At the end of each equilibration period, the bottles were removed and were immediately centrifuged in a Beckman Centrifuge at 3000 revolutions per minute for 15 minutes. At the end of the centrifuge, a sample of the supernatant water was withdrawn for direct analysis of PAHs by high performance liquid chromatography (HPLC). The remaining supernatant was removed from the centrifuge bottle and analyzed for dissolved organic carbon (DOC). Fresh electrolyte solution was added to the

centrifuge bottles and re-equilibrated for the next stage of desorption. At the end of the experiment, the solids from the bottles were analyzed for chemical concentrations and organic carbon content.

For the PCB experiments, water from four centrifuge bottles was combined and transported in a refrigerated container to U.S. Army ERDC for chemical analysis, since larger volumes were required for analysis. As for the PAH experiments, 12 replicates were used, so each stage of the PCB experiments yielded 3 replicates. At the end of the third stage, the solids from three centrifuge bottles were sent to ERDC for chemical analysis.

Analytical methods

PAHs: Water samples were analyzed for PAHs by HPLC using a fluorescence detector. A gradient method based on U.S. Environmental Protection Agency (EPA) SW-846 Method 8310 (U.S. EPA 8310) was used for the analysis. Chemical concentrations on sediments were obtained by HPLC using a fluorescence detector after the solids were extracted with a 50:50 mixture of hexane:acetone using an ultra-sonication procedure (EPA SW-846 Method 3550). The extract was solvent-exchanged with acetonitrile and analyzed by HPLC. Organic carbon content of dried sediment samples were analyzed using a Perkin Elmer CHN analyzer. The total organic carbon (TOC) content of the water samples were analyzed directly using a Shimadzu 500 TOC analyzer.

The K_d was calculated after each stage of desorption from the ratio of the chemical concentration on the sediment ($W_{s,i}$) and the true concentration in water ($C_{w,i}$). Equation 1.1 defines K_d (L/Kg) for stage i

$$K_{d,i} = \frac{W_{S,i}}{C_{W,i}} \tag{1.1}$$

Concentrations on sediment after each stage of desorption were not measured. For the PAHs, K_d's were estimated from the measured initial average chemical concentration on sediment and the mass of chemical lost to the water in each stage due to desorption as shown in Equation 1.2.

$$W_{s,i} = \frac{W_{S,i-1} \cdot m_{ds} - C_{w,i}^{meas} \cdot V_W}{m_{ds}} \tag{1.2}$$

where $W_{S,\,i\text{-}1}$ is the chemical concentration on sediment (mg/Kg) of the i-1 stage, $C_{W,i}^{meas}$ is the measured water (solution + TOC) concentration of stage i, m_{ds}, and V_W are the masses of dry solids and the volume of water in each equilibration bottle, respectively.

For the PCBs the sediment concentration was measured at the end of three stages of desorption, and Equation 1.2 was used to compute the chemical concentrations on the sediment at the end of stages 1 and 2.

The true chemical concentration in water (solution only), $C_{W,i}$, was calculated from the measured concentration in water, $C_{W,i}^{meas}$, by correcting for the chemical adsorbed on the organic carbon in the water using literature average K_{OC} values as shown in Equation 1.3.

$$C_{W,i} = \frac{C_{W,i}^{meas}}{1 + \rho_{TOC} \cdot K_{OC}} \tag{1.3}$$

where $C_{W,i}^{\ meas}$ was the measured chemical concentration in water (mg/L), ρ_{TOC} was the measured TOC (Kg/L) and K_{OC} was the literature average organic carbon-water partition constant (L/Kg).

PCBs: Chemical analyses for PCBs were performed using gas chromatography/mass spectrometry (GC/MS) and gas chromatography/electron capture detector (GC/ECD) based on the EPA SW-846 (US EPA Method 8082). Analysis was performed to measure the concentrations of all measurable PCB congeners and also Arochlor mixtures. The sediment concentrations were measured at the end of stage 3, and the sediment concentrations for the calculation of K_d at the end of each stage were obtained from the estimated sediment concentrations based on Equation 1.2. All other calculations were performed in the manner described for the PAHs.

Results, analysis, and discussion

Chemical concentration on sediments

All PAHs reported were the ones that could be adequately resolved analytically using HPLC. The IHC DM subsample was analyzed at Louisiana State University (LSU) for contaminant loading using HPLC prior to the K_d experiments. The results were compared with the loadings reported by the ERDC analytical laboratory from the composite sample and from the subsample of DM that was being used in the K_d experiment. Table 1-1 lists

these results. The loadings obtained from LSU analyses were used in the calculation of K_d. Figure 1-1 shows the chemical concentrations of the sediment and in water for the PAHs. Table 1-2 shows the comparison of the measured concentration of PAHs on the solids with the concentrations estimated from initial solids concentration and mass of chemical removed at each desorption stage.

Table 1-1. Comparison of PAH loading in IHC dredged material subsample.

	Loading (mg/kg)		
Analysis by	ERDC Composite	ERDC Reach 5	LSU Reach 5
Naphthalene	2.65	4.49	4.7 ± 1.4
Acenaphthylene	0.33	0.315	
Acenaphthene	1.74	4.33	
Fluorene	2.19	4.48	
Phenanthrene	6.93	13.7	13.1 ± 0.5
Anthracene	2.28	4.07	4.9 ± 0.4
Fluoranthene	10.6	28	
Pyrene	16	27.2	35.4 ± 5.1
Benzo(a)anthracene	6.69	14	18.4 ± 2.3
Chrysene	9.49	20.2	30.5 ± 6.6
Benzo(b)fluoranthene	7.52	16	
Benzo(k)fluoranthene	4.6	12	9.2 ± 1.3
Benzo(a)pyrene	7.32	15.4	18.5 ± 1.3
Dibenzo(ah)anthracene	1.26	2.25	
Benzo(ghi)perylene	5.19	11.4	11.7 ± 1.7
Indeno-1,2,3-pyrene	4.84	12.6	

Table 1-2. Comparison of contaminant loadings at end of experiment.

	Loading (mg/kg)		
	Initial	Final _Estimated	Final Measured
Naphthalene	4.7 ± 1.4	3.4 ± 0.24	
Acenaphthylene			
Acenaphthene		4.2 ± 0.2	
Fluorene			
Phenanthrene	13.1 ± 0.5	12.9 ± 0.03	14.6 ± 0.4
Anthracene	4.98 ± 0.4	4.95	2.7 ± 0.3
Fluoranthene			
Pyrene	35.39 ± 5.1	35.25	30.6 ± 0.9
Benzo(a)anthracene	18.4 ± 2.3	17.8	
Chrysene	30.54 ± 6.6	30.4	26.4 ± 0.8
Benzo(b)fluoranthene			
Benzo(k)fluoranthene	9.21 ± 1.3	9.2	8.4 ± 0.3
Benzo(a)pyrene	18.49 ± 1.3	18.4	21.3 ± 1.0
Dibenzo(ah)anthracene			
Benzo(ghi)perylene	11.7 ± 1.7	10.9	10.4 ± 2.3
Indeno-1,2,3-pyrene			

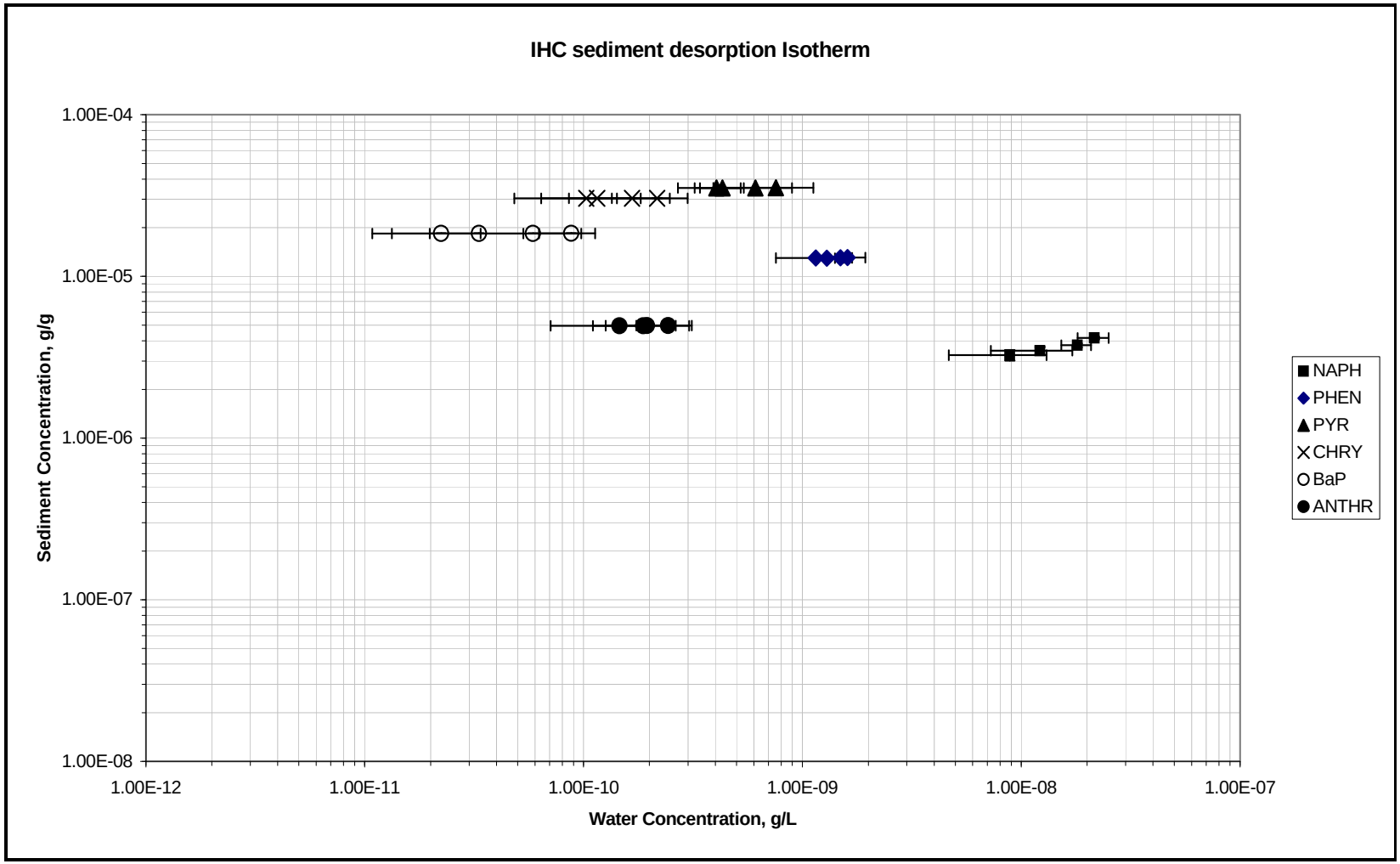

Figure 1-1. Sediment loading and water concentration at each stage of desorption.

The concentrations of PCB congeners and Arochlor mixtures on the sediment solids were measured at the end of stage 3 desorption. Table 1-3 shows sediment concentration values above detection limits for PCB congeners and mixtures.

Table 1-3. Measured PCB concentrations in the IHC sediment after three stages of desorption.

PCB Congener #	Loading (µg/kg)	PCB Congener #	Loading (µg/kg)
7	18.5 ± 1.6	151	28 ± 2.2
8	84.8 ± 8.5	170	44 ± 2.4
18	517 ± 30	171	12 ± 1.6
28	430 ± 15	180	15 ± 7.2
31	514 ± 16	183	30 ± 2.7
40	136 ± 7.5	185	7.7 ± 0.2
44	587 ± 29	191	2.6 ± 0.3
49	490 ± 20	194	19 ± 1.3
52	747 ± 21	195	9.3 ± 1.2
60	98.3 ± 4.2	196	12 ± 1.0
66	544 ± 24	201	23 ± 1.8
70	538 ± 16	203	21 ± 1.7
77	50 ± 4.3	205	2.8 ± 1.1
82	64 ± 3.7	206	7.3 ± 0.6
97	92 ± 8.8		
101	164 ± 12	Arochlor 1248	7098 ± 105
105	59 ± 3.5	Arochlor 1260	594 ± 71
114	10 ± 0.2		
118	144 ± 7.4		
141	26 ± 3.2		

Chemical concentration in water

The “true” aqueous phase chemical concentration was obtained after correction for the TOC of the aqueous phase after centrifuge using Equation 1.3. The TOC in the water phase after stage 1 was about 50 mg/L and decreased to 20 mg/L after stage 2, and 10 mg/L after stages 3 and 4. Based on the value of the K_{OC}, the TOC correction factor varied from 1.1 for naphthalene to 87 for Benzo(a)pyrene. For the PCBs, this correction was performed for only those congeners and mixtures for which a literature K_{OC} value could be found. These correction factors for PCBs ranged from

1.1 to around 300. The correction was significant as the hydrophobicity of the chemical increased.

Estimation of K_d and K_{OC}

Table 1-4 lists the sediment-water partition constants, K_d, for the PAHs measured in this study and were determined by the ratio of the sediment loading to water concentration. Figure 1-2 shows the average and the standard deviation (n=35) of K_d values for seven PAHs quantitatively resolved in this study for four stages of desorption. The mean K_d increased with increasing hydrophobicity, as expected. The mean K_d values also increased slightly toward the later stages of desorption. However, this increase in most cases is within the variation of the K_d values. Table 1-4 also lists the comparison of K_d values measured in this study to that reported in a previous report (Thibodeaux et al. 2002) for the IHC DM. For all the compounds, the K_d measured in this study is higher, sometimes by an order of magnitude. The K_d values from Thibodeaux et al. (2002) were estimated from literature average log K_{OC} values and an average organic carbon fraction of 0.14, which was similar to the sediment fractional organic carbon content (f_{OC}) measured in this study (0.137). A mechanistic explanation of the difference in these two sets of K_d is not possible from the available information. However, one conjecture could be that the disparity might be due to differences in the nature of the organic carbon. The literature average is composed of experimental data sets from various sediments, and no consistent information on the characterization of the organic carbon was available to construct a trend.

Table 1-4. Measured and reported K_d for PAHs in IHC dredged material.

	K_d (mean, L/kg) Measured	K_d[a] Reported
Naphthalene	298 ± 113	180
Acenaphthene	1,030 ± 199	
Phenanthrene	13,344 ± 8,413	2,858
Anthracene	29,691 ± 4,707	3,358
Pyrene	77,706 ± 14,084	13,370
Benzo(a)anthracene	17,226	
Chrysene	235,953 ± 68,884	
Benzo(k)fluoranthene	2,011,866 ± 1,275,580	106,201
Benzo(a)pyrene	600,776 ± 286,706	269,853
[a]Thibodeaux et al. (2002)		

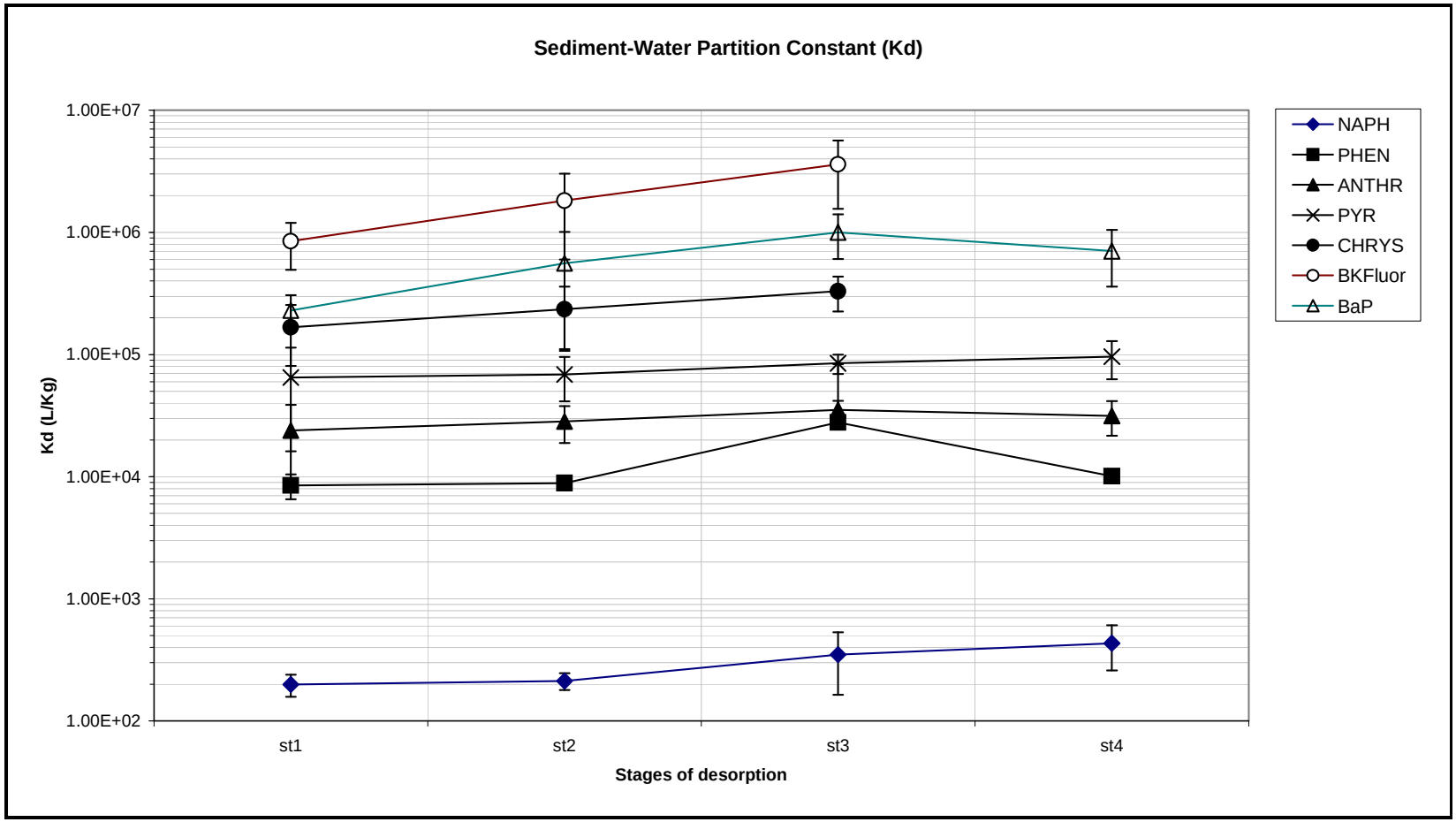

Figure 1-2. Sediment –water partition constant (K_d) in four stages of desorption.

Table 1-5 lists the measured K_d's for the quantifiable PCB congeners and mixtures in this study. No previous data for K_d from IHC could be found to compare. The experimental K_d's obtained in this study were translated to K_{OC} using Equation 1.4 and the initial f_{OC} of 0.138 ± 0.0025:

$$K_{OC} = K_d / f_{OC} \tag{1.4}$$

Table 1-5. K_d for PCBs in IHC dredged material measured in this study.

PCB Congener #	K_d (L/Kg) Mean
28	$2.3 \times 10^4 \pm 9 \times 10^3$
31	$8.5 \times 10^4 \pm 6.8 \times 10^4$
40	$1.4 \times 10^4 \pm 4.2 \times 10^3$
44	$2 \times 10^4 \pm 7.5 \times 10^3$
49	$6.6 \times 10^4 \pm 2.8 \times 10^4$
60	$3.7 \times 10^4 \pm 1.4 \times 10^4$
66	$2.1 \times 10^4 \pm 8 \times 10^3$
70	$7.6 \times 10^4 \pm 3.3 \times 10^4$
101	$1.5 \times 10^4 \pm 6.4 \times 10^3$
138	$1.6 \times 10^5 \pm 8.5 \times 10^4$
180	$2.4 \times 10^5 \pm 1.2 \times 10^5$
Arochlor 1248	$8.7 \times 10^3 \pm 2.7 \times 10^3$
Arochlor 1260	$3.6 \times 10^4 \pm 9.2 \times 10^3$

The estimation of the organic-carbon normalized log K_{OC} values from the measured K_d values provides an opportunity to compare these experimental results with published values. Table 1-6 lists the comparison of the log K_{OC} from this study, obtained using Equation 1.4, with experimental average literature log K_{OC} values (Mackay et al. 1992) for PAHs. Figure 1-3 shows the measured log K_{OC} values at each stage of desorption. Considering the level of uncertainty for each chemical, our measurements were in good agreement with the literature. The comparison of log K_{OC} values for PCBs is shown in Table 1-7. Figure 1-4 shows the comparison of experimental (this study) and the experimental literature average log K_{OC} values for the PCBs analyzed in this study. The mean log K_{OC} values obtained in this study fall within one standard deviation of the literature average log K_{OC} values.

Table 1-6. Log K_{oc} values for PAHs – comparison with experimental literature average.

	Mean Log K_{OC} (L/kg) (Estimated in this study)	Mean Log K_{OC} (L/kg) (Literature average)
Naphthalene	3.29 ± 0.15	3.07 ± 0.55
Acenaphthene	3.81 ± 0.03	4.02 ± 0.76
Phenanthrene	4.86 ± 0.1	4.31 ± 0.49
Anthracene	5.31 ± 0.08	4.54 ± 0.59
Pyrene	5.71 ± 0.1	5.08 ± 0.48
Benzo(a)anthracene	5.11 ± 0.11	5.33 ± 1.22
Chrysene	6.17 ± 0.13	5.43 ± 1.45
Benzo(k)fluoranthene	7.01 ± 0.25	6.09
Benzo(a)pyrene	6.53 ± 0.25	6.24 ± 1.43

Table 1-7. Log K_{oc} values for PCBs – comparison with literature average.

PCB Congener #	Mean Log K_{OC} (L/kg) (Measured in this Study)	Mean Log K_{OC} (L/kg) (Literature Average)
28	5.19 ± 0.2	5.3 ± 0.02
31	5.69 ± 0.3	5.57 ± 0.3
40	4.98 ± 0.15	5.57
44	5.13 ± 0.2	5.1 ± 0.63
49	5.63 ± 0.23	5.71
60	5.39 ± 0.19	5.67
66	5.19 ± 0.2	5.15 ± 0.45
70	5.69 ± 0.24	5.77 ± 0.85
101	5 ± 0.21	5.35 ± 0.83
138	6.01 ± 0.26	6.24 ± 0.86
180	6.18 ± 0.26	6.36 ± 0.82
Arochlor 1248	4.78 ± 0.14	5.09 ± 0.5
Arochlor 1260	5.4 ± 0.12	6.19 ± 0.91

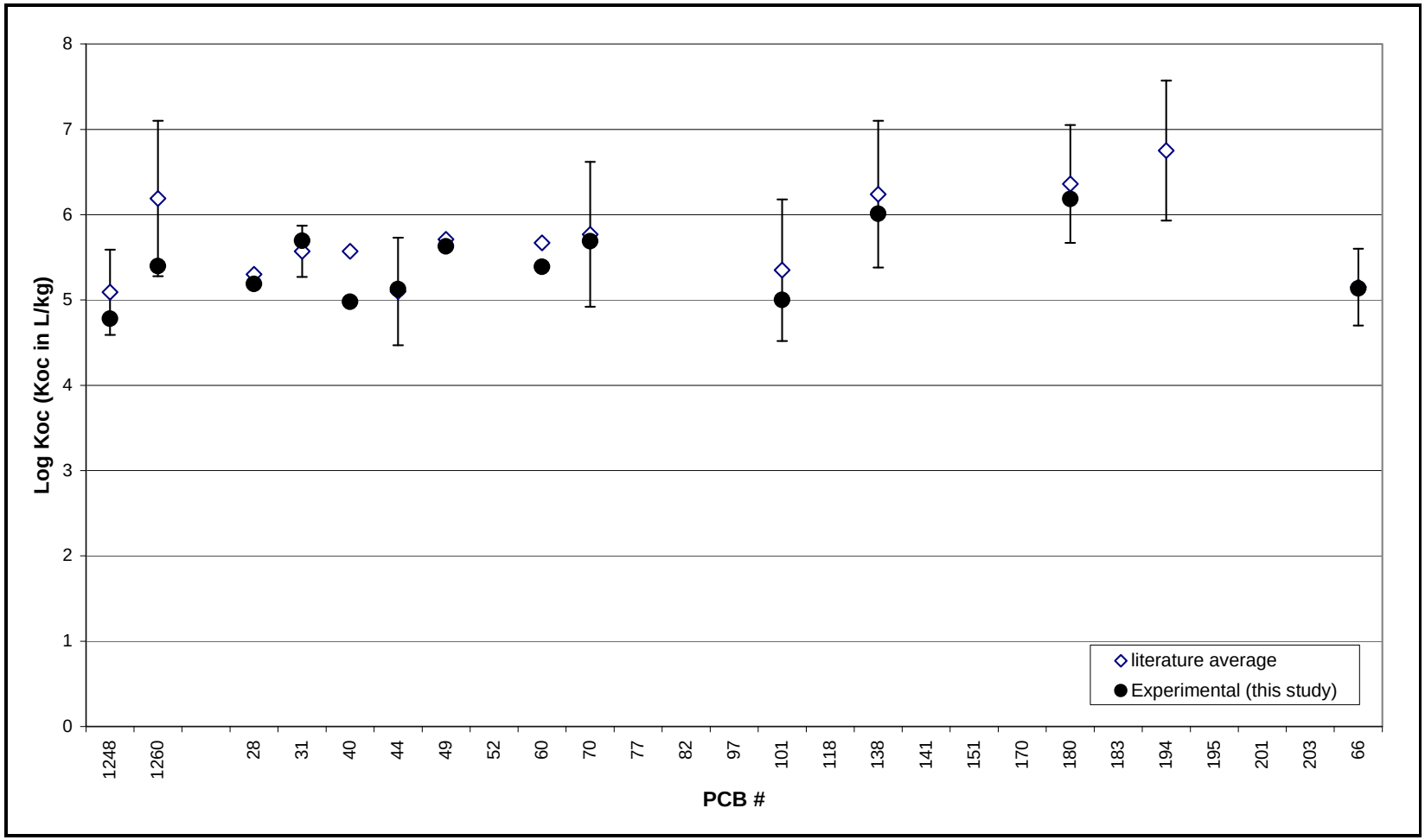

Figure 1-3. Plot of Sediment-organic carbon partition constant - Log K_{oc} for PAHs as a function of desorption stage.

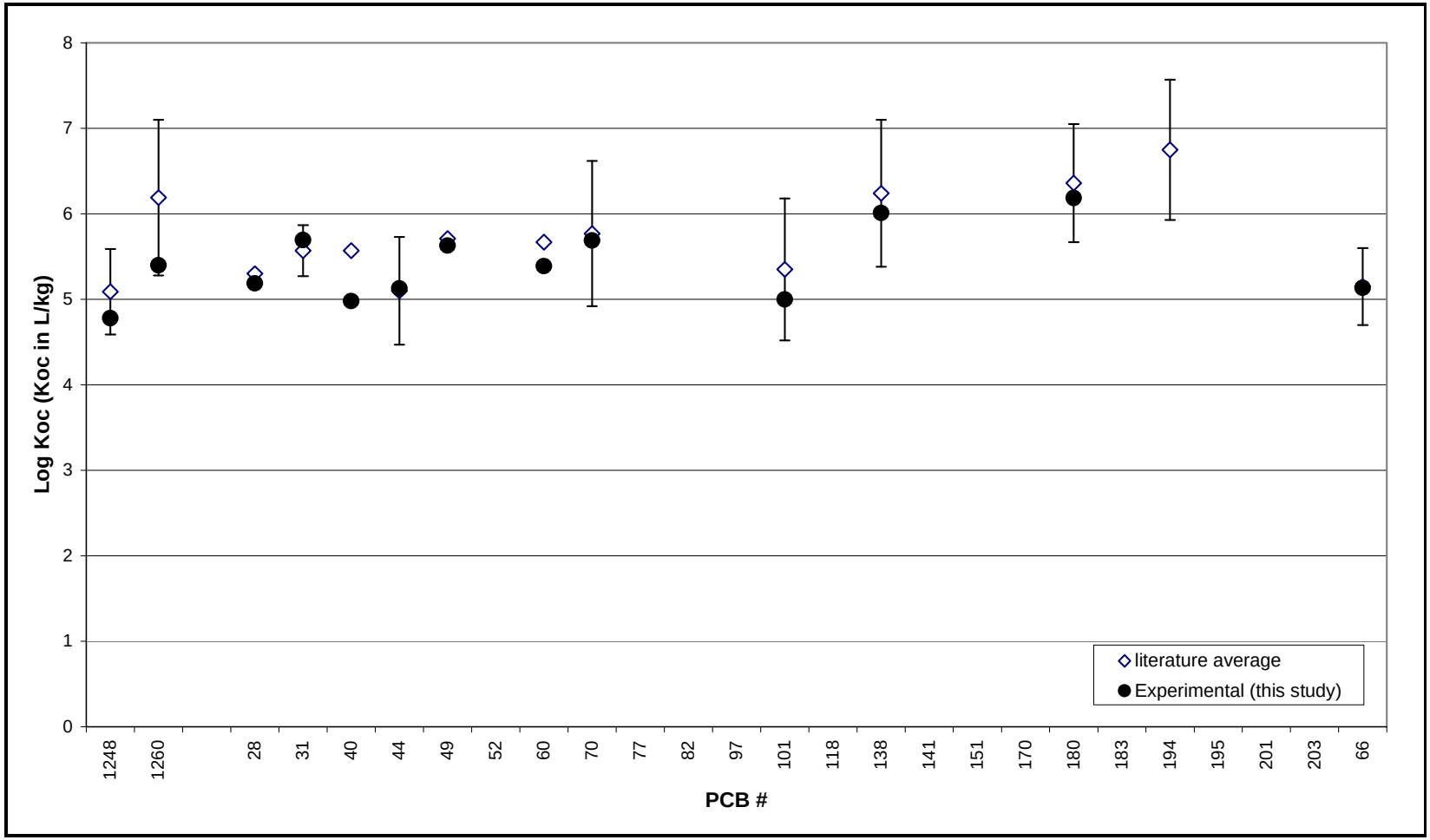

Figure 1-4. Comparison of literature average and experimental values of log K_{OC} for PCBs.

It was observed that, after the first two centrifugings, the water surface in each bottle contained a small aggregate of organic carbon and oil dispersions. Some of these aggregates were removed from the bottle when the water was replaced between successive stage of desorption and the remaining suspended material adhered to the inner walls of the bottle. It was not possible to accurately estimate the amounts that had separated from the bulk of the sediment during centrifuge and that which was removed after each desorption stage. At the end of the fourth stage of desorption of the PAHs experiment, five replicates of solids samples from two of the bottles in the K_d experiment were analyzed for fractional organic carbon and the mean value was 0.12 ± 0.006 (compare with the initial value of 0.138 ± 0.0025). The average total initial organic carbon estimated in a bottle was about 290 mg. The measured organic carbon content in the solids at the end of four runs was about 250 mg. The total estimated organic carbon removed after four stages of desorption was about 4 mg. The balance of 35 mg of organic carbon in each bottle is unaccounted for. The TOC balance closure was 88%. However, this discrepancy does not significantly impact the estimation of the log (K_{OC}) values (0.5 – 1.3% change).

Relationship between K_{OC} and K_{OW}

Both K_{OC} and K_{OW} are indicators of hydrophobicity; therefore, a strong correlation between the two quantities is expected. A relationship between the measured K_{OC} values and the literature average octanol-water partition constant, K_{OW} values was obtained. This procedure was explored as a method to extrapolate the K_{OC} of the PAHs and PCBs that were below detection limits in this study. K_{OW} is a good alternative indicator of hydrophobicity and reliable values exist for most PAHs. For the PCBs, K_{OW} values were not available for a number of the congeners. Table 1-8 shows the literature average values of the log K_{OW} (Mackay et al. 1992) for 16 PAHs and a few PCBs measured in the sample. Figure 1-5 shows the plot of the correlation of our measured log K_{OC} versus log K_{OW} in addition to measured log K_{OC} values for the PAHs. The bold black line represents the correlation of our data. Equation 1.5 shows the linear correlation obtained for the experimental log K_{OC} data and the literature average log K_{OW} data.

$$\log(K_{oc}) = 1.063 \cdot \log(K_{ow}) - 0.0772 \quad (1.5)$$

Table 1-8. Literature average values of log K_{OW}.

PAHs	Log (K_{OW})	PCBs Congener #	Log (K_{OW})
Naphthalene	3.3 ± 0.3		
2-Methyl Naphthalene	4.0 ± 0.3	28	5.5 ± 0.3
Acenaphthylene	3.9 ± 0.2	31	5.6 ± 0.4
Acenaphthene	4.0 ± 0.3	40	5.6 ± 0.6
Fluorene	4.2 ± 0.1	44	5.7 ± 0.5
Phenanthrene	4.5 ± 0.4	49	6.0 ± 0.3
Anthracene	4.5 ± 0.2	60	5.9 ± 0.6
Fluoranthene	5.1 ± 0.2	66	6.0 ± 0.4
Pyrene	5.0 ± 0.2	70	5.9 ± 0.9
Benzo(a)anthracene	5.8 ± 0.2	101	6.4 ± 1.0
Chrysene	5.8 ± 0.1	138	6.8 ± 0.3
Benzo(b)fluoranthene	6.3 ± 0.3	180	7.1 ± 0.2
Benzo(k)fluoranthene	6.3 ± 0.3		
Benzo(a)pyrene	6.4 ± 0.6	Arochlor 1248	6.0 ± 0.2
Dibenzo(ah)anthracene	6.5 ± 0.5	Arochlor 1260	6.6 ± 0.8
Benzo(ghi)perylene	7 ± 0.3		
Indeno-1,2,3-pyrene	6.6		

Table 1-9 compares the linear correlation parameters shown in Equation 1.5 with correlations available in literature. Figure 1-5 also shows the correlations between the literature and this study The correlation obtained in this study is reasonably good and can be applied to predict the K_{OC} of other PAHs. Table 1-10 lists log K_{OC} values for PAHs in IHC sediment that were estimated using literature average log K_{OW} with Equation 1.5. Table 1-10 also shows K_d values obtained from the log K_{OC} shown in Table 1-10. This procedure gives a common algorithm for estimating the sediment-water partition constants for all the PAHs. This equation, however, has the limitation that it is empirically fit using K_{OW} values of PAHs only and may not be applicable for other classes of semi-volatiles (such as pesticides or PCBs) or volatiles that may be present in the IHC sediment.

Table 1-9. Comparison of log K_{OC} and log (K_{OW}) correlation for PAHs and PCBs: log (K_{OC}) = a log (K_{OW}) + b.

Reference	a	b	r^2
PAHs			
This report	1.063	-0.0772	0.84
Lyman et al. (1982)	0.937	-0.006	0.95
Karickhoff et al. (1979)	1.0	-0.21	1
Means et al. (1980)	1.0	-0.317	0.98
Mackay (1992)	0.96	0.045	0.97
PCBs			
This report	0.515	2.254	0.36
Kenaga and Goring (1980)	0.544	1.377	-
Di Toro et al. (1991)	0.983	0.00028	-

Table 1-10. PAH Log K_{OC} - estimated from Log K_{OW} – Log K_{OC} correlation for this study (Equation 5) and corresponding K_d using f_{OC}.

PAH	Log K_{OC}	K_d
Naphthalene	3.53	464
2-Methylnaphthalene	4.17	2064
Acenaphthylene	4.12	1826
Acenaphthene	4.22	2276
Fluorene	4.39	3367
Phenanthrene	4.71	7017
Anthracene	4.69	6682
Fluoranthene	5.39	33612
Pyrene	5.23	23284
Benzo(a)anthracene	6.04	149599
Chrysene	6.07	160997
Benzo(b)fluoranthene	6.61	560982
Benzo(k)fluoranthene	6.61	560982
Benzo(a)pyrene	6.73	734309
Dibenzo(ah)anthracene	6.86	1009413
Benzo(ghi)perylene	7.36	3189180
Indeno-1,2,3-pyrene	6.92	1140825
Units for K_{OC} and K_d are L/Kg.		

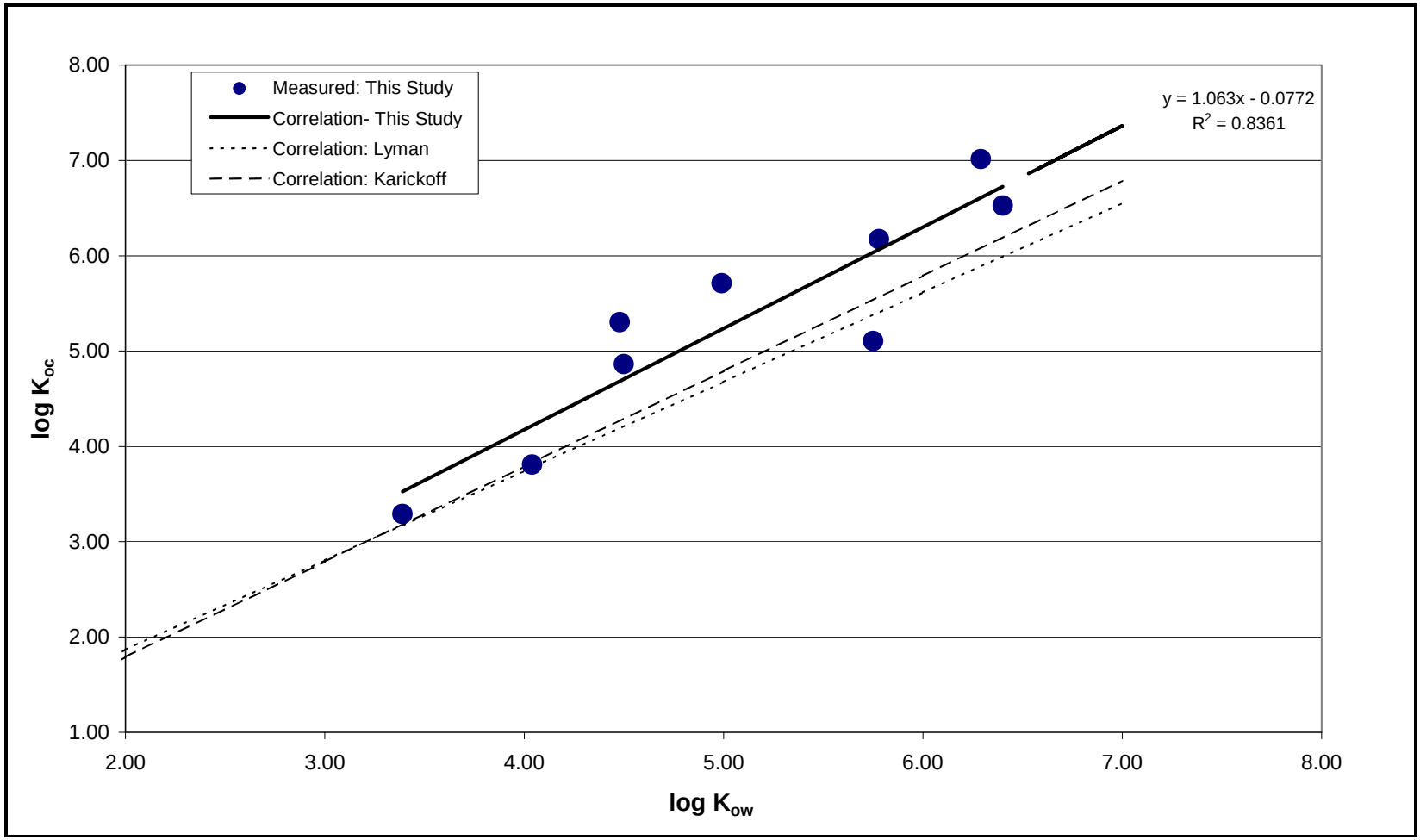

Figure 1-5. Correlation of log (Koc) and log (Kow) for PAHs in IHC sediment.

Figure 1-6 shows the plot for the log K_{OC} and log K_{OW} for the PCBs analyzed in this study. The correlation is not as good as that for the PAHs. Equation 1.6 was the linear correlation obtained from this plot and is written:

$$\log(K_{oc}) = 0.515 \cdot \log(K_{ow}) + 2.254 \quad (1.6)$$

Two other relationships that correlated log K_{OC} to log K_{OW} of PCBs were obtained from literature and are also listed in Table 1-9. The correlation obtained from this study for PCBs falls between these two correlations (Figure 1-6). Table 1-11 shows the list of log K_{OC} values that were estimated using Equation 1.6 and the corresponding K_d values for some PCBs in the IHC sediment.

The project results show the traditional and theoretically correct linear relationship between the K_{OC} values measured and the hydrophobicity of the PAHs as represented by the log (K_{OW}) values. The normalized K_{OC} values were calculated from the measured K_d values. The calculated log (K_{OC}) values were in reasonable agreement with literature average log (K_{OW}). Since all chemicals of concern in the IHC DM were not quantified in the experimental K_d determination, this procedure of estimating the log (K_{OC}) from the literature average log (K_{OW}) by the linear relationship, and then using the site-specific organic carbon content, f_{OC}, to estimate the K_d is recommended. With reference to the other chemicals of concern in the IHC DM—VOCs and pesticides—our recommendation at this stage is to use the literature average experimental values for K_{OC} in combination with site-specific organic carbon measurement for the estimation of K_d. Since the PAHs and PCBs do not follow the same correlation based on molar volume, using either correlations for pesticides or VOCs is not recommended.

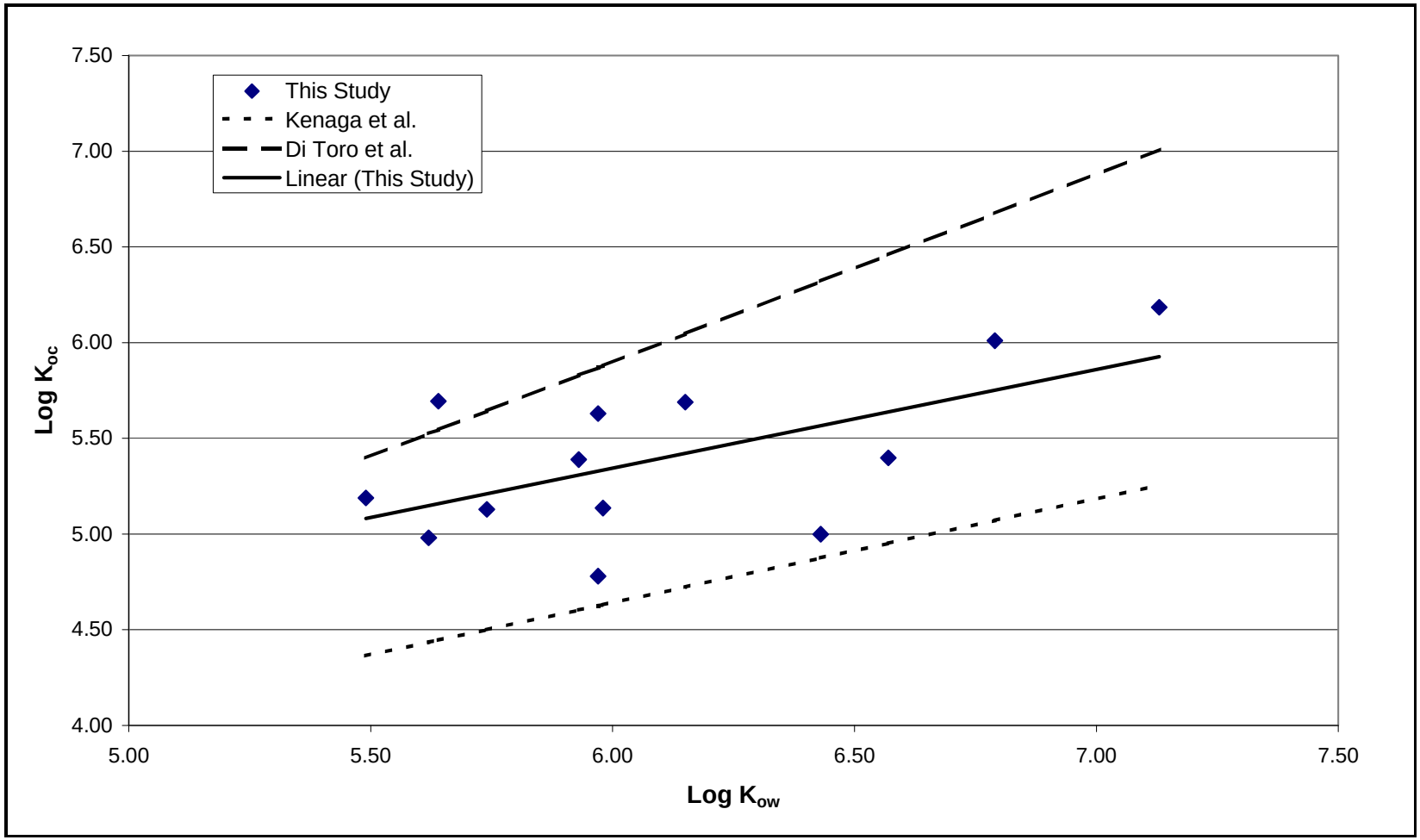

Figure 1-6. Correlation of log (Koc) and log (Kow) for PAHs in IHC sediment.

Table 1-11. Log K_{OC} and K_d for PCBs in IHC - estimated from log K_{OW} – log K_{OC} correlation for this study (Equation 6).

PCB Congener #	Log K_{OC}	K_d	PCB Congener #	Log K_{OC}	K_d
7	4.85	9760	137	6.09	168065
8	4.82	9198	138	5.75	77755
15	4.95	12227	141	5.96	124947
18	5.08	16643	153	5.93	117755
28	5.08	16643	155	5.86	99742
31	5.15	19882	156	6.17	203179
40	5.15	19416	159	6.08	166084
44	5.21	22386	170	5.91	112299
49	5.32	29405	171	6.03	147512
50	5.23	23473	180	5.93	116366
52	5.29	26744	185	6.09	168065
54	5.27	25809	187	5.91	112299
60	5.31	28043	194	6.24	239871
66	5.34	29756	202	6.37	322648
70	5.42	36402	206	6.53	465992
77	5.43	37275	207	6.27	254524
86	5.57	51342	208	6.41	354755
87	5.53	47252	Arochlor 1016	4.85	9760
97	5.69	67441	Arochlor 1221	4.03	1481
101	5.57	50737	Arochlor 1232	4.38	3278
118	5.92	114995	Arochlor 1242	4.68	6678
128	5.91	112299	Arochlor 1248	5.34	29405
129	5.90	108375	Arochlor 1254	5.44	38170
136	5.73	73278	Arochlor 1260	5.64	59900
Units for K_{oc} and K_d are L/Kg.					

Air-Water Partition Constants, Henry's Law constant, H

Project scope and objectives

The objective of this project was to determine experimentally the partition constants for PAHs/PCBs between IHC pore water and air. Laboratory experiments were conducted to measure air-water equilibrium partition constants for IHC sediment. The air-water equilibrium partition constant, K_{AW}, or the Henry's Law constant, H, is a parameter that facilitates the estimation of vapor phase concentrations of chemicals in air, if estimates of the pore water concentration are available. In the modeling of volatile losses from exposed DMs, the ratio K_d /H represents the parameter K_{SA} or

the sediment-air equilibrium partition constant. This quantity represents the thermodynamic limit of the vapor concentration of a chemical, when the concentration in the solids is known. The determination of H (the primary dependent variable in the model) will allow for the estimation of pore vapor concentrations. Estimates of H in literature vary widely mainly due to the different methods of estimation. The primary obstacle in the measurement of H for semi-volatile hydrocarbons such as PAHs and PCBs is the low vapor pressure of some of these chemicals. Direct measurement of the water and vapor phases in contact after equilibration is the preferred method for the estimation of H, but the low vapor pressures and water solubilities of some of these compounds lead to uncertainties in their estimation. The majority of the reported values of H are for exchange between air and distilled or DI water. The pore water in the IHC DM has a TOC close to 50 mg/L. This concentration may have an effect on the air-water equilibrium partition constant.

Experimental methods

H Measurement

Several methods have been used to measure H for a variety of organic compounds by direct ratio of an aqueous and vapor phase in equilibrium with each other. When the chemical is volatile, static methods such as the Equilibrium Partitioning in Closed Systems (EPICS) method (Gossett 1987) can yield significant concentration differences to resolve H. For semi-volatile chemicals such as PAHs and PCBs, however, static methods may not yield sufficient concentrations in the vapor phase. Large volumes of vapor space are necessary to conduct static experiments for these types of chemicals. Alternatively, a liquid stripping method has been used in the past for the measurement of H for PAHs (Mackay et al. 1979; Bamford et al. 1999; DeMaagd et al. 1998). In this method, humidified air is bubbled through an aqueous solution to strip the PAHs from the liquid phase into the vapor phase. The volume of the vapor phase is proportional to the flow rate and the time interval of collection. The vapor phase PAH concentration is measured by trapping the chemicals in the vapor stream over a period of time. The Henry's Law constant is estimated by the ratio of the vapor phase concentration and the average aqueous phase concentration over the interval of vapor phase collection. The prerequisite for these experiments is that the residence time of the vapor phase in the liquid is sufficient for it to be in equilibrium with the aqueous phase.

The experimental apparatus constructed for this scheme is illustrated in Figure 1-7. The apparatus consisted of a glass column 5 cm in diameter and 120 cm long, fitted with a coarse glass sparger near the base of the column. Bottled pure air (designated as "Zero Air") was supplied through the sparger through a regulating valve, flow meter, and a humidifier to prevent water loss from the glass column. The air flow rate was maintained between 60-100 mL/min. The air exiting the bubble column was sent through an XAD-2 (polymeric resin) trap to collect the PAHs in the exit stream. The flow rate of the exit air was monitored to check for leaks in the system. Water level was set at 80 cm based on Bamford et al. (1999) that a 60 cm height was sufficient to achieve equilibrium even at a higher air flow rate. The flow rates used in this study were lower than those used by Bamford et al.; therefore, the residence time is expected to be sufficient for the water and vapor to achieve equilibrium condition. Water samples were withdrawn from the top of the bubble column. The entire system was housed in a temperature controlled wooden box and maintained at 25°C. From this apparatus, H was estimated by the direct ratio of the average vapor phase concentration, C_A^{air}, measured over the time interval of vapor collection, and the average aqueous phase concentration C_A^{aq}, which was the average concentration over that time interval.

The underlying assumption in this liquid stripping method was that absorption of chemical in the gas occurs only in the bulk of the gas bubble as governed by H. However, there have been recent reports on the effect of 'adsorption' of chemicals on the surface of bubbles for gas bubbles with a relatively small volume compared to the surface area. The adsorption has been found to be significant for very small—on the order of tens to hundreds of microns—droplets (Smith et al. 1996; Mackay et al. 1990; Hoff et al. 1993), particularly for hydrophobic organic compounds. This will result in the over-estimation of the air-water partition constant. The adsorption effect was not taken into account in previous reports of this method to measure H for PAHs (Bamford et al. 1999; DeMaagd et al. 1998). In this study, the bubble column was fitted with a coarse sparger that generated bubbles in the range of several hundreds of microns to a few millimeters in diameter, which is expected to minimize surface adsorption on the bubbles.

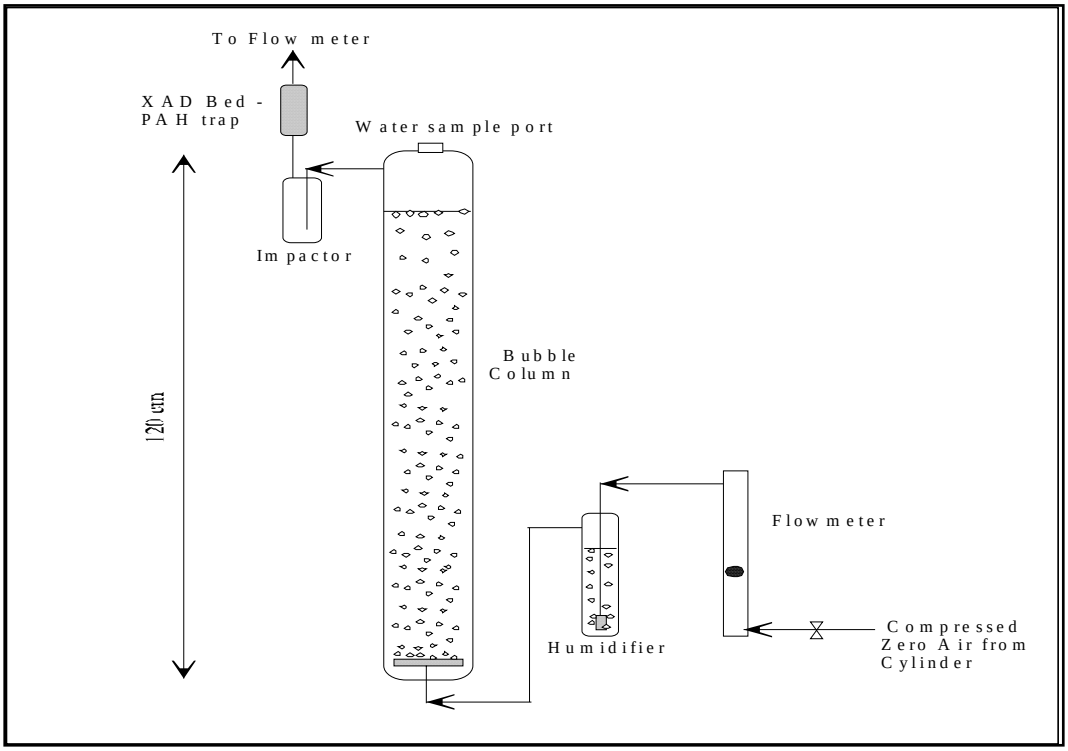

Figure 1-7. Schematic of experimental setup to measure Henry's Law constant by liquid stripping.

Polyaromatic hydrocarbons

Six PAHs were chosen as tracers to represent the entire spectrum of the 16 common PAHs. These were naphthalene (NAPH), phenanthrene (PHEN), pyrene (PYR), chrysene (CHRYS), benzo(a)pyrene (BaP) and benzo(ghi) perylene (BghiP). Aqueous solutions were prepared by dissolving pure crystals of these chemicals in DI water and IHC pore water for several days followed by filtration through a 0.7 μm glass fiber filter. Two glass columns were loaded with aqueous solutions prepared with these chemicals in DI water and IHC porewater. The experiment was divided into two phases to accommodate the measurement of the PAHs with different relative volatility in the group. NAPH and PHEN are PAHs with relatively higher volatility; therefore, collection intervals of 1 day were sufficient to measure chemical concentrations. For the low volatility compounds in the list—PYR, CHRYS, BaP and BghiP—the experimental time interval for sample accumulation and collection was 7–10 days. This division in the experimental runs was necessary to achieve detectable concentrations in the vapor phase for the low volatility compounds and to prevent vast differences in the aqueous phase concentrations for successive samples for the higher volatility chemicals.

Polychlorinated biphenyls

Separate experiments were conducted with two Arochlor mixtures – 1248 and 1260. These mixtures were chosen because they have been reported present in the IHC DM. Aqueous solutions were prepared by adding a small volume (1 mL) of a concentrated standard solution of the Arochlor mixture into 2-L volumes of IHC pore water and DI water and stirring for several days. The solutions were filtered through a 0.7 mm glass fiber filter and used in the experiment. Several experimental runs were conducted with sampling intervals varying from 12 hours to 3 days.

Analytical methods

Polyaromatic hydrocarbons

Water samples were analyzed immediately after collection for NAPH and PHEN using HPLC with a fluorescence detector. The adsorbent resin (XAD) traps were extracted with acetonitrile and analyzed within 1 day. For the other four PAHs, water samples (50–100 mL) were withdrawn and extracted with hexane. The hexane extract was separated from water, concentrated using a gentle stream of nitrogen and solvent-exchanged with acetonitrile for analysis in HPLC. A gradient method based on EPA SW-846 method 8310 (website: *http://www.epa.gov/SW-846/pdfs/8310.pdf*).

Polychlorinated biphenyls

The PCBs in the water and XAD (air samples) were extracted using the same methods used for the PAHs. The extracts were analyzed in a gas chromatography system using an electron capture detector. Two types of quantitative analyses were performed on the chromatographic data obtained. The total Arochlor peaks were quantified by summing all the peaks and calculating H for the Arochlor mixture. Nine individual congeners, present in the IHC DM and also part of the Arochlor mixtures, were identified by individual chemical standards. These standard congeners (shown in Table 1-12) were purchased from Accustandard. The data from the experiments conducted with Arochlor 1248 were used to quantify the H for congeners 18, 31 40, 52, 66, and 101. The data from experiments run with Arochlor 1260 were used to quantify the H for congeners 101, 151, 183, and 194. The congeners selected also represent the range of chlorines in the Arochlor mixtures.

Table 1-12. Congeners identified in the Arochlor mixture.

Congener IUPAC #	Predominant Arochlor	# of Chlorines
18	1248	3
31	1248	3
40	1248	4
52	1248	4
66	1248	4
101	1248, 1260	5
151	1260	6
183	1260	7
194	1260	8

Results and discussion

Polyaromatic hydrocarbons

Vapor phase concentrations could be obtained for only five of the six PAHs used in this study. BghiP vapor phase concentrations were below detection limits; therefore, H values were not obtained for this chemical. Table 1-13 lists the measured H values for the five PAHs measured in this study. The table compares the H values from aqueous solutions in DI water and in the IHC porewater. The table also compares data obtained in two previous studies by Bamford et al. (1999) and DeMaagd et al. (1998).

The value of H was observed to decrease with an increase in the molar volume of the PAH. At 25°C, the value of H in DI water did not vary significantly with that in the IHC porewater. T-test results showed that the test statistic was consistently lower than the t-value for all PAHs. This concludes that the organic carbon present in the IHC porewater does not have any significant effect on the air-water partition constant for PAHs. The H values obtained in this study compare favorably with those obtained from other studies. Figure 1-8 shows a plot of the log H (in $Pa.m^3/mol$) versus the molar volume for the DI water and IHC porewater experimental data with linear regression lines through both experimental datasets.

Table 1-13. Experimental Henry's Law constant values for PAHs – comparison between DI water, IHC pore water, and literature values.

Compound	Molar Volume (cm^3/mol)	Henry's Law constant (-)				
		DI –water	IHC pore water	Literature Average, Mackay et al. (1992)	From Bamford et al. (1999)	From DeMaagd et al. (@20 C)
Naphthalene	147	0.012 ± 0.007	0.011 ± 0.006	0.02 ± 0.0001		0.018
Phenanthrene	199	0.0022 ± 0.0005	0.0029 ± 0.0007	0.0016 ± 0.0003	0.0017 ± 0.0001	0.0012 ± 0.0001
Pyrene	214	0.0007 ± 0.00006	0.00092 ± 0.000025	0.00056 ± 0.0002	0.00069 ± 9.9×10^{-5}	0.0008 ± 0.0002
Chrysene	251	0.0003 ± 0.00022	0.0003 ± 9.8×10^{-5}		0.00022 ± 9.9×10^{-5}	
Benzo(a)pyrene	263	9.3×10^{-5} ± 6.2×10^{-5}	8.5×10^{-5} ± 4.1×10^{-5}			1.37×10^{-5}

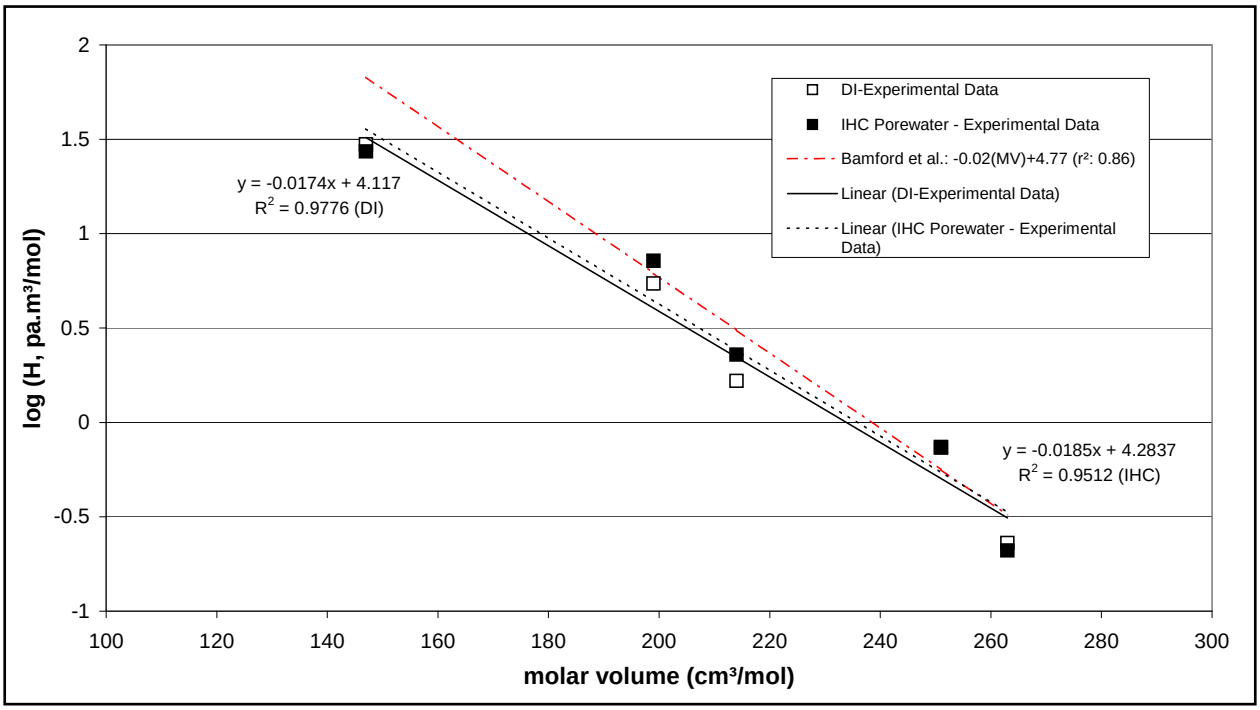

Figure 1-8. Henry's Law constant for PAHs – correlation with molar volume.

The equations were—

DI water:

$$\log H\ (Pa\text{-}m^3/mol) = -0.0174 * MV\ (cm^3/mol) + 4.117 \quad (1.7)$$

IHC pore water:

$$\log H\ (Pa\text{-}m^3/mol) = -0.0185 * MV\ (cm^3/mol) + 4.284 \quad (1.8)$$

The correlation from Bamford et al. (1999) was

$$\log H\ (Pa\text{-}m^3/mol) = -0.02 * MV\ (cm^3/mol) + 4.77 \quad (1.9)$$

The correlations for both the DI water and IHC experiments were good (r^2 of 0.98 and 0.95, respectively). The correlation from Bamford et al. (1999) compares well with the correlation obtained from the experimental data in this study.

To extrapolate the H values for other PAHs by correlation with molar volume is a convenient method since the saturated vapor pressure and the solubility also correlate with molar volume. On the basis of the molar volumes of all the PAHs and the correlation obtained in this study, Table 1-14 lists the suggested values of dimensionless H for 15 PAHs of concern in the IHC sediment for which molar volume measurements are available.

Table 1-14. Suggested values of H based on correlation with molar volume for 15 PAHs in IHC at 25°C.

PAH Chemical	Molar Volume, cm^2/mol	Estimated Henry's Law constant ($Pa.m^3/mol$)	Estimated Henry's Law constant (-)
Naphthalene	147	36.66	0.015
Acenaphthylene	173	12.11	0.0049
Acenaphthene	166	16.32	0.0066
Fluorene	188	6.39	0.0026
Phenanthrene	199	4.00	0.0016
Anthracene	197	4.36	0.0018
Fluoranthene	217	1.86	0.00075
Pyrene	214	2.11	0.00085
Benzo(a)anthracene	248	0.49	0.0002
Chrysene	251	0.44	0.00018
Benzo(b)fluoranthene	268.9	0.20	8.22×10^{-5}
Benzo(k)fluoranthene	268.9	0.20	8.22×10^{-5}
Benzo(a)pyrene	263	0.26	0.00011
Benzo(ghi)perylene	277	0.144	5.82×10^{-5}
Dibenzo(a,h)anthracene	300	0.054	2.19×10^{-5}

Polychlorinated biphenyls

Table 1-15 shows the measured H values for the nine congeners and the Arochlor mixtures in IHC pore water, DI water, and literature average values. Though the values of the Arochlors are reported here, it is not recommended to use a single value of a physical property such as H for a mixture of individual chemicals. It is recommended that each congener be treated as an individual compound. An attempt is made here to correlate the H values of the PCB congeners to a representative physical property. Figure 1-9 also displays the experimental H values shown in Table 1-15 in graphical form. For most of the congeners under consideration, the error bars overlap for the measured H, suggesting that there is no significant difference between the three sets of data. Most of the environmental properties, such as aqueous solubility or vapor pressure of PCB congeners, do not exhibit a correlation to the chlorine number of the PCBs (Mackay and Shiu 1986). In this study, the H values also did not show any correlation with the chlorine number. This observation is in agreement with those made in several earlier reports of measured H in literature (Mackay and Shiu 1986; Murphy et al. 1983; Atlas et al. 1982) and also from the calculations of H from reported vapor pressures (Bidleman 1983;

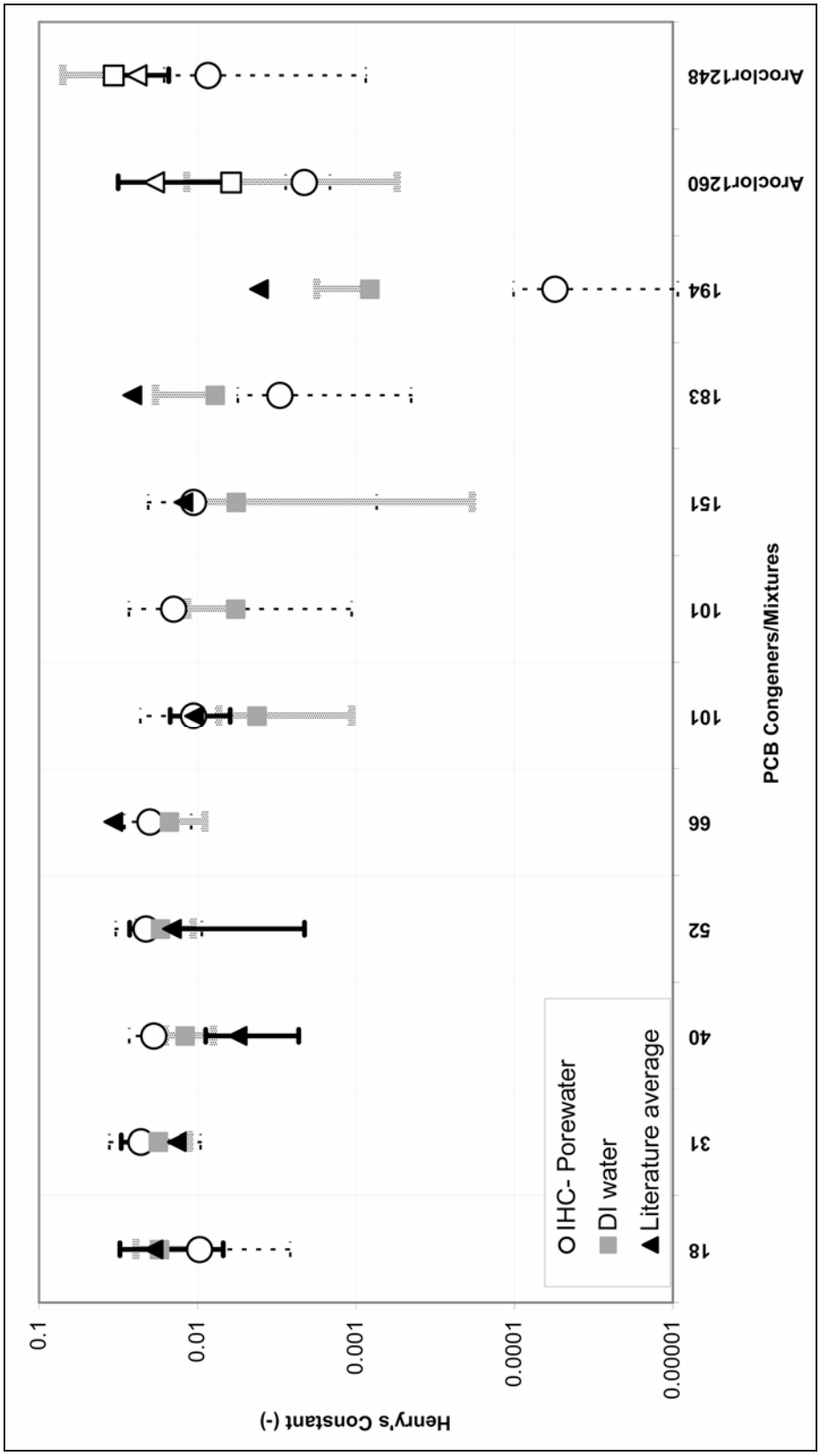

Figure 1-9. Henry's Law constant for PCB congeners.

Westcott et al. 1981; Westcott and Bidleman 1981) and solubilities of PCBs. The H values for PCBs vary around a mean value, which is 0.012±0.008, 0.012±0.01, and 0.017±0.01 for IHC pore water, DI water, and literature average. Mackay and Shiu (1986) suggested that it may be appropriate to use a mean value to represent all PCB congeners. In the absence of the measured values of H for all congeners or a suitable correlation, this mean value may be used to estimate H for any congener.

Table 1-15. Experimental Henry's Law constant values for PCBs – comparison between DI water, Indiana Harbor and Canal Porewater and literature values.

PCB Congener #	IHC Porewater	DI water	Literature average
18	0.01 ± 0.0071	0.017 ± 0.0071	0.019 ± 0.012
31	0.023 ± 0.013	0.018 ± 0.006	0.013 ± 0.017
40	0.019 ± 0.008	0.012 ± 0.004	0.006 ± 0.003
52	0.021 ± 0.012	0.017 ± 0.006	0.014 ± 0.012
66	0.02 ± 0.009	0.015 ± 0.006	0.034
101	0.012 ± 0.013	0.005 ± 0.004	0.011 ± 0.004
151	0.011 ± 0.01	0.006 ± 0.005	0.012
183	0.003 ± 0.003	0.008 ± 0.01	0.026
194	0.00006 ± 0.00005	0.0008 ± 0.001	0.0041
Arochlor 1248	0.009 ± 0.008	0.034 ± 0.037	0.024 ± 0.037
Arochlor 1260	0.002 ± 0.001	0.006 ± 0.006	0.019 ± 0.013

Correction of H for temperature T_2, different from 25°C (298K), may be obtained from the van't Hoff equation (Equation 1.10)

$$\ln\frac{H(298)}{H(T_2)} = \frac{-\Delta H^0}{R}\left(\frac{1}{298_1} - \frac{1}{T_2}\right) \tag{1.10}$$

where ΔH^o is the enthalpy of volatilization from an aqueous solution. R is the universal gas constant. The value of ΔH^o may be obtained experimentally by measurements at different temperatures or from literature. At this stage, it is recommended to use any published values of the enthalpy and, in the absence of these, use the correlation for temperature relationship provided by Bamford et al. (1999) as a first estimate for PAHs. Similar correlations were also derived from experimental measurements of multiple PCB congeners by Bamford et al (2002). These correlations are applicable for each Chlorine number group (e.g., tri-chloros and tetra-chloros).

H values for VOCs, especially benzene, have been well established using different methods, and the values reported in literature are very reliable (Kotchetkov et al. 2001). In the absence of site-specific H values for pesticides, the recommended option is to use literature average experimental values.

References

American Society for Testing and Materials. 2002. Method E1195-01. "Standard test method for determining a sorption constant (Koc) for an organic chemical in soil and sediments.

Atlas, E., R. Foster, and C. S. Giam. 1982. Air-sea exchange of high molecular weight organic pollutants: Laboratory studies. *Environmental Science and Technology* 16: 283-286.

Bamford, H. A., D. L. Poster, and J. E. Baker. 1999. Temperature dependence of Henry's Law constant of thirteen polycyclic aromatic hydrocarbons between 4°C and 31°C. *Environmental Toxicological Chemistry* 18: 1905-1912.

Bamford, H. A., D. L. Poster, R. E. Huie, and J. E. Baker. 2002. Using extrathermodynamic relationships to model the temperature dependence of Henry's Law constants of 209 PCB congeners. *Environonmental Science and Technology* 36: 4395-4402.

Bidleman, T. F. 1983. Estimation of vapor pressures for nonpolar organic compounds by capillary gas chromatography. *Analytical Chemistry* 56: 2490-2496.

DeMaagd, P. G. J., T. E. M. van Hulscher, H. V. D. Heuvel, A. Opperhuizen, and D. T. H. M. Sijm. 1998. Physicochemical properties of polycyclic aromatic hydrocarbons: Aqueous solubilities, n-octanol/water partition coefficients and Henry's Law constants, *Environmental Toxicological Chemistry* 17: 251-257.

Gossett, J. M. 1987. Measurements of Henry's Law constants for C1 and C2 chlorinated hydrocarbons. *Environmental Science and Technology* 19: 202-208.

Lyman, W. J., W. F. Reehl, and D. H. Rosenblatt, eds. 1982. Handbook of Chemical Property Estimation Methods, Environmental Behavior of Organic Compounds. New York, NY: McGraw-Hill.

Hoff, J. T., D. Mackay, R. Gillham, and W. Y. Shiu. 1993. Partitioning of organic chemicals at the air-water interface in environmental systems. *Environmental Science and Technology* 27: 174-2180.

Kochetkov, A., J. S. Smith, R. Ravikrishna, K. T. Valsaraj, and L. J. Thibodeaux. 2001. Air-water partitioning of organo-silicon compounds. *Environmental Toxicological Chemistry* 20: 2184-2188.

Kommalapati, R. R., K. T. Valsaraj, and W. D. Constant. 2002. Soil-water partitioning and desorption hysteresis of volatile organic compounds from a Louisiana superfund site soil. *Environmental Monitoring and Assessment* 73(3): 275-290.

Mackay, D., and W-Y. Shiu. 1986. A critical review of aqueous solubilities, vapor pressures, Henry law constants and octanol-water partition coefficients of the polychlorinated biphenyls. *Journal of Physical Chemistry Reference Data* 15: 911-929.

Mackay, D., W-Y. Shiu, and R. P. Sutherland. 1979. Determination of air-water Henry's Law constants for organics in dilute solutions. *Environmental Science and Technology* 13: 333-337.

Mackay, D., W. Shiu, K. T. Valsaraj, and L. J. Thibodeaux. 1990. Air-water transfer: Role of partitioning, *Air Water Mass Transfer,* Gulliver, J.S. and Wilhelm, S., eds. American Society of Civil Engineers, New York, NY.

Mackay, D., W-Y. Shiu, and K. C. Ma. 1992. Illustrated handbook of physical- chemical properties and environmental fate for organic chemicals. Vol. 1-5. Lewis Publishers, MI.

Murphy, T.J., J. C. Pokojowczyk, and M. D. Mullin. 1983. *Physical Behavior of PCBs in the Great Lakes*, Mackay, D., Paterson, S., Eisenreich, S.J., and Simmon, M.S., eds. Ann Arbor Scientific, Ann Arbor, MI.

Smith, J.S., K. T. Valsaraj, and L. J. Thibodeaux. 1996. Bubble column reactors for wastewater treatment. 1. Theory and modeling of continuous countercurrent solvent sublation*, Industrial Engineering Chemistry Resource* 35: 1688-1699.

Thibodeaux, L.J., R. Ravikrishna, and K. T. Valsaraj. 2002. Volatilization rates from dredged material and soils – a literature review with application to Indiana Harbor and Canal, Final Report. U.S. Army Corps of Engineers, Chicago District, Chicago, IL.

U.S. Environmental Protection Agency. 2005. *EPA Method 8310*. Polynuclear Aromatic Hydrocarbons– Analysis by Liquid Chromatography, SW-846 Methods, 1986. *www.epa.gov*. (28 October 2005).

_____. 2005. *EPA Method 8082*. Polychlorinated Biphenyls (PCBs) by Gas Chromatography, SW-846 Methods, 1986. *www.epa.gov*. (28 October 2005).

_____. 1996. *EPA Method 3550*. Test Methods for Evaluating Solid Waste – Physical/Chemical Methods, SW-846 Methods, 1986.

Westcott, J. W., C. G. Simon, and T. F. Bidleman. 1981. Determination of polychlorinated biphenyl vapor pressures by a semi micro gas saturation method. *Environmental Science and Technology* 15: 1375-1378.

Westcott, J. W., and T. F. Bidleman. 1981. Determination of polychlorinated biphenyl vapor pressures by capillary gas chromatography, *Journal of Chromatography* 210: 331-336.

2 Exposed Dredged Material CDF Emission Model and Wind Tunnel Results

Introduction

The objectives of the investigation were to obtain experimental data and develop a science-based volatilization process model for soil-to-air chemical emissions from dredged materials (DM). Wind tunnel volatilization experiments were conducted using Indiana Harbor and Canal (IHC) DM to produce data for modeling efforts. A literature review revealed that most chemical evaporation data (i.e., flux to air) are derived from natural soil-like sources and are based on laboratory-scale experiments that typically used small mass quantities and small evaporative surface areas, and contained soils not of bed-sediment origin. With one exception, all were laboratory-scale evaporation experiments. As a result, models are based on natural soils rather than DM-like soils. However, the model results generally matched that of the "field" experiment except for the drying process found in the sediment bed. It was decided that a large-scale lysimeter/wind tunnel (L/WT) experiment was the best compromise between the laboratory-scale simulations and field-scale measurements. The large evaporative surface areas and DM mass contained within the wind tunnel allowed close mimicking of the drying/consolidation/cracking/etc. processes that occur in the field. In addition, the L/WT apparatus has the advantages over the field in the ability to control the wind conditions and air sampling to make precise measurements of water content, water losses, surface area cracking, and other aspects of chemical flux measurements. Using the IHC DM as the contaminant source material will provide critical data needed for estimating emissions at this particular site. The results of the experiment will provide the process understanding and the parameter quantification that are keys to developing a more realistic chemical flux model. The two key objectives of this research are to: (1) obtain field-like chemical flux measurements for IHC Confined Disposal Facility (CDF) DM and (2) update the existing U.S. Army Corps of Engineers (USACE) commissioned emission flux model (Thibodeaux 1989).

Background

As established in a recent literature review of models and data, considerable information is available discussing the evaporative chemical release process from natural soils (Thibodeaux et al. 2002). The fundamental theory of the process is well established and generally verified by numerous sets of laboratory-scale data. Essentially it is a three-step transport process:

1. The chemical is sorbed to the solid phase of the DM and desorbed into the adjoining air-filled pores characterized by the ratio of the Henry's Law constant to the sediment-water partition constant.
2. The effective chemical diffusion coefficient in the vapor-phase of the porous media, quantified by D_e, moves the chemical to the air-soil interface.
3. The chemical species moves through a thin boundary film on the air-side of the interface before being mixed with bulk air currents in the atmospheric boundary layer.

An equation based on the Lavoisier mass-balance principle connects the flux, n, and the average chemical concentration, C_s, in the soil column. The major uncertainty in the transport process model appears to reside with Step 2 — diffusion of chemical vapor molecules through the open pores of the soil, as outlined next.

It is well known that the fraction of air porosity, ε_1, is a key variable in regulating the effective diffusion coefficient, D_e. The well known Millington and Quirk (1961) correction, which is $D\varepsilon_1^{4/3}$, is used to modify the molecular diffusivity, D, for the presence of solid particle blocking and tortuous pathways. Typical agricultural soils behave ideally because they maintain rather uniform ε_1 values so that a constant D_e can be used for predicting pesticide and volatile hydrocarbon emissions. Due to the high initial water contents and large clay fractions, DM soils appear to behave very non-ideal. One field-scale test using IHC DM displayed an emission-to-air behavior that could not be quantified by a constant D_e as typically used in these models (Ravikrishna et al. 2001). Post-experiment analysis suggested that a complex behavior of $\varepsilon 1$ with time was the likely factor. It was hypothesized that the observed flux behavior was the result of water evaporation and the simultaneous volume shrinkage of the DM column (i.e., consolidation). Surface cracks were noted to appear early on in the

evaporation process. A critical review of this first field test appears in Thibodeaux (2002).

Experimental materials and methods procedure

Dredge material sources

Sediment samples from five separate reaches of the IHC were collected in July 2003. The objective of sample collection was to obtain sediment samples representative of the material to be dredged in regard to location, quantity, and amount of contamination. A total of fifteen 55-gallon (200 liters) metal drums were filled with sediment and shipped to the U.S. Army Engineer Research and Development Center (ERDC), Vicksburg, MS, in a refrigerated truck (Saichek 2003). All containers were stored in a refrigerated trailer (4°C) until ready to be mixed.

Sediment handling and analysis

The DM solids had consolidated during transportation and storage time and significant amounts of water had accumulated at the top of each container. Motorized propeller mixers were used to homogenize the drum contents before the material was transferred to the lysimeter where further mixing was conducted to homogenize all 15 drums. One 55-gallon drum was removed for use in plant up-take studies. Once filled, the sediment was raked evenly to form a uniform (3 to 4 cm – height variations) surface, 46 cm in depth.

Five separate samples were taken from the homogenized DM in the lysimeter and analyzed for physical and chemical parameters (Table 2-1).

Table 2-1. Soil parameters for IHC DM at 25°C.

Parameter	Units	Average	Minimum	Maximum
Organic Carbon Fraction	%	0.096		
Naphthalene	mg/kg	2.65	Undetectable	2.90
2-Methylnaphthalene	mg/kg	Undetectable	Undetectable	1.2*
Phenanthrene	mg/kg	4.27	2.40	6.50
Acenaphthene	mg/kg	1.63	Undetectable	2.20
Fluoranthene	mg/kg	7.95	4.80	10.00
Fluorene	mg/kg	1.60	Undetectable	1.70
Pyrene	mg/kg	9.47	4.20	12.00
Particle density	g/ml	2.41		
Bulk density	g/ml	0.88	0.47	1.27
Air-filled Porosity, ε_1	-	0.17	0	0.5
Initial Moisture fraction	%	55.7	27.7	96
* lower limit of detectability				

Initial sediment contaminant concentrations for polyaromatic hydrocarbons (PAHs) and polychlorinated biphenyls (PCBs) were determined by gas chromatrography/mass spectrometry (GC/MS) analysis (U.S. Environmental Protection Agency [EPA] Method 8270) and GC analysis (EPA Method 8082), respectively (Appendix II). Once mixed, the lysimeter was moved into a temperature-controlled (23-25°C) building housing the wind tunnel. The sediment was covered with a thick layer of black plastic and the wind tunnel was lowered onto the lysimeter and sealed using gasket material and numerous bolts.

Wind tunnel design

The design of a wind tunnel constructed at ERDC Vicksburg was based on one used to measure selenium volatilization from soils (Dungan et al. 2000). A lysimeter of height 0.46 m (1.5 ft) x width 1.22 m (4 ft) x length 4.57 m (15 ft), designed to simulate surface water runoff (Price et al. 1996), was used as the base of the wind tunnel. A rectangular tunnel of height 0.91 m (3 ft) x width 1.22 m (4 ft) x length 4.57 m (15 ft), open at each end, was placed on top the lysimeter. The tunnel contained window panels along one side and on top for access and to view the inside of the tunnel. The soil-filled lysimeter served as the bottom of the wind tunnel. Figure 2-1 shows a schematic of the tunnel.

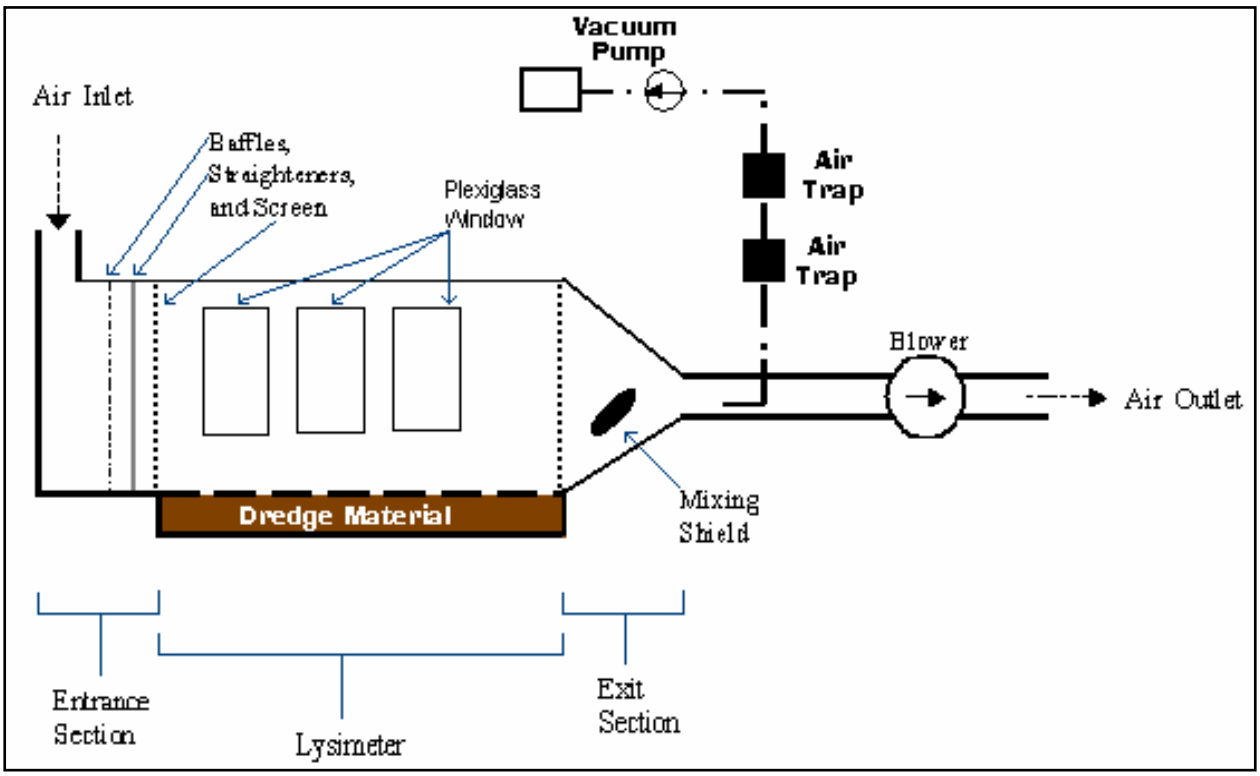

Figure 2-1. Wind tunnel schematic.

An 11.2 W (15 hp) blower was used to draw outside air into the wind tunnel via an aluminum duct located outside the building with an opening at 4.57 m (15 ft) above the ground. Once in the entrance zone the air stream is straightened and the flow evenly distributed using a three-part section consisting of a honeycomb, a baffle, and screens. The baffle was made of sheet plywood with teardrop shaped holes to better distribute the inlet air-flow arriving in the duct. A thin aluminum sheet of honeycomb cells 1.27 cm (0.5 in.) X 15.2 cm (6 in.) length was added to further straighten the flow. A stack of four wire screens were placed last to further assist in shaping the velocity profile over the lysimeter. Velocity profiles within the tunnel were measured using hotwire and impellor anemometers at locations of 1.22 m (4 ft), 2.44 m (8 ft), and 3.66 m (12 ft) from the entrance screen.

Air sample collection apparatuses were located both within the tunnel section and in the exit section outside of the tunnel. A thin circular metal disk angled at 45 degrees to the wind and placed 30 cm upstream of the sample device was the “mixing body” used to homogenize the air stream (Ruscheweyh 1984) prior to sampling. This gas mixing system has been shown to be very effective in producing uniform concentrations in

converging gas streams. The blower unit is located a few feet beyond the air sample port. The air exits at a height of 9.14 m (30 ft) above the ground.

Wind speed and profile

The stack of devices (baffles, honeycombs, and screens) installed in the L/WT inlet section shaped the airflow above the soil surface in an attempt to conform it to field-like conditions. Measurements taken in the 30 cm region above the soil displayed the turbulent boundary layer profile shape with friction velocities and surface roughness heights commonly found at field sites. These results are evidence that the chemical transport processes in the air boundary layer above the soil were realistic simulations of field conditions.

Experimental methodology

The first of a series of four experimental runs was initiated the day following lysimeter loading. The plastic was removed from the sediment surface and the sediment was raked again to a uniform consistency. A soil temperature probe (Campbell Scientific, Logan, UT) was inserted into the DM approximately 2.54 cm (1 in.) in depth from the sediment surface. Soil water content reflectometers (Model CS616, Campbell Scientific) were inserted 30.48 cm (12 in.), 15.24 cm (6 in.), and 2.54 cm (1 in.) below the sediment surface in the middle section of the wind tunnel. Soil temperature and moisture were collected on a CR200 data logger (Campbell Scientific) during the course of each experimental run. Wind speed, air temperature, and relative air humidity in the wind tunnel were monitored during each run using sensors obtained from Texas Instruments [TI], Dallas, TX. Data were collected and recorded on a Solus data logger (TI). All probes and sensors were removed prior to each new experiment to enable water addition and sediment remixing and then replaced in the same locations in the wind tunnel.

In the first experimental run, a representative air sample of the main air stream was collected on contaminant-specific air sampling tubes (Orbo 44, Supelco, Inc.) located in a separate chamber outside the wind tunnel (Figure 2-1). Air was pulled through the sampling tubes at a rate of 1.7 L/min using a GAST vacuum pump. This rate was selected based upon trap capacity specifications. Samples were collected continuously and removed at sample times of 6 hours, 3 days, 7 days, 13 days, 21 days, and 28 days

after air was supplied across the sediment surface. Inlet air concentrations were periodically measured and determined to be free of the contaminants of interest. The traps were solvent extracted and the solvent analyzed for PAHs and PCBs according to EPA Methods 8270 and 8081.

Before experimental Run II began, 30 liters of water were added to the sediment in the wind tunnel and mixed to approximately 1 ft (0.3 m) in depth. The sediment surface was again smoothed and measurements were taken to determine unevenness of the material throughout the tunnel. In order to increase trapping capacity and increase the sample detection limits, larger traps were constructed of the same material as the Orbo 44 traps (Supelpak-2). Air was pulled through these larger traps at 10 L/min. Samples were collected both outside and inside the wind tunnel to draw a comparison between sampling techniques in both locations. Samples were collected 2 days, 5 days, 9 days, and 15 days after air was supplied across the sediment surface. Traps were extracted and analyzed as stated previously.

A third run was initiated after adding 279 liters of water to the DM. Sediment was mixed to approximately 1 ft (0.3048 m) in depth. The run was discontinued after a sampling error was detected; all analytical results were below detection limits.

A fourth and final run using the larger traps as described in Run II was initiated immediately following Run III. A total of 242 liters of additional water was added and mixed into the sediment. The sediment had consolidated and mixing was conducted to approximately 8 to 12 in. (20.32–30.48 cm) in depth. The sediment surface was again smoothed to prevent as much unevenness in the surface as possible. Samples were collected 2, 5, 9, 13, 19, 26, 33, and 40 days after air was supplied across the sediment.

Experimental results

The primary observation from the L/WT apparatus was the chemical flux to air from the DM mass. From measured mass (ng) quantities collected onto adsorbent traps, the exit concentrations in air, C_A (ng/m^3), of selected chemical species were obtained. The volumetric airflow rate, Q_1 (m^3/s), was measured as well. From these measured quantities the chemical flux to air, N_A (ng/m^2.h), was obtained from:

$$N_A = Q_1 C_A / A \quad (2.1)$$

The DM surface area was A (m²). The measured fluxes for the three chemicals appear in Figures 2-2 through 2-4.

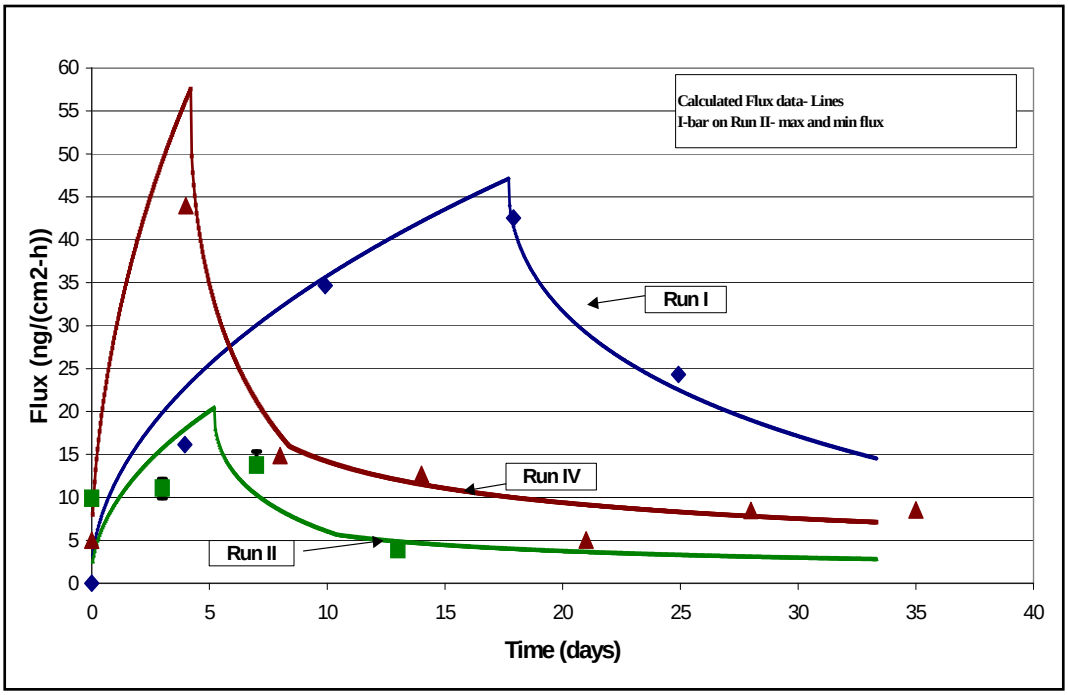

Figure 2-2. Naphthalene flux – measured versus model-estimated.

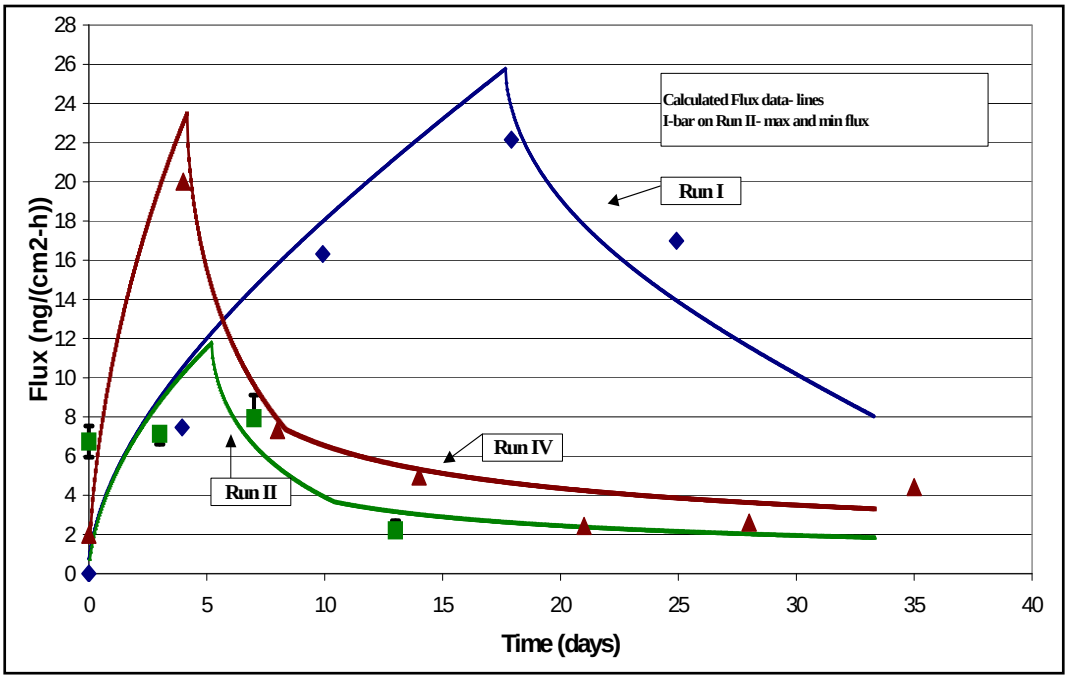

Figure 2-3. 2-Methylnaphthalene flux – measured versus model-estimated.

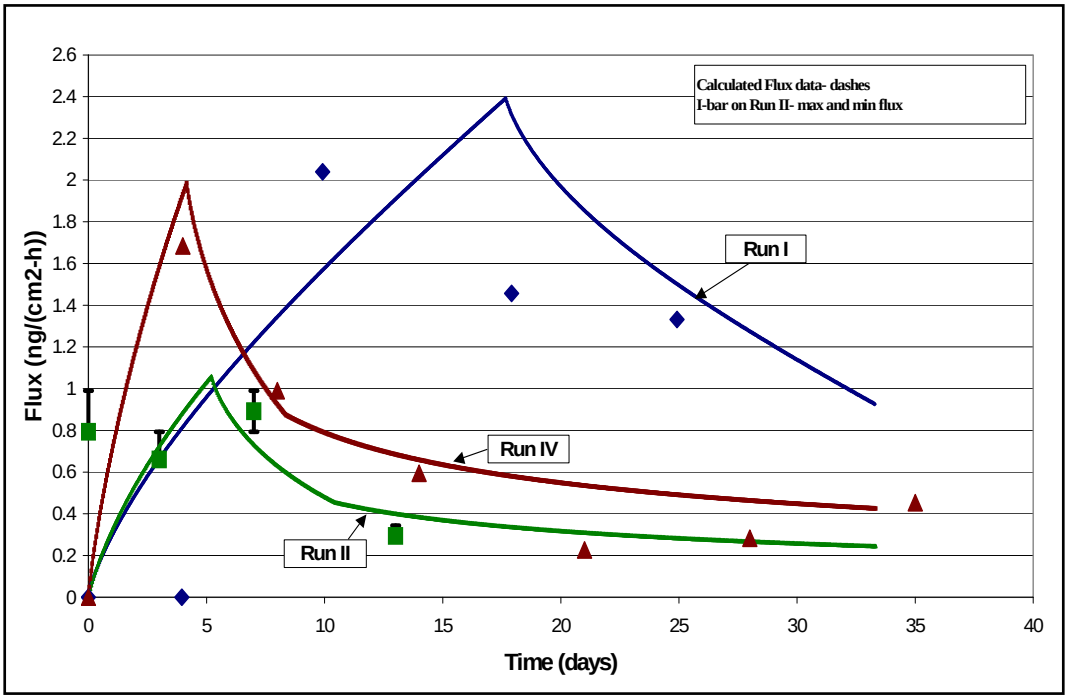

Figure 2-4. Phenanthrene flux – measured versus model-estimated.

Due to the low chemical loading levels in the collected IHC DM, only naphthalene, 2-methylnaphthanlene, and phenanthrene fluxes were quantifiable. Collected mass quantities for other PAHs were too low or too few in number to be useful. Three successive experimental runs were performed in order to capture the variations of the flux measurements. The experimental run times were 670 hours (28 days), 360 hours (15 days), and 959 hours (40 days) for Runs I, II, and IV, respectively. The flux data for naphthylene (NAPH), M-NAPH, and PHEN displayed the same general trends with time. Fluxes for NAPH varied between 0 and 50, those for M-NAPH varied between 0 and 25, and PHEN fluxes ranged from 0 to 2 ng/cm^2.h. Sample time intervals varied for each run; initially, a 6-hour interval was used. As air concentrations decreased, however, the sample collection time intervals were extended to 48 hours and 96 hours with some requiring 194 hours (8 days) in order to obtain measurable quantities on the adsorbent traps. In addition to NAPH, M-NAPH, and PHEN, small quantities of acenaphthylene were observed. Occasionally, even smaller quantities of pyrene and fluorene near the detection limit of < 0.10 µg/mL were noted. The data associated with these low levels, however, were judged to be unreliable for flux interpretation purposes. The flux data on these chemicals appear in Appendix A along with other physical variables during the experimental runs. The following paragraphs

describe the time-behavior patterns for the observed NAPH, M-NAPH, and PHEN fluxes; focusing on NAPH due to the higher chemical fluxes.

Run I

As Run I began, 2.6 m^3 of DM was placed in the lysimeter. The air velocity was adjusted to an average of 1.16 m/s (2.60 mph). A ponded/soupy water layer existed on the surface of the DM initially. After 3 days the ponded water was no longer visible. The time period for the evaporative removal of the ponded/soupy water layer covering the bed is t_b, defined as the Regime 0 time period. During this time period the NAPH flux was initially 21 $ng/cm^2.h$, but decreased rapidly and values were below detection limits (<0.10 ug/mL) after 72 hours (3 days), which marked the end of Regime 0. Regime 0 does not appear on Figures 2-2, 2-3, or 2-4, so the days referred to below do not match the abscissa in the figures. See Figure 2-5. The values of t_b = 3, 2, and 5 days respectively for Runs I, II, and IV. The days used in the following presentation of results include the t_b values; Figures 2-2, 2-3, and 2-4 do not. Fluxes measured during Regime 0 are not representative of a drying bed process but are for a ponded CDF process. The appropriate models appear in the Ponded CDF emission model section (page 101). During Regime 0 the observed fluxes were of very short duration and represent a small chemical mass quantity. This type flux burst with rapid die-off is typical of chemical evaporation from a thin water layer containing a finite soluble fraction.

The increasing chemical flux period is defined as Regime I. Regime I commences when the chemical flux increases above the detection limit. Once the surface water layer is gone, further chemical volatilization must occur from within the porous bed material. Chemical diffusivities in water-filled pore spaces are much smaller than those found in air-filled ones; typically they are 100 to 1000 times smaller. The formation of air-filled chemical pathways must occur so as to maintain the highest vaporization fluxes. The loss of liquid water by evaporation converts water-filled pore spaces to air-filled ones, and this is referred to as the process of “dry patch” formation. Dry patch formation is defined as Regime I.

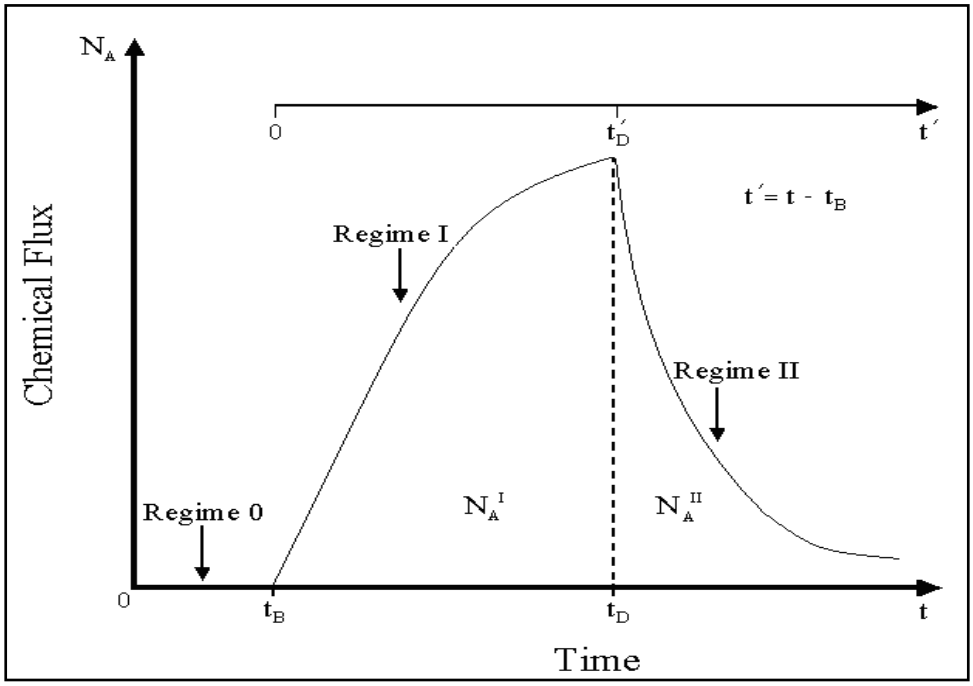

Figure 2-5. Exposed dredge sediment regimes.

It is assumed that the reappearance of a measurable chemical flux is due to the formation of dry patches on the surface of the DM. This process proceeds slowly because the bed solids continue to consolidate and free water is forced upward. Since water evaporates faster than any that is forced up, ponded water does not develop on the surface. The majority of consolidation-produced water appeared to end on Day 7; it was reported that the overall surface was "beginning to dry." On Day 11 cracks on the surface of the DM became apparent. The chemical flux increased as water-free porous surface areas (i.e., patches) increased with time. Some water was observed at depth in the soil cracks on Day 15, indicating consolidation was still occurring. The surface of the DM had receded from 2.5 to 3.8 cm below the top of the lysimeter. On Day 20 the sediment level had decreased 5.1 cm. This decrease amounts to 228 liters of water evaporated from the lysimeter. The surface cracks were 1 to 1.2 cm in width and 2.5 cm in depth on Day 20, and 2 cm in width and 6-8 cm in depth on Day 26. On Day 21, the NAPH flux reached a maximum value of 49 ng/cm^2-h. This occurrence marked the end of Regime I.

The falling chemical flux period is defined as Regime II. On Day 28 the final NAPH flux measurement was 28 ng/cm^2-h. Surface layer (~2 cm) soil moisture content measured on composite samples for Days 0, 12, 15, and 21 fell from 94 to 79, 62, and 55%, respectively. In general, these

measurements correspond to the observed water evaporation losses. Clearly, the solids consolidation process produces water, which travels upward since the bottom of the lysimeter is sealed; no leachate was collected or withdrawn. This water expression due to consolidation opens the soil pore spaces and affects the chemical flux to air. As introduced, these three regimes will be used to characterize the chemical and water behavior in the lysimeter: Regime 0 is the ponded period, Regime I is the surface patches formation period, and Regime II is the dry surface period.

These water regimes influence the NAPH flux rate. Regime 0 occurs early on after filling the lysimeter with DM; rapid solids consolidation produces ponded water on the surface. The second water regime, Regime I, is characterized by less rapid consolidation, high water contents with continuing water evaporation. Relative dry soil surface patches and numerous cracks appeared on Day 14. Between Days 7 and 14 (approximately) the soil pore spaces increasingly contain air rather than water. At 25°C, the chemical diffusivity for NAPH in air is 185 cm^2/h, where it is only 0.02 cm^2/h in water. Since the air-filled pores dominate the chemical transport within the soil, the flux gradually increases over the period as shown in Figure 2-2 for Run I. Soil temperature and percent relative humidity (%RH) varied with the incoming outdoor air and ranged from 15 to 25°C and 65 to 90% over the period. Dry surface patch areas with air-filled soil pore spaces begin to appear at the end of Regime 0. In effect Regime I is characterized by surface drying that converts a porous but water-filled DM soil surface to one containing air-filled surface patches. When the patches cover the entire surface, the maximum chemical flux occurs and defines the time, t_D[7]. This occurrence marks the end of Regime I and the start of Regime II.

High chemical fluxes cannot be maintained once the surface is dry. Chemical depletion occurs from the upper soil layers, but the diffusion path length increases with time. Since the chemical needed for evaporation originates well below the interface, the flux decreases. A dramatic decrease in flux occurred between Days 21 and 28.

In summary, Regime 0 contains free water on the surface of the DM; Regime I has air-filled pore spaces gradually replaced by water-filled ones; and Regime II represents full air-filled soil pore spaces and a cracked surface. The chemical flux pattern responds to the three water-dominated regimes. Considerable bed consolidation occurs throughout Regimes I and II. The flux versus time behavior of M-NAPH and PHEN shown in

Figures 2-3 and 2-4 are very similar to that of NAPH for Run I. The three water regimes similarly affect all the chemical fluxes. Flux is low when a ponded condition exists and increases as the water evaporation opens soil pores to achieve a maximum flux value. Upon reaching a maximum flux, chemical depletion from the dry upper layers precedes producing progressively lower fluxes to a low value on Day 28. The dramatic effect of chemical depletion with time is better appreciated in viewing the Run IV data, which are also shown in Figures 2-2 and 2-3.

Run II

At the end of Run I, the airflow was stopped and approximately 30 liters of water was added and mixed into the surface soil to produce a uniform mud layer without a significant water layer. The wind speed was again set at 1.16 m/s (2.60 mph), while the soil temperature and %RH values were similar to values in Run I. On Day 6 the surface was still moist, and cracks developed on Day 7. This cracking continued so that by Day 15 (at the end of the experiment) several cracks had appeared (1–2 cm in width and 5-8 cm in depth). Four large cracks 2 cm wide by 8–11 cm in depth existed on the surface soil. The 30 liters of water did not replace the 228 liters lost during Run I. A Regime 0 with ponded water never truly developed. Regime 1 characterized by dry surface patch formation was short lived. The maximum flux occurred at $t_D' = 7$ days, compared to 16 days to achieve t_D' in Run I. Figures 2-2 through 2-4 show data for NAPH, M-NAPH, and PHEN with increasing fluxes during this period as air replaced water in the pores. As time increased beyond $t_D 7$ the flux decreased; a value of 5 ng/m^2-h occurred for NAPH on Day 11.

Replicate samples, n=3 of sorbent tubes, at each sample time were analyzed on Run II. The measured flux range appears in Figures 2-2 through 2-4 as a vertical bar at each time. The peak fluxes were lower than those in Run I by approximately 70%. This occurrence of lower fluxes has no definite explanation at this time. Mixing of the chemical-depleted surface layers may have produced a lower soil concentration and resulted in lower fluxes. Because insufficient water was added, the peak flux value may have been missed during sampling. The maximum may have occurred between Day 5 and Day 9. Nevertheless, this short time-period experiment displayed some of the same patterns observed with Run I. The temperature for Run II ranged from 14 to 23°C. The turnaround time between Runs I and II occurred in a single 24-hour period, 23–24 October 2003. The DM mass in the lysimeter was not returned to its initial water

content. Soils at depth in the lysimeter were well consolidated during the 29 days of Run I and not remixed with the surface layers. The top surface of the DM level in the lysimeter was down 13 cm when Run II started and likely affected the air flow velocity and distribution over the bed. In combination, these factors may have produced the lower fluxes.

Run IV

At the conclusion of Run II, a more aggressive procedure was adopted for mixing-in water in an effort to return the DM mass to its initial water content and uniform consistency. Before Run IV commenced, another sediment re-wetting and re-working activity occurred. A total of 520 liters (0.52 m^3) of water was added in five batches and mixed into the soil. Some ponded water appeared on the surface after the mixing. This run was the longest of the three, lasting 40 days. Seven flux observations were made for NAPH and M-NAPH, and six were made for PHEN over the period. These appear in Figures 2-2 through 2-4, respectively. Although a full restoration of the DM to initial water conditions did not occur, it was sufficiently reconstituted that it displayed the three water regimes observed during Run I.

At the start the surface was wet and the average level was 10 cm below the top of the lysimeter. The DM had been in the lysimeter for 4 months (120 days), and the layers near the bottom of the 45 cm soil column were well consolidated and resisted break-up/re-wetting with the implements used for mixing. More aggressive water-soil mixing equipment may have damaged the bottom liner and resulted in water leakages. Initially, low fluxes were observed from the wet surface. Air temperatures ranged from 3.00 to 12°C and %RH ranged from 50 to 90%. Within 2 days small cracks appeared on the surface. On Day 9 the cracks were 1–2 cm in width and extended 6–8 cm in depth. Air porosity was dominant in this now dry soil, and the same magnitude of maximum chemical fluxes observed in Run I reappeared but occurred much earlier in time. The maximum flux occurred on Day 9 for Run IV whereas it occurred on Day 21 for Run I. Soil drying occurred more rapidly in Run IV because the DM mass contained less water than it did in Run I.

The chemical flux versus time behavior for Run IV displayed an outstanding feature not previously observed. The flux dropped rapidly from the maximum and after approximately 10 days leveled off to what appeared to be near-constant fluxes. These persisted for approximately 15

to 20 days. The final average soil surface level was 11.5 cm below the top of the lysimeter, down 1.5 cm from the start, and displayed some tendency to continue to consolidate. Soil cracks at the finish were 2.5 to 4 cm wide at the surface and extended 18 to 29 cm deep; however, the consolidation likely occurred in the top 10 to 15 cm reworked zone rather than at deeper depths in the soil column.

The above discussion was dominated by the observations on NAPH and M-NAPH. In the opinion of the investigators, the flux measurements for NAPH and M-NAPH were more reliable than those for PHEN, which appear in Figure 2-4. The fluxes for PHEN were roughly 10 times lower than those for M-NAPH and 20 times lower than those observed for NAPH. Due to its low Henry's Law constant, the measured fluxes for PHEN were low as expected even though it is present in the DM at the highest loading; see the sediment loading values in Table 2-1.

Small mass quantities were collected during air sampling, challenging the detection limits of the chemical analysis. Because of these factors the flux data for PHEN were devalued and not used to adjust key model parameters. The final model was applied to PHEN and the data used in comparison because it represents chemicals with vastly lower Henry's Law constants. Figure 2-4 shows the model versus data results for PHEN.

Summary of L/WT PAH emission data

A complex series of chemodynamic processes control and influence the chemical release and the flux of semi-volatile PAHs to air from the IHC DM. Solids consolidation and water expressed from the bed are major factors. The presence of ponded water provided a diffusion barrier on the surface keeping the fluxes low at the start of the volatilization process. During drying as unsaturated soil is produced, air-filled pore spaces encourage increased volatilization rates. These increased emission rates occur because, as noted previously, chemical diffusivities in air are more than 5000 times larger than those in water. The gradual drying process delays the onset of the maximum observed flux. During this period, dry soil patches appear on the surface and grow in number as time progresses. The maximum fluxes were manifested after 7 to 20 days depending on the initial DM water content and the water evaporation rate. Beyond these maximums, the observed chemical fluxes decreased with increasing time. The rate of decrease was nonlinear with increasing time and measured fluxes remained nearly constant for up to 30 days. Additional discussions

concerning the flux versus time behavior patterns appear in the theoretical analysis section.

Chemical volatilization model development

The soil-to-air chemical volatilization modeling is based on observations made within a L/WT designed and operated using conditions similar to those found in the outside environment. Each of the experimental runs displayed chemical flux events classified into three water regimes described below. A conceptual graphical description of the three regimes is shown in Figure 2-5 in order to clearly identify the key aspects of each in the combined water-chemical evaporation-emission process.

Regime 0

After the DM was transferred from the drums into the lysimeter, it was nearly completely submerged under a layer of water. Only two chemical phases, liquid and solid, exist during this regime leaving the bed pore spaces between the solid particles saturated with water. The depth of this water layer was controlled by the topological variations of the DM surface. Regime 0 ends at time t_b when the water layer is effectively absent from the DM surface. Emissions of the contaminants during this time occurred by the chemicals "diffusing" from the water to the bulk air above. Fluxes from this regime were generally very low. Volatile emissions for the ponded scenario are not within the scope of this study. The ponded scenario is important for hydraulic-dredge-generated DM, however, and it will be addressed in another report. Regime 0 is therefore not modeled and is considered further only in relation to Regime I.

Regime I

At the end of Regime I, free standing water is absent, but wet DM remains. As the water consolidation-evaporation process continues, dry patches ~2 cm deep are formed on the surface of the DM. These patches continue to develop and completely cover the surface at time, t_D. Throughout this period, the air-filled pore-space patch areas increase from 0 to 100% as shown in Figure 2-6.

These patch areas appear as the water-filled pore spaces are converted to gas-filled ones. The surface drying time period begins at the end of Regime 0 until the entire surface layer is covered with dry patches, written

as: $t'_D = t_D - t_b$. It is an empirical parameter controlled by the combined consolidation and evaporation processes that drives liquid from the surface layer. The above equation defines the relationship between the run time, t, and the model time, t'.

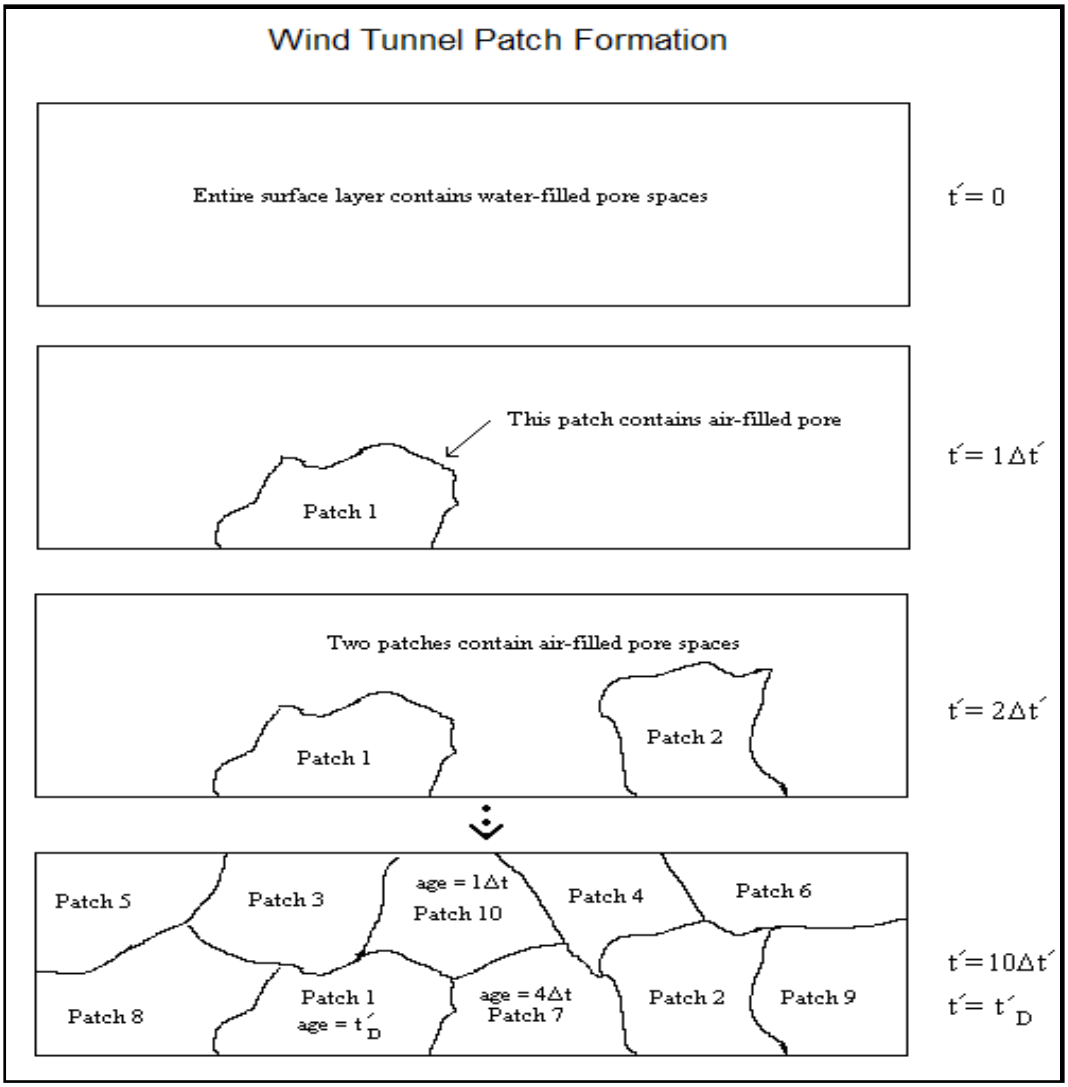

Figure 2-6. Linear patch age distributions on DM surface.

At the end of Regime I, a uniform distribution of equal size dry patches is assumed to exist. Figure 2-6 illustrates the size and age distribution for a hypothetical 10-patch surface. The first patch formed has an age of t'_D. After time interval Δt, the second patch was formed; its age at time t'_D will be t'_D-Δt. The ten patches have ten ages from the longest at t'_D to the shortest at age Δt. Alternatively, rather than 10 patches, the drying time period t'_D may be divided so as to produce n patches. For example, if 1 hour is a convenient value for the time interval Δt, then the number of patches in

the model is n= t'_D /Δt. For n time periods, the last patch formed has age equal to t'_D- (n-1)Δt.

Regime II

Regime II commences after the last dry patch is formed. At the beginning of this regime, air-filled pores are present throughout the entire surface of the DM bed. The chemical contaminant desorbs from the damp solid phase and diffuses through the porous, air-filled soil layers and into the bulk air above. The maximum chemical flux occurs at time t'_D. The evaporation/consolidation process continues, but at a slower rate. As it does, further pore openings widen in the present air-filled pore spaces and more are created at a deeper depth. Surface cracks form and widen as well. Chemical movement from the DM surface layer causes depletion. Deeper residing chemical quantities have a longer and more tortuous diffusion path to traverse to get to the interface, which lowers the flux. This chemical depletion process was demonstrated in the laboratory for porous soils (Valsaraj et al. 1999). The flux continues to decrease with increasing time. The next section contains a mathematical model developed to quantify these described flux behavior patterns.

Flux equation

The basic flux equation used in this study has been shown to provide reasonable estimates of chemical volatilization from natural and agricultural soils to air (Thibodeaux et al. 2002). A Lavoisier's species mass balance was used in developing the equation for the case of a soil column of infinite depth containing an air interface at the top. A total of three phases (soil, air, and water) are assumed to be present. The model also assumes a uniform chemical loading concentration, C_S, throughout the soil column. The following algorithm describes the instantaneous flux for a chemical species through the air-filled pore-spaces, then through the air boundary layer and finally entering the bulk air above:

$$N = \frac{C_f\left(\frac{C_s \cdot H}{K_d} - C_{ai}\right)}{\sqrt{\frac{\pi \cdot t'}{D_{a3} \cdot \left(\varepsilon_1 + \frac{K_d \cdot \rho_b}{H}\right)}} + \frac{1}{K_G}} \tag{2.2}$$

where:

N = flux from DM to air in g/m²s
C_s = chemical loading onto the DM in g/kg (dry solid)
H = dimensionless Henry's Law constant
K_d = soil-to-water chemical partition coefficient in m³ per kg
D_{a3} = effective air-space soil diffusivity in m²/s
ε_1 = air-space porosity of the soil in volume air per volume soil
ρ_b = bulk dry density of the DM in kg/m³
K_G = overall air-side mass transfer coefficient in m/s
t' = time in seconds
C_f = dimensionless flux calibration

The above equation was incorporated in modeling algorithms developed for Regimes I and II. A model simulation using beds of finite thickness and infinite thickness indicates that identical fluxes are achieved for bed thicknesses of 3 cm or greater. Laboratory experiments with three PAHs for 35 days of evaporation showed chemical losses occurred in only the top 2 cm of the sediment (Valsaraj et al. 1999.) As illustrated in Figure 2-5, the chemical flux to air from the surface of the DM consists of two regimes. The two-regime conceptual structure described previously forms the basis upon which to formulate the chemical emission process model.

Chemical flux in Regime I

The time-period t'_D (hr) will be divided into a number, n, of equal time-intervals (Δt) as noted in Equation 2.2 above. Each time interval will have an average flux dependent on the age of the patch. The number of dry patches is also n (numbers) and their rate of appearance (i.e., n/ t'_D) will be assumed to be constant with time. For the first time interval (i=1) one patch exists; its area is $A1/A = \Delta t/t'_D$; where A is the total surface area of the DM emission source and A1 is the surface area of a dry patch. The patch flux is computed as the average of flux at each time $t'=0$ and $t'=1\Delta t$ by applying Equation 2: this flux is denoted as N(1). This newly formed patch has the highest flux since t' is small. The average flux for the entire emission source is denoted by $N_A(1)=N(1) . A_1/A$. For the second time interval, i=2, patch 1 has increased in age; its flux is the average of flux at each time $t'=1\Delta t$ and $t'=2\Delta t$; it is denoted as N(2). It has a slightly smaller flux now since it has aged. Equation 2.2 accounts for the decrease in flux at its new age. The flux of Patch 2 is N(1), which was the previous value for Patch 1. The average flux for the emission source consisting of two patches

is: $N_A(2)=[N(1)+N(2)] \cdot A_1/A$. In general for the i^{th} patches the emission source flux is:

$$N_A^I(i) = \frac{A_1}{A}\sum_{k=1}^{i} N(k) = \frac{\Delta t}{t'_D}\sum_{k=1}^{i} N(k) \tag{2.3}$$

The ratio A_1/A is a constant and $t'=i\Delta t$. This equation relates the flux for each time interval $t'= t'_D$. As total patch size increases so does $N_A(i)$. The general shape of the function reflecting the increasing fluxes of Regime I as expressed by Equation 2.3 is $N_A(t')$ vs. t'. For numerical computation of the flux using Equation 2.3, a time interval, Δt, for patch formation must be selected. Realistic values are 1/2 to 1 hour. Large time intervals such as 8 hours will not realistically capture the time varying flux early in the patch formation process. Time intervals of minutes or less increase the numbers of patches and intervals but may not necessarily increase computational accuracy. Numerical computations performed have shown that the N(i) function remains unchanged in magnitude as Δt takes on values less than 1 hour. At time t'_D, the flux $N(t'_D)$ is at its maximum value. Up until that time, new patches were being formed. As time progresses beyond t'_D, Regime II commences and no new patches are formed.

Chemical flux in Regime II

At the start of Regime II, the surface of the emission source is covered with a mosaic defined as "j patches" of equal size and a linear decreasing age distribution ranging from Δt to t'_D. The oldest patch has age t'_D and the youngest has age Δt. As time progresses, all the patches become older. For example, the emission source flux for the sum of all n patches at $t'=t'_D+\Delta t$ is:

$$N_A^{II}(t'_D + \Delta t) = \frac{A_1}{A}(N(\Delta t) + N(2\Delta t) + \ldots + N(t'_D + \Delta t)) \tag{2.4}$$

Where N is the average of the individual patch fluxes across each age interval. Each patch is Δt older. The oldest patch has age $t'_D+\Delta t$. Since the number of patches remains constant at n and, as time progresses, their individual fluxes decrease, the sum decreases as well. In general the emission source area flux for the time $t'=t'_D+j\Delta t$ starting with j=1 can be expressed as:

$$N_A^{II}(t') = \frac{A_1}{A} \sum_{k=0}^{n-1} N\left[(k+j)\cdot \Delta t\right] \quad (2.5)$$

The functional behavior of this equation is illustrated in Figure 2-5. As with Equation 2.4 the individual patch average fluxes, N, are computed from Equation 2.2. As j increases, so do t' and the N_A function of Equation 2.5. It displays a decreasing flux with increasing time since the flux from individual patches decreases with increasing age (i.e., t' becomes large in Equation 2.2). Figure 2-6 shows the patch times corresponding to the fluxes N_A^I and N_A^{II}.

Model applications of wind tunnel data

The structure of the emission model and the associated flux algorithms were presented above. A two-regime emission structure defined by t'D (the surface drying time) along with Equations 2.3 and 2.5 constitute the quantitative process model. Equation 2.2 is embedded and used to compute the chemical fluxes needed at the appropriate times and patch ages. The model was fitted to the measured fluxes obtained in Runs I, II, and IV. The model calculated and the measured fluxes appear in Figures 2-2, 2-3, and 2-4 for NAPH, M-NAPH, and PHEN, respectively.

Several transport, thermodynamic, and soil parameters are needed for Equation 2.2. These include the chemical molecular diffusivities in air (D_{a3}), Henry's Law constants (H) and the soil-to-water partition coefficients (K_d). These numerical values appear in Table 2-2 in addition to the chemical loading and the air-filled soil porosities. Direct measurements were available for the IHC DM for all the parameters except the diffusivities, which were estimated based on Fuller, Schettler, and Gidding's algorithm (Fuller et al. 1966). The following procedure was used in fitting the two-regime soil-drying model to the flux measurements.

The calibration process began with a visual inspection of the graphical representations of the measured fluxes versus model-estimated fluxes for each chemical. These fluxes appear in Figures 2-2, 2-3, and 2-4. First the ponded flux time-period, t_b, of Regime 0 was estimated for each run, and the time positions, t, were readjusted by subtracting t_b from the run time so that Regime I begins at the origin (i.e., t'=0). These adjustments are reflected in the data points re-plotted with the new times as shown in Figures 2-2, 2-3, and 2-4. The t_b's appear in Table 2-3.

Again, based on a visual inspection, the drying time, t'_D, was determined. The conceptual schematic shown in Figure 2-5 is used as a guide; based on the data in Figures 2-2 and 2-3 for each run the t'_D values are chosen. It is somewhat a "judgment call" to establish at what time the maximum flux occurs faced with sparse data sets such as those appearing in Figures 2-2 and 2-3. This t'_D is a key adjustable parameter in the two-regime drying model. Nevertheless, reasonable values can be obtained and these appear in Table 2-3 for each run. The same values of t_b and t'_D were used for each chemical.

In order for the model to mimic the measured flux versus time data for each chemical-unique value of K_G, the air-side mass-transfer coefficient (MTC) was needed. This is a parameter that controls the rate of the flux rise with increasing time. Its maximum value also influences its rate of flux decrease for times beyond t'_D. The numerical values of K_G appear in Table 2-3. A "flux calibration factor," C_f, was needed to scale the absolute magnitude of the model-computed fluxes. Positive C_f values were needed to adjust the computed fluxes to the measured ones. These C_f values appear in Table 2-3. Figures 2-2, 2-3, and 2-4 contain the Regime I and II measured fluxes and the model predicted fluxes based on the above calibration procedure for NAPH, M-NAPH, and PHEN, respectively.

Table 2-2. Transport and thermodynamic parameters of IHC DM at 25°C.

Parameter	Units	NAPH	m-NAPH	PHEN
Molecular diffusivities, D_{a3}	cm^2/h	252.8	234.1	215.1
Molecular weight	g/mol	128	156	178
Henry's Law constant, H_C	-	0.0198	0.0178	0.0021
Solid-to-Water partition Coefficient, K_d	L/kg	260	1440	7017

Table 2-3. Emission model calibration parameters.

Parameter	Units	NAPH	m-NAPH	PHEN
t_b, ponded flux time interval (Run I/II/IV)	hours	3 / 2 / 5	3 / 2 / 5	3 / 2 / 5
t_D, drying time (Run I/II/IV)	hours	425 / 125 / 100	425 / 125 / 100	425 / 125 / 100
K_G, air-side mass transfer coefficient	cm/h	672	640	604
C_f, flux calibration factor (Run I/II/IV)	-	17 / 4 / 10	50/ 15 / 27	12 / 4 / 7

Discussion of results

The traditional approach to the subject of drying beds of solids employs the concept of the constant-rate period and the falling rate period (Perry 1950). Moisture (i.e., water) is the "drying" chemical of primary focus in this traditional field where uniform granular solids particles typically constitute the beds. Water is present in DM in copious amounts and likely undergoes both a constant rate and a falling rate-drying period. The data shown in Figures 2-2, 2-3, and 2-4 clearly demonstrate that this traditional approach does not apply to NAPH, M-NAPH and PHEN evaporation (i.e., drying) since there is no constant rate period. Nevertheless, the presence and behavior of water in the DM is a significant process factor. The published literature on traditional, nonconsolidating solids drying by water evaporation is voluminous. Because the combined processes of water consolidation, ponding, runoff, and evaporation are exceedingly complex in the case of DM drying, an empirical approach containing some theoretical aspects of the traditional drying process was adopted. This approach was used for Regime I, as developed previously. The essence of the approach is the idea that "dry surface" patch areas of air-filled soil pore spaces is assumed to appear linear with time and to occupy the entire emission surface at time t'_D. A linear function is consistent with the concept of moisture evaporating from the surface of the bed at a constant rate. Once the surface becomes dry, the water evaporation rate falls. It is assumed that the constant water evaporation rate period ends at the drying time, t'_D. A chemical flux to air process was superimposed onto the constant rate period and is consistent with the dry patch formation process. This interpretation allowed the development of a simple computation procedure for the chemical emission flux behavior during Regime I. The ability of the model to mimic the observed increasing chemical fluxes (i.e., zero to maximum) is apparent in Figures 2-2 and 2-3.

Since the water behavior controls t'_D, theoretically it should be independent of contaminant chemistry. All volatile substances should display the same observed t_D since it reflects a water lost event. This appears to be so for the NAPH, M-NAPH, and PHEN flux data; the t'_D values appear in Table 2-3. However, t'_D, the drying time, is different for each experiment. Rewetting the DM solids to original water content after Run I was unsuccessful. Only a fraction of the original water was reintroduced and, as a consequence, the drying times for Runs II and IV were shorter. The t'_D values of 125 and 100 hours were needed for Runs II and IV compared to 425 hours for Run I. Nevertheless, based on this limited data set, it

appears that the semi-theoretical dry patches model is consistent with traditional solids-water drying concepts.

The highest chemical fluxes occur from the individual patches when they are first formed. Setting t=0 in Equation 2-2 yields the highest flux, which occurs when the airside MTC, K_G, controls the process. High fluxes are seen as each new patch is formed. The numerical value of K_G therefore plays a dominant role in the magnitude and shape of the rising fluxes characteristic of Regime I. The chemical flux from a patch quickly diminishes as time increases according to the $t^{-1/2}$ relationship in Equation 2.2. Therefore, the numerical value of K_G is an important adjustable parameter in Equation 2.2 for mimicking the flux behavior in Regime I. The K_G values of NAPH, M-NAPH, and PHEN appear in Table 2-3 and are based on a visual fitting of the model fluxes to the data.

Theoretically, for a constant wind speed, the effective K_G in the wind tunnel should be constant and therefore independent of experimental run. This is the case, apparently, because the wind speed was kept constant for all three runs and the same numerical values of K_G resulted. The K_G values are chemical dependent and a function of molecular diffusivity in air D_a. The calibrated K_G values were correlated with D^n where $n \cong 0.64$. This result is consistent with boundary layer theory where $K_G \cong D^{0.67}$. In addition, numerical values of K_G's for organic chemicals similar in size have been reported in the range 1 to 10 m/h and depend on wind speed (Thibodeaux and Scott 1985). Therefore the 6 to 7 m/h range for the effective K_G's observed in the L/WT tunnel are very consistent with this range of values.

The two adjustable parameters needed for this two-regime emission model, t'_D and K_G, have a good theoretical basis and are well constrained as to their numerical magnitudes. They cannot be arbitrarily adjusted in order to force model versus data congruence. A flux calibration factor, C_f, was created as a multiplier to Equation 2.2 because it gave consistently low flux estimates. Nine values of C_f were needed; these appear in Table 2-3 and range from a +5 to +50. The C_f's for M-NAPH are larger than those for NAPH; the averages being 31 and 10, respectively. PHEN displayed the lowest C_f values with an average of 8. Such model versus data flux deviations have been observed in laboratory experiments with soils that behave very unlike DM (Thibodeaux et al. 2002). In the case of soils, however, the model predictions were typically higher numerically than the

measurements. Natural soils typically do not undergo the particle consolidation process like DM. At this time the causes of the direction and magnitudes of C_f are unknown. The following provides a plausible reason for the C_f magnitudes being larger than unity.

Bed consolidation with water expressed in the upward direction followed by evaporation may have contributed in a significant way to the measured fluxes being larger than the model predictions. A single batch of DM was used in the three separate experiments. The mud level decreased 5.1 cm (2 in.) at the end of Run I. Each inch is equivalent to 140 liters of water (H_2O). Thirty liters of H_2O was added and the bed surface remixed prior to Run II. Compared to those measured in Run I, the maximum fluxes of both chemicals were lower in Run II by a factor of three. Approximately 520 liters of water were added after Run II and the bed remixed prior to Run IV. The maximum fluxes returned to the levels of those observed in Run I. It appears that when massive quantities of water were being mobilized from the bed, similar to what happened in Runs I and IV, high chemical fluxes were observed. Much lower fluxes occurred in Run II; where little water was present to mobilize through the combined consolidation/evaporation process. No water was lost downward or collected as leachate. The upward moving water may be transporting fine particles to the surface of the bed where they are deposited.

The solids-water mixing and homogenization process that occurred in the lysimeter prior to each run may have contributed to the placement of a thin soil layer containing elevated chemical concentrations on the DM surface. The solids-mixing process produces a supernatant rich in fine particles since the sand and silt fractions settle rapidly. In effect, this combined mixing-settling event is a crude fractionation process that produces a “raffinate” phase consisting primarily of large particles and some water. This phase is overlaid by a “supernatant” phase consisting of fine particles in suspension. As the water evaporates in Regime 0, these fines are deposited on the surface. These fines, which include the clays and organic colloids, typically contain higher chemical loadings (i.e., C_S in mg/kg) per unit mass than the average. Pilot-scale and laboratory-derived evidence supports the surface layer enrichment process.

A pilot-scale demonstration of a Saginaw River, MI sediment washing treatment was performed using individual equipment modules roughly the size of the L/WT apparatus (EPA 1994). DM daily feed quantities of 8 to

20 m^3 were "washed" through a series of devices consisting of hydrocyclone separators, dense media separators, attrition scrubbers, sand recovery and dewatering screens, and final clarifiers. Eight particle-size classes were used to assess the effectiveness of the washing. The largest was 430 μm sand and the smallest was 30 μm fines. Since contaminant concentration/volume reduction is simply an artifact of the partitioning for the contaminants among these grain sizes, an extensive effort was made to monitor these as they moved through the soil washing system. Approximately 19% of the feed was in the < 30 μm range. The total organic carbon (TOC) enrichment factor (i.e., concentration in discharge stream to the feed concentration) was nearly 20 for the particulate organic fraction (size > 109 μm). PCBs with mean feed concentration of 1.2 mg/Kg as total Arochlors displayed a mean enrichment factor of 3.8 with a maximum of 9.4 in the clarifier solids. Separate laboratory bench-scale test enrichment factors of 6.2 were observed for the PCBs in the Saginaw sediments. In another laboratory study, PAHs in New Jersey/New York harbor sediments were separated into size fractions and further separated into low and high density fractions in an effort to better understand the factors controlling sequestrations and desorption in the field (Rochne et al. 2002). The PAH concentrations were found to be greatly increased in the low-density fraction and not predictable by equilibrium partitioning theory. For the Piles Creek sediment, the low density-to-bulk concentration total PAH ratio was 19, while that for Newton Creek was 3.2. In addition, it was found that the PAH partition coefficients (i.e., K_{oc}) were nearly 10 times larger for the low-density fraction.

The above studies illustrate that elevated chemical concentrations appear in the fines and/or low-density particle fractions. Generally the enrichment factors ranged from 3 to 20. The evaporation of a standing water layer above a DM solid bed will deposit fines particles with elevated chemical concentrations on the bed surface. Chemical volatilization may be driven by the enriched interface concentration producing higher fluxes than represented by the average concentration in the DM. Run II had too little water moving upward, so the surface received little or no concentration enhancement; therefore, the maximum fluxes for NAPH and M-NAPH were three times lower compared to Runs I and IV. Since the average concentration was used in the model rate equation to compute the fluxes, the predicted results should be lower, and they were. The flux calibration factors for Run II were correspondingly lower than those required for Runs I and IV. It appears that the upward particle-bound

chemical mobilization process that results from bed consolidation and evaporation may contribute to the high measured fluxes. The chemical emission algorithm, Equation 2.2, used in the predictive model originates from theories and laboratory testing of chemical transport in surface soils that do not consolidate; therefore, water is not expressed upward. Although this is a logical explanation for the model versus data mismatch and the need for the C_f corrections, other factors or processes may be involved.

Model field application

Freshly applied DM from mechanical dredging will likely behave differently from that used in the L/WT. If the DM retains the low in-situ water content of the sediment bed when deposited upon the CDF surface, only limited consolidation will occur. The small quantities of expressed water will run off to a designated ponded basin prepared for its collection. Evaporation of water from the surface of the exposed DM solids will commence immediately, and dry surface patches will likely appear fairly rapidly. In the L/WT the DM was homogenized and water mixed in to produce uniform chemical concentrations, which was necessary for making consistent measurements needed for flux model comparison. The L/WT was not designed for runoff applications, so water had to move upward then evaporate to depart the DM mass. This process kept the DM surface supplied with moisture and prevented it from drying quickly. Two model parameters, t'_D and C_f, must be addressed in translating the L/WT results to the field. In regard to translating the L/WT experimental results to the field, mechanical and hydraulic delivery of DM to the CDF must be considered separately.

Mechanical DM delivery

For mechanical delivery, the DM is placed into the CDF at near in-situ sediment water content. Because the L/WT operation better simulated the aspects of hydraulic DM delivery that results in a ponded situation, the drying times were very long (4 to 18 days). In this regard the L/WT experiments did not simulate the field drying solids conditions representative of mechanical DM delivery. This section contains discussion for translating the results to a drying solid-bed CDF operation. Drying times in the field will depend primarily upon the local wind speed, temperature, and the air's relative humidity. Except for extended rain periods, the field drying times will be rapid and are better represented by the low-end of the L/WT

values. Times much less than 4 days and in the 8 to 24-hour range may be reasonable under excellent soil-drying conditions. The value selected for t'_D is left to the judgment of the user. The tipping and spreading of DM "lifts" deposited from trucks, for example, produces a complex geometric footprint surface containing a range of drying times. In reality t'_D for a particular tip may not be attainable. A default value of 24 hours takes into account the dominance of the solar factor in drying.

Without the occurrence of Regime 0 in the field, the use of a model flux enhancement factors, C_f, greater than unity are not necessary. In the field, rapid water runoff will allow little opportunity for a continuous layer to develop on the DM surface. Without its presence and subsequent evaporation, no surface layer deposit with enhanced chemical concentrations can be formed. For a CDF receiving solid DM such as typically derived from mechanical dredging operations, a C_f =1 is recommended.

Hydraulic DM delivery

Normally during hydraulic dredging or mechanical dredging followed by hydraulic slurry, which is the current IHC plan, the CDF contains ponded water and appropriate models are available for estimating these emissions. However, exposed surfaces containing solids do occur during the life cycle of a ponded CDF. Deltas are formed in the vicinity of the pipeline slurry entering the CDF. Also a drying solids bed is formed during the latter days of filling when the ponded water is drained away prior to closure. The use of the drying solids emission model is appropriate in both these cases.

The two primary parameters mentioned as being key parameters are t_D and C_f. During the ponded water period of the CDF operation, time is sufficient for the bed to undergo significant consolidation. This process occurred on the L/WT during the 2-month experimental time period and frustrated efforts to re-water the DM between experimental runs. It is therefore reasonable to assume that the resulting exposed drying solids bed is nearly identical to that of mechanical delivery. Therefore, the drying time, t_D, comments and recommendation for that case apply as well. However, the C_f for the hydraulic DM delivery is likely to be much greater than unity. The C_f values observed in the L/WT experiments for the three PAHs tested ranged between 4 and 50. Those values for experiment Run I were 12, 17, and 50 where slurry preparation likely best represented hydraulic pipeline slurrying in the field and are recommended.

The topics discussed above should provide the user with some type of approach to deal with modeling long-term emissions. Further guidance in applying the model to the field appears in Thibodeaux et al. (2002).

References

Fuller, E. N., P. D. Schettler, and J. C. Giddings. 1966. Industrial Engineering Chemistry 58(5): 18.

Millington, R. J., and J. M. Quirk. 1961. Permeability of porous solids. *Trans. Faraday Soc.* 57: 1200-1207.

Perry, J. H. (ed.). 1950. *Chemical Engineers' Handbook*. New York, NY: McGraw-Hill Book Co. 800-808.

Price, R. A., J. G. Skogerboe, and C. R. Lee. 1996. A rainfall simulator/lysimeter system for predicting surface-runoff water quality. *Water Quality* 439-441.

Ravikrishna, R., K. T. Valsaraj, D. D. Reible, L. J. Thibodeaux, C. B. Price, J. M. Brannon, T. E. Myers, and S. Yost. 2001. Air emission flux from contaminated dredged materials stored in a pilot-scale confined disposal facility. *Journal of Air and Waste Management Association* 51: 361-373.

Rochne, K. J., M. Shor, L. Y. Young, G. L. Taghon, and D. S. Kasson. 2002. *Environmental Science and Technology* 30(12): 2636-2644.

Ruscheweyh, H. 1984. A mixing system for gas flow. *Journal of Wind Engineering and Industrial Aerodynamics* 16: 189-199.

Saichek, R. 2003. The collection of water and sediment samples from Indiana harbor and canal. CELRC-TS-HE, Chicago, IL: USACE Chicago District and Vicksburg, MS: U.S. Army Engineer Research and Development Center.

Thibodeaux, L. J. 1989. Theoretical models for evaluation of volatile emissions to air during dredged material disposal with applications to New Bedford Harbor, Massachusetts. Miscellaneous Paper EL-89-3, Vicksburg, MS: U.S. Army Engineer Research and Development Center.

Thibodeaux, L. J., and H. D. Scott. 1985. Air/soil exchange coefficients. *Environmental Exposure from Chemicals*. W. B. Neely and G. E. Blau (eds.) Vol. 1, Chapter 4, Boca Raton, FL: CRC Press.

Thibodeaux, L. J., R. Ravikrishna, and K. T. Valsaraj. 2002. Volatilization rates from dredged material and soils—A literature review. Final Report. Chicago, IL: USACE Chicago District and Vicksburg, MS: U.S. Army Engineer Research and Development Center.

U.S. Environmental Protection Agency. 1994. Pilot-scale demonstration of sediment washing for the treatment of Saginaw river sediments. EPA 905-R94-09. July 1994.

Valsaraj, K. T., R. Ravikrishna, B. Choy, D. D. Reible, L. J. Thibodeaux, C. B. Price, S. Yost, J. M. Brannon, and T. E. Myers. 1999. Air emissions from exposed contaminated sediments and dredged material. *Environmental Science and Technology* 33, 142-149.

Appendix 1A: Experimental Data

Table A-1. Emission flux data.

Time (days)	NAPH Flux (ng/cm²-hr)	m-NAPH Flux (ng/cm²-hr)	PHEN (ng/cm²-hr)
Run I			
0.1	18.65	0.00	0.00
2.5	0.00	0.00	0.00
6.0	16.16	7.46	0.00
10.9	34.68	16.32	2.04
18.9	42.54	22.15	1.46
24.4	24.31	16.98	1.33
Run II			
1.0	9.31	6.74	0.7925
1.0	10.10	7.53	0.9906
1.0	9.91	5.94	0.7925
3.5	11.09	7.13	0.6604
3.5	9.91	6.60	0.7925
3.5	12.15	7.13	0.6604
7.0	15.35	9.11	0.9906
7.0	13.77	7.92	0.8915
7.0	13.67	7.83	0.7925
11.0	3.92	2.21	0.2941
11.0	3.77	2.16	0.2941
11.0	4.75	2.70	0.3431
Run IV			
1.0	6.74	3.76	0.00
3.5	5.02	1.98	0.00
7.0	43.99	20.01	1.68
11.0	14.86	7.33	0.99
16.0	12.68	4.95	0.59
22.5	5.04	2.43	0.23
29.5	8.49	2.60	0.28
36.5	8.55	4.42	0.45

Table A-2. Physical conditions during experimental runs.

	Wind Speed Range (miles/hr)	Air Temperature (°C)	Air Relative Humidity Range (%)
Run I	2.12 – 3.77	14.7 – 25.1	60.8 – 91.4
Run II	2.12 – 3.77	13.6 – 23.3	60 – 89.4
Run IV	2.12 – 3.77	1.4 – 17.6	49 – 89.6

3 Chemical Volatilization Models for Dredging Operations with Application to IHC-Type Site Conditions

Introduction

Indiana Harbor and Canal

The Indiana Harbor and Canal (IHC) are in East Chicago, Lake County, IN. Plans are ongoing for U.S. Army Corps of Engineers (USACE) to dredge the sediment as an aid to navigation. Figure 3-1 shows the IHC site in relation to the East Chicago regional area. Figure 3-2 shows the proposed layout of confined disposal facilities (CDF) cells. The material to be dredged from the IHC and disposed into the CDF contains contaminants such as polyaromatic hydrocarbons (PAHs), polychlorinated biphenyls (PCBs), oil and grease, chromium, and lead. USACE Chicago District is developing CDF operational parameters, as well as estimating emissions from the CDF to satisfy air registration requirements, based in part on the analysis and results of the volatile emissions predictions using the models developed in the study and presented in this report. The concentrations reported in Table 3-1 were those of composite samples obtained for emission experimental studies in the laboratory and do not adequately represent the high degree of concentration found at the IHC.

Project Scope

This chapter, a product of work requested by the USACE Chicago District, provides predictive chemodynamic models for estimating air emissions from selected activities associated with dredging contaminated sediments. Although developed specifically for the IHC, the models are generally applicable for dredging and associated operations with the dredged material (DM) in CDF. The overall effort was an updating of and extension of theoretical model concepts first developed and made available by USACE (Thibodeaux 1989). As part of this work, several computer programs were produced and tested with IHC-type site conditions. Following is a brief review of chapter contents and air emission models.

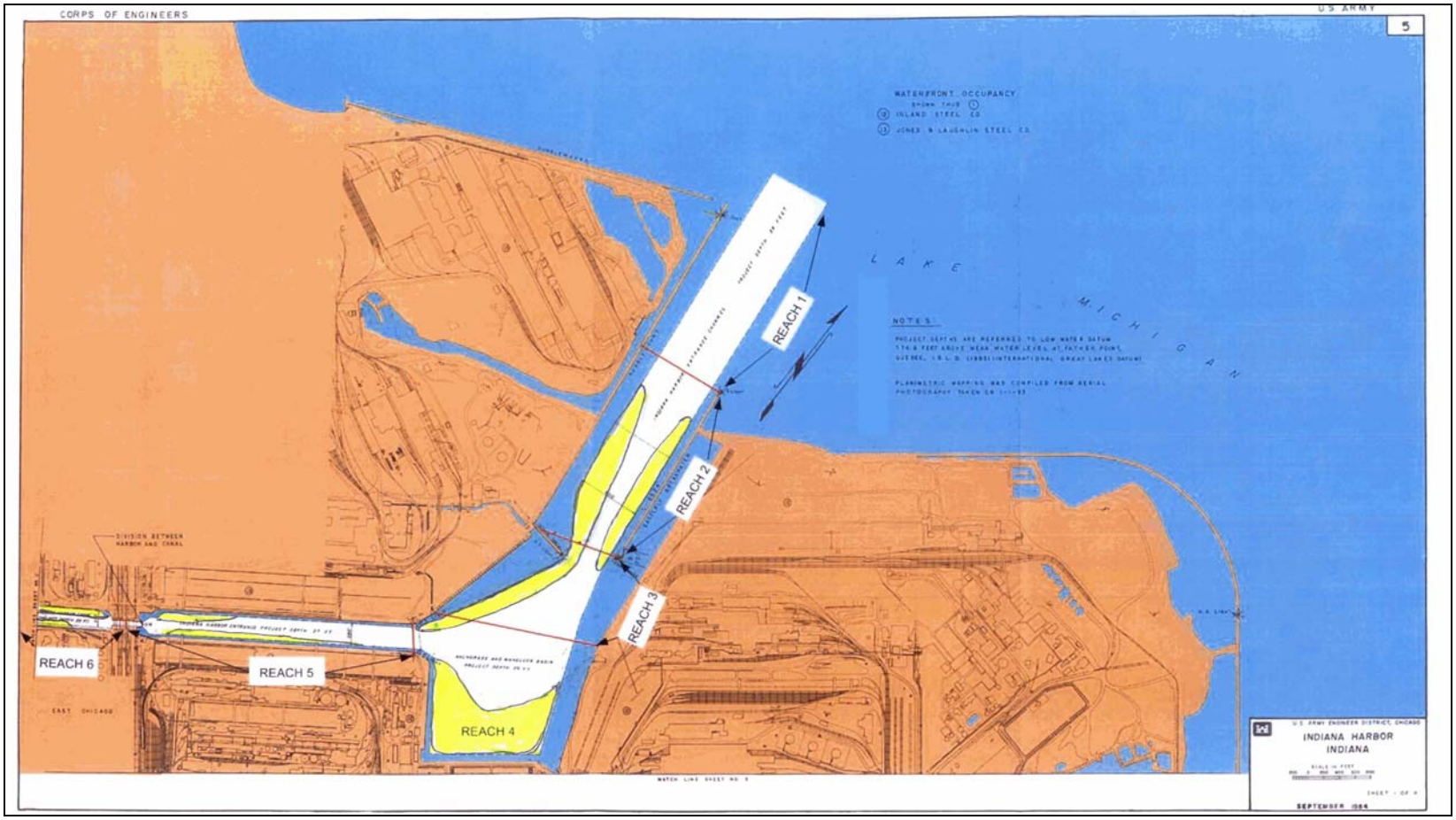

Figure 3-1. Indiana Harbor and Canal – channel reaches.

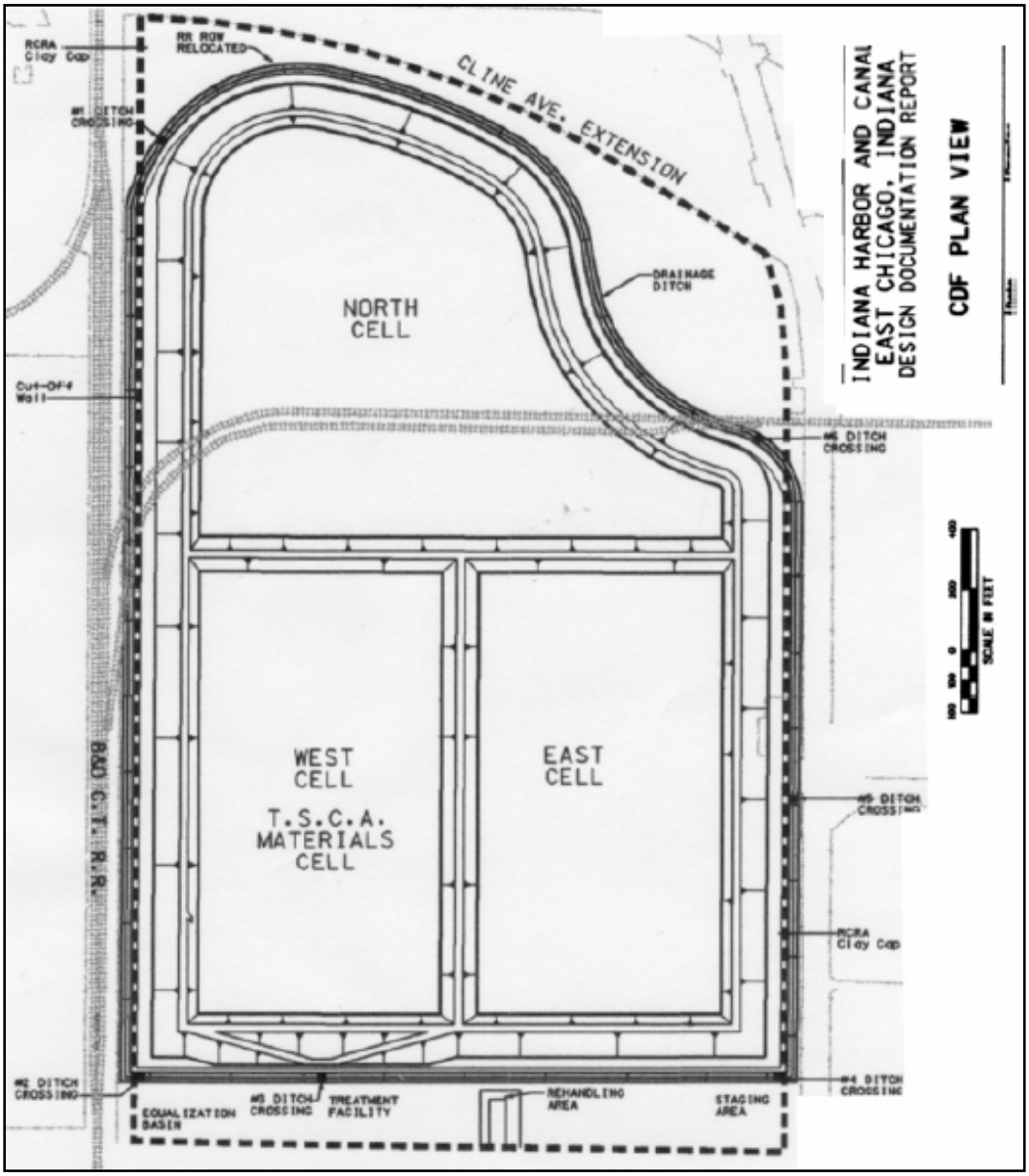

Figure 3-2. IHC CDF design and layout.

Table 3-1. IHC sediment analysis.

Compound	Concentration μg/kg
Naphthalene	2650
Phenanthrene	6930
2-Methyl Naphthalene	1760
PCB-1248	5103
PCB-1260	500
Chromium	290
Copper	213
Lead	437
Zinc	2440
Manganese	1560
Total Organic Carbon	96000
Oil and Grease	3.29×10^7

The next section of this chapter contains an overview of the general volatilization modeling approaches used. The general nature of the dredging and disposal site requires both soils type chemical source models and water source models. Steady-state chemical flux equations and phase equilibrium models were used to quantify the chemodynamic processes. Generic forms of these equations are presented.

The third section focuses on dredging operations in various water-bodies and the factors associated with the sediment extraction process that produces chemicals in water that are subsequently released to the air. Several cases involving dredging in flowing and nonflowing water-bodies are modeled. In the absence of chemical transport coefficients unique to dredge-generated water turbulence, alternative means of estimating numerical values were proposed. Example model applications that included emission flux calculations were performed followed by a discussion of the numerical results.

The fourth section of this chapter is concerned with the development of an emission model for exposed DM placed in the “dry” CDF. This task involved an extensive experimental work component. The DM holding section of a large laboratory wind tunnel, capable of simulating key field-scale aspects of the emission process, was filled with IHC site sediments and operated for several months at U.S. Army Engineer Research and Development Center (ERDC), Vicksburg, MS. Based on chemical flux

measurements to air for several PAHs an appropriate theory-based predictive model was developed. Due to the unique nature of this work product, a separate document was produced and appears as Chapter 2.

The fifth section is concerned with model development for DM placed in a ponded CDF (PCDF). The emission model combined the dredging unit and the settling pond. The connection of the two units with fluid streams allows the needed DM slurry-water to be obtained from the water body and/or from the clarified water pond (i.e., recycle water). Example model applications with and without recycle were performed and flux to air emissions numerical results obtained and discussed.

The final section of the chapter summarizes key aspects of the content and includes conclusion and recommendations.

General volatilization model theory and approach

General model development

In evaluating the fate of chemicals in the environment, fundamental concepts are needed to describe the behavior of these interactions. The mobility of a species is quantified using a mass balance around a system of chemical gradients, sources, and sinks, which quantify the variations and form the basis for chemical transport through the media and across interfacial boundaries by various mechanisms. The transfer involves the movement of chemical in the environment between the atmosphere, hydrosphere, and geosphere. The geosphere represents the primary focus of these models since they include both water bodies and soil-like surfaces.

Soil models

A literature review of chemical volatilization from sediment or dredge material was performed to determine current theory and transport models available for application to dredging (Thibodeaux et al. 2002). Most of the applications for this theory are designed for use in the modeling of volatilization of chemicals from dry soil. Early work on chemical volatilization focuses on the emissions of pesticides to the atmosphere from relatively dry soil on farmlands and upon industrial chemicals from “land farms” (i.e., waste applications on soil surfaces). This research began to unfold as scientists discovered that, in the absence of appreciable mass transfer due to water movement, diffusion processes in the soil account for the

movement of pesticides to the soil surface to replace that lost by volatilization (Mayer et al. 1974). The research analyzed several models against volatilization data to find that indeed, under negligible wind speeds, the surface was still renewed through diffusion in the pore spaces. This matched closely the experimental values compared to the models assuming that the concentration goes to zero under these conditions. This showed the process to be diffusion-controlled instead of through interfacial resistance.

Most of the models of this time were directed towards specific conditions instead of general transport processes. Further work was performed by scientist from University of California Riverside and U.S. Department of Agriculture (USDA) showing the critical process of gas phase molecular diffusion on the process of surface concentration renewal. The research was intended to supply a general volatilization model for estimating pesticide emissions from soil (Jury et al. 1980, 1983, 1984a, 1984b, and 1984c). A more complex model by Cohen et al. (1988) showed that the volatilization model could assume a linear isothermal diffusion, neglecting natural convection within the soil to adequately describe the chemical flux for a long duration.

Assuming equivalent levels of biological activity, the soil models cited above are not representative of modeling volatilization from DM because of the difference in pore-space composition and compaction. For natural soil models, the pore spaces typically contain some air and the soils are completely consolidated. In consolidated soils, the solids have compacted themselves through gravity settling processes to the point of constant pore-space volume. The exposed DM process is relatively dynamic with time in that the pore spaces change from being completely water-filled to being partially air-filled through evaporation and bed consolidation occurring throughout the process. The ongoing process acts to provide a driving force for upward water movement in a CDF. Downward movement is generally retarded because the floor is effectively nonpermeable.

A recent literature review compiled the published chemical flux data from laboratory and field experiments and evaluated a simple algebraic flux equation to model volatilization from DM and soils (Thibodeaux et al. 2002). The purpose of this model was to define the process of volatilization by using a simple equation based on a Lavoisier mass balance around the soil column assuming semi-infinite boundary conditions. The equation

provides estimates based on describing the chemical pathway of desorption from solid particles into the water film, desorption from the water solution to pore air, gas phase molecular diffusion to the surface, depletion of surface concentration over time, resistance of solid/air interface, and transport to the bulk air above.

Modeling drying DM chemical evaporation is required for estimating emissions from most dredging operations since it is present regardless of the method of transporting the sediment to the CDF. When the sediment is truck-delivered to the CDF after mechanical dredging, the material arrives at the CDF as mud. In the event of hydraulically transporting the DM to the CDF, the water layer above will eventually be removed producing exposed mud. In all cases of dredging, the emissions from the drying DM will be of high importance due to the direct contact of mud with air. This drying mud process may provide significant emissions to air with an impact on the local environment.

Water models

The following models deal with the chemical flux from a liquid (i.e., water) to a gas (i.e., air). To determine emissions from a dredging operable unit (DOU) or ponded CDF, chemical mass balances are conducted to provide aqueous concentrations in the water column for estimating evaporation to the air. For both of these cases, the balance is performed under steady-state conditions. In representing these phenomena, the concepts of developing theory surrounding both a driving force and its transport resistance are needed. Chemicals placed into one of these mediums will transfer a portion of the initial mass into the adjoining phase in the drive to achieve equilibrium. Each phase will contain a chemical flux, shown in Equation 3.1. The flux from water to air is:

$$n_A = {}^1k'_{A2} \cdot \left(\rho_{A2} - \rho_{A2i}\right) = {}^2k'_{A1} \cdot \left(\rho_{A1i} - \rho_{A1}\right) \tag{3.1}$$

See the glossary of symbols (Appendix 3A) for the specific definitions of the individual mass-transfer coefficients (MTCs) and concentrations in water and air.

The chemical transport from water to air is dependent on the resistance to mass transfer across the interface and an overall chemical concentration gradient, $\Delta\rho_{A2}$. It is the concentration gradient that acts as the driving

force for the movement of chemical from the water to the air. For a given chemical concentration in air, there is an associated equilibrium concentration in the water, ρ^*_{A2}, related by H_x, the dimensionless Henry's Law constant. Mass transferrence across the air-water interface occurs when the equilibrium concentration within the air is less than the water concentration. The overall evaporative flux of chemical A across the interface is:

$$n_A = {}^1K'_{A2} \cdot \left(\rho_{A2} - \rho^*_{A2} \right) \tag{3.2}$$

While the concentration gradient drives the system to equilibrium, the mass transfer resistance controls the rate of transfer. The overall MTC of chemical from water to air, ${}^1K'_{A2}$, is comprised of individual MTCs on both sides of the interface as dictated by the two-resistance theory shown in Equation 3.3.

$$1 \Big/ {}^1K'_{A2} = 1 \Big/ \left({}^2k'_{A1} \cdot H_x \right) + 1 \Big/ {}^1k'_{A2} \tag{3.3}$$

Both the air-side (${}^2k'_{A1}$) and water-side (${}^1k'_{A2}$) MTCs will control the rate at which chemical emissions cross through the interface into the bulk air phase. This theory has been well established in defining chemical transport resistance between two adjoining phases with interfacial equilibrium.

Phase equilibrium process

A process critical to modeling chemical volatilization is the potential for a chemical to distribute between two phases. This potential will determine the degree to which a chemical may be released through the pathways for emissions. In the DOU and CDF, the Local Equilibrium Assumption (LEA) is assumed to apply between water and solids in the pore spaces and for the suspended solid particles in the water column. A true equilibrium is likely never established, so pseudo-equilibrium is assumed to characterize the distribution of chemical between the aqueous phase and solid particle. This type of LEA can provide reasonable estimates for adjoining phase chemical concentrations (DiGiano et al. 1993).

It has been established that the hydrophobic partitioning of chemicals in phase equilibrium with solid particles is dominated by the fraction of particulate organic matter. The partitioning between solid-water, K_{A32}, is linearly dependent on the soil organic carbon-water partitioning, K_{oc}, by the following expression:

$$K_{A32} = f_{oc} \cdot K_{oc} \tag{3.4}$$

where f_{oc} = fraction organic carbon. This partition coefficient is used in all of the following models for determination of the water equilibrium concentration in pore space and in the water column from suspended solids. Also very important to modeling these processes are the equilibrium estimations for solid-air, K_{A31}, and the Henry's Law constant for air-water, H_x. The estimation of K_{A31} for wet sediments/soils can be estimated using the following relationship:

$$K_{A31} = K_{A32} / H_x \tag{3.5}$$

where K_{A31} is defined as the ratio of concentration in air to the chemical loading on the solid particles. The expression above is used in the estimation of equilibrium concentrations in the sediment modeling emissions from exposed DM. It establishes the driving force concentration gradient along with the background air concentration required in the flux equation. The sorption processes occurring between solids and air/water phases has received some study over recent years as to the exact nature of equilibrium. The work has been focused on providing better descriptions of the equilibrium interactions between air and the solid phase to include chemical properties, sediment moisture level, and temperature (deSeze et al. 2000).

Dredging and CDF models

The chemical emissions from dredging operations are assumed to be comprised of two primary source "locales." These include the DOU and the final disposal CDF site. Both generate emissions to the air that possibly affect concentration levels in the local and remote air environments. This project is an up-date of an earlier suite of models proposed for these two locales (Thibodeaux 1989). In this development, however, two types of CDF area sources, exposed DM and ponded, are treated as two separate models. The following section will highlight the development of the models for three area source locales: DOU, exposed DM CDF, and a ponded CDF.

Dredge operations emission models

The DOU defined

The chemical release from the dredging site is a function of factors such as the chemical loading on the DM solids, the type of dredge, the rate of solid extraction, the nature of the water-body, etc. The operation begins with a design plan to determine the area of dredging. This area of the water body is known as the DOU. Most remediation actions occur in two water-body types: flowing rivers or streams and nonflowing waters such as embayments, lakes, and harbors. This classification results in three different scenarios as shown in Figure 3-3.

A common case of dredging involves enclosing a section of a flowing stream with a silt curtain or other semi-permeable membrane device as shown in Figure 3-3A. The dredge location is shown in the center of a forced convection area. The surrounding curtain significantly inhibits suspended solids from exiting the DOU. Depending on the efficiency of the curtain, the downstream flow from the DOU will form a natural convection area in which volatilization continues to occur due to quantities of chemical remaining in solution. The DOU containment area will contain higher concentrations due to the close proximity of the dredge and partitioning from resuspended sediment.

The DOU illustrated in Figure 3-3B is similar to the previous without an enclosure around the targeted extraction area. The absence of an enclosure results in the generated chemical mass moving directly downstream into the natural convection area where it decreases in concentration as the volatiles are lost to air and are dispersed in the rest of the flow.

In the scenario depicted in Figure 3-3C, dredging is performed inside a harbor, bay, or other enclosed water body such as a lake. It is assumed that no or very limited hydraulic flow is inside the enclosure. This case is handled differently from the previous DOU types because of this no-flow condition. Within this DOU, turbulent dispersive chemical transport occurs from the forced convection zone outward into the natural convection zone. A dispersion model will be used to describe the chemical concentration profile within the latter.

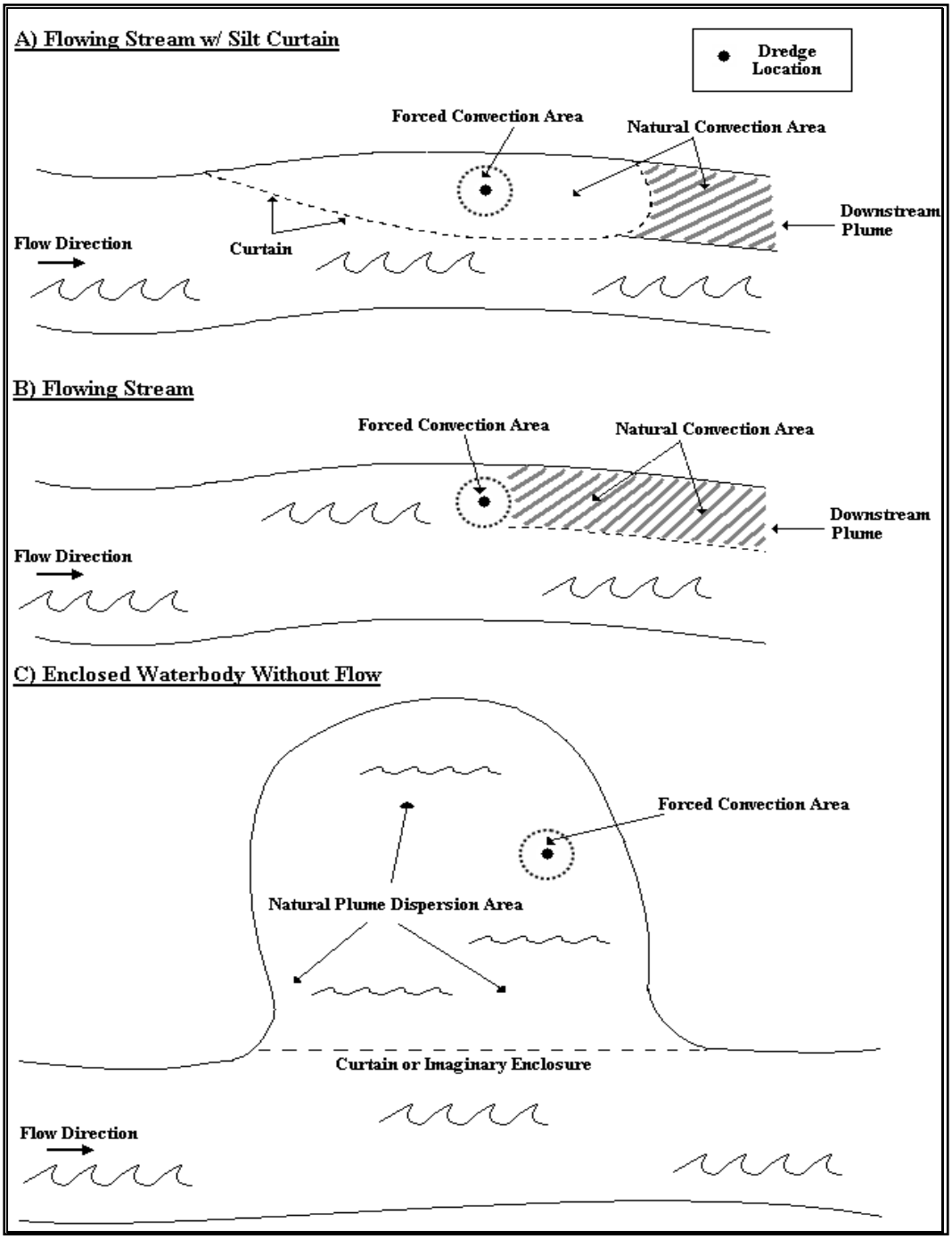

Figure 3-3. DOU classifications.

Due to the complexity and uncertainties about the chemodynamic processes involved, modeling the dredge-generated chemical release fractions to water and eventually to air from particle suspensions is in an early stage of development. Early on, batch desorption equilibrium models, based on available partition coefficients, were used to describe the solid and associated soluble PCB distribution at the point of dredging (DiGiano et al.

1993). Steady-state flow models incorporating so-called turbidity generating units (TGU) for quantifying the total suspended solids (TSS) levels produced by the dredge were coupled to the particle-to-water equilibrium model and used to simulate the dredging chemical release at three field sites (Thibodeaux and Duckworth 2001). General concepts of a transient toxic constituent loss and transport model for both solids and chemical incorporating a kinetic approach rather than equilibrium approach has been proposed (Hayes 2001; Malcolm Pirnie/TAMS-Earth Tech 2003). In application to the proposed dredging of the Hudson River PCB-contaminated site, the steady-state version was used. A steady-state multimedia chemical fate model was developed and applied to the Bayou Bonfouca PAH-contaminated field site (Sanchez et al. 2002). Of the targeted chemical mass, 0.42 to 1.13% was estimated as lost by volatilization from the DOU. The mass losses of total PAHs to air were estimated to be 8,913 kg for the 1-year dredging time period. A similar range of percentage volatile losses were projected for several other field sites (Sanchez 2001). The approach adopted here for model development is based in large part on the above steady-state modeling that uses a mass-transfer kinetic approach rather than an equilibrium partition approach.

Forced and natural convection zones

Both natural and forced convection MT processes can occur on either side of the interface, and the magnitude of the coefficient is controlled by the degree of fluid turbulence. Under static conditions with no flow of water or wind, the chemical movement will depend on the slow process of molecular diffusion through the water and air. With wind and water motion, the turbulence occurs in both phases. The turbulent eddies propel the chemical in the water to the interface and away from the interface in the bulk air. So the level of fluid convective turbulence heavily influences both the local water-side and air-side MTCs.

The characterization of turbulent driven processes has been a highly researched area in chemodynamics over recent years, and numerous correlations exist. The natural convection-induced MTCs are fairly well understood and correlations exist. Thus, the natural convection MTC can be determined using the appropriate equations in the following sections. Those equations used to determine the forced convection-induced MTCs will require further evaluation since mechanical turbulence generation is very device-specific. It is becoming increasingly important to develop better coefficients for estimating chemical emissions. Currently no empirical

expressions have been developed specifically for estimating dredge-induced MTCs. Since no studies have been performed for dredge operations, approximate alternative approaches are reviewed that may provide reasonable estimates. These methods, based on existing theories and similar mechanical devices, are expected to give only reasonable approximate values.

As was developed and is currently the practice for air emissions from surface impoundments (Springer et al. 1984), it is convenient to create so-called "forced" or "natural" convection mass transfer zones (see Figure 3-4). By separating the two processes into these area zones, the estimation procedures can more accurately account for the different transport processes occurring in each (i.e., forced and natural). In accounting for the different fluxes for each zone, Equation 3.2 becomes:

$$n_A = \left(\left({}^1K'_{A2FC} \cdot A_F + {}^1K'_{A2NC} \cdot A_N \right) / A_{DOU} \right) \cdot \left(\rho_{A2} - \rho^*_{A2} \right) \tag{3.6}$$

where:

A_F = area of DOU under direct influence of the dredging activity
A_N = area of DOU beyond the dredge influence
A_{DOU} = the total DOU area; all in m^2

Figure 3-3 also illustrates these zones within each of the DOU scenarios. Combining both the area in the DOU with forced convection and natural convection will give A_{DOU}. In Figure 3-4, the inner circular zone shown surrounding the dredge contains wind, hydraulic, and mechanical turbulence and is referred to as the forced zone, A_F. The area beyond the forced zone is influenced by wind and hydraulic turbulence only and is designated as the natural zone, A_N. The procedure for estimating the areas of the two zones is given later in this chapter.

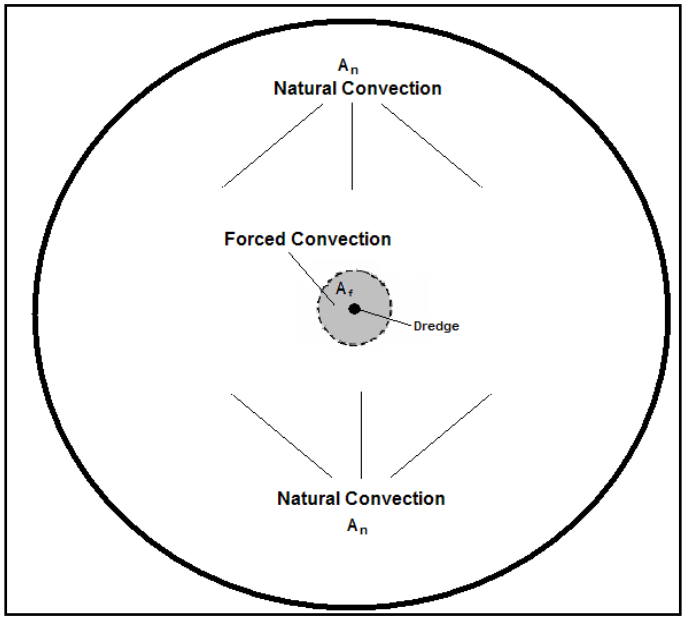

Figure 3- 4. Forced and natural convection zones.

In a forced convection process, the mechanical dredge device generates most of the bulk fluid turbulence. Since the transport of chemical in the bulk fluid phase can also be attributed to natural forces, the combination of water-side MTCs in the forced zone are added:

$$ {}^{1}k'_{A2FC} = {}^{1}k'_{A2NC} + {}^{1}k'_{A2D} \tag{3.7} $$

The mechanical effects of the dredge may be estimated from similar types of equipment that are known to increase turbulence in the water column such as surface aerators, boats, and cyclic mechanical devices. In a following section, details on these forced convection liquid-side MTCs induced by such equipment will be developed. In the natural convection zone, the bulk water turbulence is the result of both the stream flow hydraulic portion and the wind-induced water turbulence portion. These MTCs are computed from readily available algorithms in the literature. The air-side MTC is available in algorithm form as well (see Thibodeaux 1996). This MTC is assumed to be the same for both zones.

Air-side mass transfer coefficient

This aspect of mass transfer has been well established and appropriate equations are available to estimate $^{2}k'_{1A}$, the air-side MTC. The mechanical devices analyzed in the following discussion are assumed to create significant disturbance on the liquid-side only. Chemical transport on the air-

side from the interface to the bulk air is enhanced by air turbulence in this region. Wind speed and air stability are the important parameters that characterize this level of turbulence. Details on both the water-side and air-side coefficients will be developed following a discussion of dredges.

Dredges and water turbulence

An effort is made toward closely representing the operational aspects of both mechanical and hydraulic dredges and their influence on water turbulence. The mechanical dredge bucket moves up and down through the entire water column to physically act upon the entire vertical distance from the bed to the surface of water column to create turbulence for this forced convection zone. Although not always moving vertically, the cutterhead/auger portion of the hydraulic dredge can produce turbulent eddies throughout the water column by its suction activity and the side-to-side sweeping motion of the support ladder near the bottom of the water column. The near-bottom turbulence is likely greater than higher up in the water column. The cutterhead/auger section suctions water along with sediment from the bottom, inducing water currents up to a certain height in the water column that (because of mass continuity) requires a downward direct component. To a lesser degree, the hydraulic dredge arm (i.e., ladder) connecting the cutterhead/auger to the dredge barge stirs the upper water column. Nevertheless, natural convection results in induced turbulence that causes water containing high solution concentrations to be transferred upward toward the surface, elevating the concentration at the interface to sustain the emission to air process.

In the development of the MTCs for mechanical and hydraulic dredges, understanding and appreciation of the turbulent eddy formation process enables the selection of similar representations in the absence of directly applicable ones. Such similar processes will be presented and discussed in the following sections with the fundamental idea of representing the increased rate of water transport and turbulence generation on the water side of the interface. These processes are approached from a theoretical or fundamental perspective as well as a practical perspective. So, in the absence of specific studies of this MTC for dredges, three approaches that, to a degree, roughly mimic some of the key water turbulence generation processes will be presented. In the case of the mechanical dredge, the surface renewal theory and the surface aerator model will be presented. In the case of the hydraulic dredge, a motor vessel re-aeration model will be presented.

Surface renewal model

The theory of surface renewal was first developed by Dankwerts in 1951 to describe the resistance at the air-water interface for a general mass transfer process. Previous to this development, the penetration theory was developed for surface water exposed to a gas phase for some time period, then cycled away by turbulence, to reappear later and be exposed again, etc. In developing the surface renewal theory, Dankwerts proposed the distribution of the rate of surface renewal (i.e., exposure) parameter, s, to describe many ages of exposure. He chose an exponential distribution function for s with the adjoining phase as a realistic approach to the process. It resulted in the MTC, ${}^{1}k'_{A2}$, of chemical being related to its diffusivity in water, $\mathcal{D}_{A2}$, and the surface renewal parameter, s, by:

$$ {}^{1}k'_{A2} = \left(\mathcal{D}_{A2} \cdot s\right)^{1/2} \tag{3.8} $$

The surface renewal rate, s, is in units of s^{-1}, and the diffusivity coefficient in water in units m^2/s. If the diffusivity in water is constant, the MTC will vary directly with the square root of the renewal rate. The downward moving mass of water induced as the bucket descends through the column and later reverses as it ascends, produces an upward moving mass, forcing surface water to the bottom and bottom water to the surface. Some level of water motion most likely occurs through the entire water column. Upcurrent is deflected upon encountering the surface to cause so-called “cats paws” turbulence patterns on the water surface and a similar deflection upon contacting the bottom. The sum of all this water motion effectively creates a circular pumping action that brings chemical laden water from the bed region and delivers it to the surface region where it can encounter the interface and vaporize. The mechanical dredge can be represented using this theory because the up and down motion of the bucket through the interface roughly mimics the renewal rate concept. The s should be closely related and proportional to the cycle time of the bucket (τ_{bucket}). The relationship between the two variables is as follows:

$$ s = k/\tau_{bucket} \tag{3.9} $$

where k is some proportionality constant.

Although the surface renewal model approach is simplistic, it provides a means of estimating the order-of-magnitude of the water-side MTC and

captures the relative changes with dredge bucket cycle time. It will be assumed that k = 2 in Equation 3.9; this quantifies that the bucket disturbs the air-water interface twice per cycle. The first disturbance occurs when the bucket enters the water and the other when leaving it. Combining the two disturbances yields:

$$ {}^{1}k'_{A2} = \left(2\mathcal{D}_{A2}/\tau_{bucket}\right)^{1/2} \tag{3.10} $$

This approach was suggested by John Gulliver (personal communication 2005). The diffusivity of naphthalene in water is 5.0E-6 cm²/s at 25°C. Table 3-2 contains the calculated MTCs for bucket cycle times of 0.25 to 5 minutes. The numerical values are substantially lower than those estimated using a surface aerator model correlation. See the next section where surface aerator values up to 80 cm/hr are estimated. A mechanical dredge with 250 cycles per hour (4.2 cy/min) or 0.24-minute cycle time has been proposed for the IHC site (Estes et al. 2003, 2004). Alternatively, a slower 1.5-minute cycle time results in an MTC of 1.2 cm/hr.

Table 3-2. Liquid-phase MTCs from surface renewal theory.

Dredge Bucket Cycle Time τ_{bucket} (min)	'k_{A2} (cm/h)
0.25	2.91
0.5	2.06
1.0	1.46
2.0	1.03
5.0	0.651

Surface aerator model

Surface aerators were studied vigorously in the mid-1900s as devices to increase the oxygen concentration in the water. Over the past few decades, the concepts have been optimized and are now well understood. One type of surface aerator is designed to sit on the surface of a water body and contains a set of rotating paddles or blades that stir the surface of the water column. This action displaces the surface water layers laterally from the center of the aerator so that bulk water from below will rise up, renewing the surface and releasing the chemical in solution. A surface water velocity will move out radially, but water must eventually move down as well by continuity to replace the bulk water moving up. It is essentially a practical idea for surface renewal that roughly mimics the up and down movement

of water currents induced by the dredge bucket. Both operations constantly displace the vaporization diluted surface water with concentrated bulk water from below. This water turnover device produces a continuous cycle of renewal.

Conceptually, the bucket dredge does not appear to produce the intense surface disturbance of an aerator. Instead of remaining at the surface to vigorously renew the surface, the bucket dredge moves up (and down) the water column producing high energy turbulent eddies that causes a trailing upward (or downward) water flow behind the bucket. Once the bucket dredge moves past the interface, the renewing of the surface with chemical concentrated water will decrease exponentially until the dredge breaks the surface again. Although the bucket dredge cycles up and down and the aerator rotation is continuous so as to appear to be a totally different operation, they both achieve very similar surface renewal processes that force waters at depth upward to the air interface where volatilization occurs.

For estimating the mechanical dredge contributions to the overall waterside MTC, correlations were defined using the concepts mentioned above. The following equation modified and generalized from the original oxygen form is (Thibodeaux 1996):

$$ {}^{1}k'_{A2} = 3140 \cdot \left(\mathcal{D}_{A2}/\mathcal{D}_{B2}\right)^{1/2} \cdot \left(n'_{BO} \cdot E \cdot \alpha\right) \cdot \left(f\right) \cdot \left(1.024\right)^{(T-24°C)} \qquad (3.11) $$

where

B = oxygen
A = the volatile organic compound (VOC)
n'_{BO} = the oxygen delivery of 2 to 4 lb O_2/hr • hp
E = specific power delivery efficiency of 0.65 to 0.9, dimensionless
α = dirty water to clean ratio, 0.8 to 0.85, dimensionless
T = water temperature, °C
k'_{A2} = the MTC, cm/h

The diffusivity ratio corrects the oxygen-based MTC for the VOC selected. This correlation may be used to estimate the MTC in the highly turbulent forced convective zone in the immediate vicinity of the bucket.

Without some modification, the above correlation will produce extremely high and likely unrealistic MTCs representative of a bucket dredge of

equivalent horsepower. One obvious modifying factor is the fraction of the time the bucket is in the vicinity of the air-water interface. During a typical dredge cycle, this may be no more than 10%. When the bucket reaches the bottom, the surface waters are not being directly stirred. Only when the bucket is in transit through the interface is it contributing significantly to stirring the surface waters that drive the MTC for evaporation. It seems reasonable to apply a factor f with numerical values between zero and one to account for this time fraction. A default value f = 0.05 or 5% will be assumed; however, the user may apply a more appropriate value for any particular situation. For example, if nearby structures are hampering free movement of the bucket, smaller in-water time fractions may be appropriate. For very deep water, more cycle time is used since the bucket spends a longer time in the water; in this case a 0.01 time fraction may be more appropriate. For a 300 hp mechanical dredge of lowest O_2 rating and efficiency in dirty water with f = 0.05, an MTC of 80 cm/hr results for naphthalene. Using f = 0.05 in the above example as the fraction of cycle time the bucket spends moving through the air-water interface is not unreasonable. Nevertheless, in comparison to the estimates of MTCs of the other two models, the value of 80 cm/hr is high. It is also high compared to the surface renewal model values and the motor vessel values presented next.

Motor vessels model

A third alternative transport process based on similar fundamental concepts has been developed from motorized vessels on water. The research on this re-aeration process came about to evaluate the impact of increased water turbulence due to boat traffic through a particular water body. This water mixing process is similar to the hydraulic dredge mixing process, particularly in mixing the water at the bottom of the water-column. Eventually the turbulent eddies generated here contact and impact the surface but to a lesser degree of intensity. During hydraulic dredging, the ladder supporting the cutterhead suction end moves side-to-side stirring the bottom waters. It forms large turbulent eddies similar to those surrounding a barge-type vessel moving through a shallow waterway.

As a boat moves through shallow waters, the surface and bottom waters are displaced. This displacement creates a rapid movement of water along the sides and bottom of the boat. In this regard, the action is very similar to the cutterhead/auger dredge in its displacement of water by the swing motion of the ladder through the water. Intense turbulence is less noticeable at the surface, especially for larger water depths; the higher velocities

occur at the end of the ladder near the bottom. However, residual eddies eventually reach the surface to create a continuous turnover and replacement of chemically depleted waters.

Estimates for molecular oxygen MTCs of large and small motor vessels have been made through both laboratory and field studies. A theoretical momentum balance model was developed to quantify the water-side MTC due to motor vessels moving on the Seine River in France (Thibodeaux et al. 1994). As the vessels' passage rate increased on a section of the river, too did the MTC increase. For 20 hp (15 kW) vessels, the oxygen MTCs ranged from 1.5 to 2.5 cm/hr at passage rates of 5 to 20 vessels per hour. The oxygen MTCs for 70 hp (52 kW) vessels ranged from 2.5 to 4.5 cm/hr for the same passage rates. For naphthalene the MTCs are approximately half those of oxygen. Laboratory experiments with scale-model vessels confirmed the passage frequency relationship and yielded oxygen MTCs that ranged from 0.77 to 6.4 cm/hr (Qaisi et al. 1997). This approach of estimating the water-side MTC for hydraulic dredges that create water turbulence primarily on the bottom yields numerical values similar to those for mechanical dredges that create water turbulence primarily at the air-water interface.

In summary, it appears that no correlations or theoretical models developed specifically for dredges exist. Three approximate approaches are proposed as alternatives. Based on the above, water-side MTCs in the range of 1 to 4.5 cm/hr seem appropriate for both mechanical and hydraulic dredges. Using the surface aerator correlation will yield unrealistically large values for the mechanical dredges and is not appropriate for hydraulic dredges.

Chemical release from particle-water slurries

Whereas the particle generation and water column suspended solids aspects of environmental dredges have been studied to a good degree, the related chemical release process has received less attention. A brief review of the particle process is presented below. The following paragraph contains a review of the studies performed measuring volatile chemical flux to air from contaminated sediment particles suspended in water.

Using inoculated sediment in a grid-stirred tank apparatus that closely simulates the water turbulence and suspended sediment concentrations of a dredge, the flux of semi-volatile organics to air was measured (Valsaraj

et al. 1997, 1999). The flux increased with increased suspended sediment concentration, increased with increasing Henry's Law constant, and decreased with increased sediment/water partitioning constant for the chemical. Follow-on experiments using IHC sediments produced similar results (Ravikrishna et al. 2001). The flux to air for naphthalene, anthracene, and phenanthrene decreased with time as the chemical mass was depleted. As TSS increased so did the flux to air. A transient kinetic mass-transfer model was applied to the data and it was found that the TSS level was the most critical parameter for predicting air emissions. Using an alternative laboratory-scale artificially stirred flux chamber apparatus and Stryker Bay sediment slurries with high solid-to-water ratios of 1% (10,000 mg/L) to 8% (80,000 mg/L), the evaporative flux of the PAHs and high volatility petroleum hydrocarbons were measured (Thibodeaux et al. 2004). The transient behavior followed the expected theory of the mass-transfer kinetic, but the conventional LEA model failed to capture the necessary water soluble concentrations that drive the evaporation process. The TSS levels used were much higher than those typically observed in the mud clouds near environmental dredges. The dredging-driven volatile emission models to be developed in a later section are based upon the above research involving contaminated particles in water and water-sediment slurries as the volatile and semi-volatile chemical sources.

Particle generation in the water column

The dredging of contaminated sediments in rivers or streams is often performed by using some form of particle containment enclosure, such as a silt curtain. They reduce the visible particle concentration (i.e., mud cloud) downstream from the dredge site and may aid in reducing contaminant mobility by encouraging particle settling and decreasing flow through the dredging zone. In modeling this case it is assumed that negligible suspended solids exited the DOU. This condition results in a downstream plume made primarily from chemical in solution leaving the DOU area. The DOU emission area is divided into two zones: forced convection and natural convection. These two zones were shown in Figure 3-3. The smaller forced convection zone refers to the emission area immediately surrounding the dredge where volatilization is enhanced by dredge-generated turbulence.

For the natural zone within the enclosed area of a flowing river, the emissions are not enhanced by the dredging activities, but only by wind-

generated and hydraulic currents. Outside the enclosed area, the downstream plume concentration is influenced by these natural convective mass transfer processes as well. The forced zone has an increased TSS concentration level relative to the natural zone. Both zones within a contained DOU operation are assumed to be well-mixed sections. Admittedly, this is an assumption of convenience; almost nothing is known about the hydraulic flows, TSS levels, particle settling, chemical concentration profiles both horizontal and vertical, etc. within curtained-off DOUs. Outside the contained DOU in the downstream (DS) plume section, the TSS levels are significantly lower. Order-of-magnitude TSS levels for these zones suggested by Paul Schroeder (personal communication, February 2005) are listed in Table 3-3. Downstream beyond the DOU area, water exits with a finite concentration of chemical in solution. Natural convection processes, which include the wind-generated and hydraulic flow at the water surface, influence the rate of chemical emissions in the downstream section. Although the most common containment mechanism is a silt curtain, sheet pilings can also be used to construct the containment walls of the DOU. In this case, since no flow occurs past the containment boundary, downstream chemical flux must be excluded from the emission calculations. This situation was not modeled, however.

Table 3-3. Convection zone TSS concentration levels.

Location	TSS Concentration mg/L
DOU Forced Convection Zone	~500
DOU Natural Convection Zone	~50
DS Natural Convection Zone	~0.5 to 5

The first step in the chemical pathway commences when the mechanical parts of the dredge contact the bed and cut into the consolidated sediment layers. As noted above, the most significant mass fraction is extracted and departs the water-body within the bucket extractor or is drawn by flow into the suction pipe intake of the hydraulic dredge. In this extractive action, some fraction of the targeted material becomes suspended in the water column (Sanchez et al. 2002; Sanchez 2001). Because the turbidity plumes associated with dredging have been viewed to negatively impact water quality, much literature exists on the subject. A recent review by Hayes and Wu (2001) summarizes the available studies and presents an approach for estimating re-suspension from dredging operations based on the available field data. The authors note that transport models will also be

needed for the toxic constituents associated with suspended sediment particles and the models all require a mass flux of suspended sediment (the rate of sediment loss) into the water column due to the dredging operation input. This mass flux rate, referred to as the "source strength," varies widely with dredge operation, sediment characteristics, and local conditions. The variations are both temporal and spatial in nature. The authors provide a simplified approach for estimating the particle resuspension mass flux based on dredge type and operating conditions.

The mechanical and mixing actions that occur in the immediate vicinity of the dredging operations do not discriminate against particle sizes; all sediment size fractions are initially suspended into the water column. However, sand (and larger) particles resettle quickly in the immediate vicinity except under extreme flow conditions leaving only silt and clay particles (i.e., particles smaller than 74 μm) in the water column. Steady-state transport models need the average rate of sediment mass flux leaving the "near-field" area or immediate vicinity of the dredging operations. The resuspension factor method proposed by Hayes and Wu (2001) provides a practical means of estimating the sediment flux leaving the near field, ω_{32}, and is:

$$\omega_{32} = \left(R/100\right) f_{74}\, Q_3\, \rho_3 \left(1-\varepsilon\right) \tag{3.12}$$

where:

R = re-suspension factor (%)
f_{74} = fraction of particles ≤ 74 μm-diameter in size

Since water column measurements typically include only this fraction in ω_{32} determined under field conditions, a value of $f_{74} = 1$ is appropriate when using Equation 3.12. The volumetric rate of in-situ sediment removal by the dredge is Q_3(m^3/s), and ρ_3(1-ϵ) is the in situ bed-sediment concentration in g/m^3. The latter can be measured directly or estimated based on particle density, ρ_3, and bed porosity, ϵ.

The resuspension factor, R, represents the mass of sediment suspended in the water column relative to the mass of sediment removed via dredging in units of percent. It varies with dredge type and size, sediment characteristics, dredge operational mode, and local environmental conditions. Because it is likely the most important and sensitive input variable that impacts the volatile emission process, R values should be studied carefully

before selecting numerical values for use at a particular site. The following paragraphs present a brief overview of the ranges of resuspension factors for different dredge types reported by Hayes and Wu (2001).

Resuspension factors for cutter-head dredges are based on almost 388 observations of resuspension rates from five field studies. Factors range from near 0 to 0.51% with the prepondence of values between 0 and 0.1%. The data have a mean of 0.11% and a standard deviation of 0.11%. For the available data, R of 0.31% was exceeded only 5% of the time and 0.46% only 1% of the time. These data likely represent approximate maximums for similar cutter-head dredges. The dredge sizes ranged from 10- to 18-in. and the engines were 175 to 360 hp.

A similar amount of data is available from bucket dredging studies. Buckets included standard clamshell buckets often referred to as "open" buckets to distinguish them from buckets that are fully enclosed in an attempt to reduce turbidity. Bucket sizes were 7.6, 9.2, 9.9, and 19.6 m^3 (10, 12, 13, and 26 yd^3). All operations included scow overflow; the scow receiving the DM was allowed to overflow supernatant liquid, which increased the TSS concentration in the water column. These solids are not distinguishable from the resuspension of the mechanical action of the dredges and are reflected in high R values. All the studies show higher resuspension factors than cutter-head with R values ranging from 0.16 to 0.60%. The authors note that if overflow accounts for 50% of the suspended sediments then the R values for open clamshell dredges are not substantially different from the cutter-head ones. Data available on two enclosed bucket dredging studies produced R values of 0.10 and 0.22%. The latter was for a 29.8 m^3 (39 yd^3) enclosed bucket.

Although the data sets for horizontal auger dredges were not substantial, the R values were markedly higher than any other dredge type. Fifty-seven observations were available for the matchbox dredge. The R values ranged from 0.1 to 10% and substantiate previous data that show the matchbox R values about five times higher than the cutter-head and much lower production rates.

The chemical loading on the bed-sediment solids is ω_{AO} (mg/kg dry solids). The dry solid extraction rate performed by the dredge, either hydraulic or mechanical, is M_P (kg/s). Therefore the chemical mass forced into the water column is

$$w_{AA} = M_P \cdot R \cdot \omega_{AO} / 100 \quad (3.13)$$

Once suspended in the water column a fraction desorbs into solution; however, the total mass will be used in modeling the input from the dredge.

Flowing stream with a "mud cloud" containment barrier

As shown in Part A of Figure 3-3, this DOU is defined by the physical boundary of a semi-permeable containment structure. It also includes the downstream plume section shown because significant quantities in solution move through the semi-permeable structure. Emissions to air originate from the forced and natural convection areas within the containment structure and also from the departing plume. A single chemical mass balance was performed around the contained water volume defined by the surface area of the DOU, A_{DOU} (m^2), and the average water depth, h (m). The processes include in the balance were advection in and out, mass input generated by the dredge, diffusion from the contaminated bed-sediment surface layers that form the bottom surface of the DOU, and volatilization from both the natural and forced zones (A_{NDOU} (m^2) and A_{FDOU} (m^2), respectively). A key result of the steady-state balance is the soluble concentration in the DOU that drives the vaporization, written as:

$$\rho_A = \alpha / \beta \quad (3.14a)$$

where:

$$\alpha \equiv Q_{DOU}\rho_{AS} + w_{AA} + "k_{A3}A_{DOU}\rho'_A + \left['K_{A2}A_{FDOU} + 'K'_{A2}A_{NDOU}\right]\rho_{A1} \quad (3.14b)$$

$$\beta \equiv Q_{DOU} + "k_{A3}A_{DOU} + 'K'_{A2}A_{FDOU} + 'K'_{A2}A_{NDOU} \quad (3.14c)$$

The water flow rate moving through the DOU is Q_{DOU} (m^3/s) and ρ_{AS} is the upstream inlet concentration. The w_{AA} term represents the mass of chemical placed in suspension by the dredge extraction process; see Equation 3.13. The other terms have been previously defined or appear in the list of symbols in Appendix 3A.

Several assumptions were involved in formulating the above mass balance, they are:

1. The contents of the contained portion of the DOU are well mixed (i.e., Continuous Stirred-Tank Reactor Model) and of uniform concentration,
2. The semi-permeable containment structure excludes particles entering and exiting the DOU,
3. All processes were assumed to be at steady-state, and
4. The departing plume portion of the DOU was modeled as a plug-flow transport process.

The emissions to air within the DOU originate from two sources areas, which are forced zone written as:

$$w_{AF} = A_{FDOU}\,'K_{A2}\left(\rho_A - \rho_{A1}\right) \tag{3.15}$$

and natural zone written as:

$$w_{AN} = A_{NDOU}\,'K'_{A2}\left(\rho_A - \rho_{A1}\right) \tag{3.16}$$

Numerical differences in the areas and in the MTCs regulate the respective rates although both are driven by the same soluble concentration in water. The down-stream chemical plume volatilization rate is:

$$w_{AP} = 1/\tau \int_0^{\tau} A(\tau)\, n_A(\tau)\, d\tau \tag{3.17}$$

where the flux decays exponentially with the time-of-flow, τ

$$n_A(\tau) = {}'K'_{A2}\left(\rho_A^0 - \rho_{A1}\right)\exp\left\{-{}'K'_{A2}\tau / h\left[1 + K_{A32}\rho_{32S}\right]\right\} \tag{3.18}$$

and the emission area is related to τ as well

$$A(\tau) = \tau\, Q_{DOU} / h \tag{3.19}$$

The time-of-flow, τ, commences at the boundary of the containment barrier, where $\rho_A{}^0 = \rho_A$.

The area of the DOU, A_{DOU}, is broken into two parts: the forced convective area, A_{FDOU}, and natural convective area, A_{NDOU}. These areas are required for estimating the mass evaporative rates as given by Equations 3.15 and 3.16. The A_F is estimated as the area generated by the surface aeration process (Thibodeaux 1996). Without data on area of disturbed surface

water for dredging, the data available for surface aerators is used. The aerator estimates are likely on the high side.

$$A_{FDOU} = \left(17 \text{ ft}^2 / hp\right) P \tag{3.20}$$

Here P is the dredge delivered power (hp) for >13.5 hp. In each case, the natural convective area, A_N, is determined by taking the difference between A_{DOU} and A_F as

$$A_{NDOU} = A_{DOU} - A_F \tag{3.21}$$

See Figure 3-4.

Flowing river without containment barriers

Part B of Figure 3-3 illustrates the DOU for dredging in a flowing stream without the use of a containment barrier. It consists of a well-mixed area of forced convection containing the dredge extractor and a downstream plume similar to the previous case. Without the presence of a semi-permeable barrier, suspended solids can move in and out of the forced convection zone. Including this factor the resulting model incorporates the same processes as the previous one. A chemical mass-balance yields the soluble concentration within the forced convection zone similar to Equation 3.14:

$$\rho_A = \gamma / \delta \tag{3.22a}$$

where

$$\gamma \equiv Q_{DOU} \rho_{AS} \left[1 + K_{A32} \rho_{32S}\right] + w_{AA} + "k_{A3} A_{DOU} \rho'_A + 'K_{A2} A_{FDOU} \rho_{A1} \tag{3.22b}$$

and

$$\delta \equiv Q_{DOU} \left[1 + K_{A32} \rho_{32S}\right] + "k_{A3} A_{DOU} + 'K_{A2} A_{FDOU} \tag{3.22c}$$

The ρ_{32S} in both Equations 3.18 and 3.22 is the suspended solids generated by the dredge; this quantity is equal to M_p R/ Q_{DOU} plus the entering stream suspended solids, ρ^o_{32S}. Due to the possibility of high solids generation, the w_{AA} term may force the concentration in both Equations 3.18 and

3.22 beyond the equilibrium solubility limit. To avoid this thermodynamic impossibility, ρ_A is limited to values less than or equal to the solubility in water. The emission rate to air is given by Equation 3.15, and the down-stream chemical plume volatilization rate is similar to Equation 3.20. The chemical emissions are estimated by using the MTCs appropriate for this natural convective zone. In addition to the water-to-air volatilization MTCs, Equations 3.20 and 3.22 contain a sediment-to-water MTC denoted by $'''k_{A3}$.

It is well established that environmental dredging is not 100% efficient and that a bottom contaminant residue layer is formed because of re-suspended particle fall-back and incomplete capture of the targeted sediment layers (Sanchez et al. 2002; Thibodeaux and Duckworth 2001). This fall-back produces a surface layer estimated to be several centimeters in thickness on the bed throughout the DOU (Reible et al. 2003), which then becomes a source of soluble chemical transported into the water column. A residual layer of 10 cm in depth was used for the Fox River, WI study. This situation is illustrated in Figure 3-5 for the case of a contained DOU; however, it applies to all DOUs modeled. Within the containment area and downstream from the forced convection zones, a fresh residual

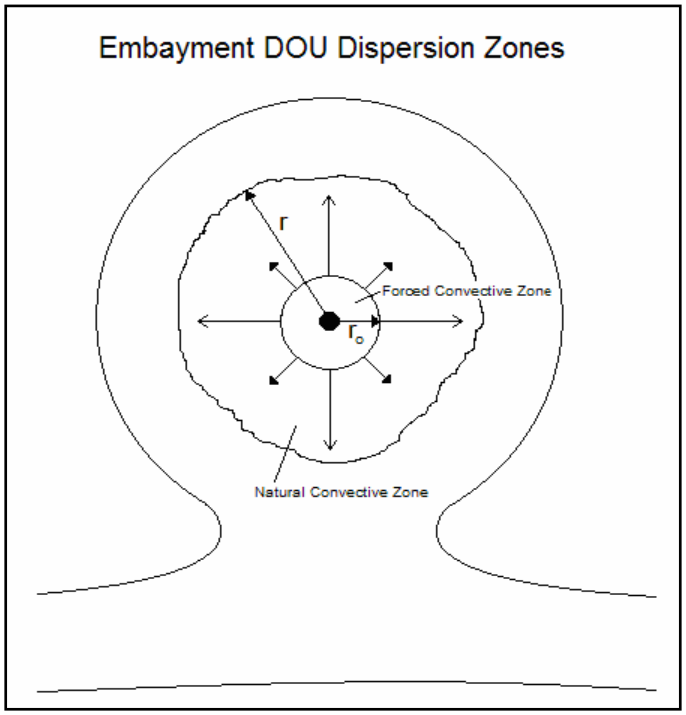

Figure 3-5. Radial chemical dispersion in embayment waters.

layer is assumed to be continually produced. Chemical mass-transport from the interface of this surface layer through the benthic boundary layer is a well-known process. The mass flux, n_{diss} (kg/m² s), from the bed to the water column is:

$$n_{diss} = "k_{A2}\left[w_a/K_{A32} - \rho_{A2}\right] \tag{3.23}$$

where $"k_{A2}$ is the bottom-water MTC in cm/hr.

Field data and correlations are available to estimate this MTC for both flowing streams and wind-induced bottom turbulence (Thibodeaux 1996). During the dredging time periods and beyond, this residual layer will continue to deliver a soluble fraction to the water column. For the residual layer at steady-state during nondredging time intervals, the chemical dissolution rate into the water column is equal to the evaporation rate to air resulting in a steady-state "background" concentration ρ_{A2SS} (g/m³) given by:

$$\rho_{A2SS} = \left[w_a/K_{A32}\right]\left["k_{A2}/\left("k_{A2} + {}^2K_{A1}\right)\right] \tag{3.24}$$

Numerical calculations using this result indicate that a freshly formed surface layer with chemical loading near w_a will contribute significantly to the water column concentration and the vaporization rate. This justifies its appearance in equations 3.14 and 3.22.

Barge emissions

Typically, a mechanical dredging operation uses a barge for receiving the DM. The DM within the barge will be comprised of a layer of standing water with high concentrations of TSS somewhat representative of the conditions in the forced convection zone. To account for barge emissions, therefore, the area of forced convective emissions should be increased by the surface area of the barge if this equipment is to be included as part of the emission sources.

Enclosed embayment

The chemical flux from a DOU located within an embayment involves a different modeling approach. The chemical is undergoing turbulent diffusion away from the forced convection zone by wind and wave action rather

than hydraulic flow. As in the previous models, the area inside the forced convection zone of radius r_o is assumed to be comprised of a uniform chemical concentration. In this case, however, a lateral turbulent diffusion process transports the chemical within the natural convection zone as shown in Figure 3-5. A steady-state chemical mass balance on the forced zone includes terms for rate of input from the dredge and the bed residual layer. The outputs are evaporation and turbulent diffusion to the surrounding natural convection zone of concentration, ρ_{ss}. The result is:

$$\rho_A = \frac{\varepsilon}{\varphi} \tag{3.24a}$$

$$\varepsilon = W_{AA} + A_{Dou}\left[{}'k_{A3}\rho_A' + {}'k_{A2}\rho_{A1}\right] + 4\pi hD\rho_A \tag{3.24b}$$

and

$$\phi = A_{Doa}\left({}''k_3 + {}'k_{A2}\right) + 4\pi hD \tag{3.24c}$$

where D(m^2/s) is the lateral turbulent mass diffusivity in the waters of embayment. A line source dispersion approach was used to describe the turbulent chemical transport from the forced convection zone into the natural convection zone of the embayment DOU. A line source with length $2\pi r_o$ rather than a radial-source yields slightly higher estimates of the chemical concentration, plus the mathematics are simpler. A steady-state mass balance in the natural convection zone results in the 2nd order ordinary differential equation:

$$D\frac{d^2\rho}{dr^2} - \left(\frac{{}''k_{A3} + {}'k_{A2}}{n}\right)\rho = -\left[\frac{{}''k_{A3}\rho_A' + {}'k_{A2}\rho_{A1}}{n}\right] \tag{3.25a}$$

With boundary condition

$$\rho_A\left(r = r_o\right) = \rho_A^{0\,0} \tag{3.25b}$$

and

$$\left|\frac{d\rho}{dr}\right|_{r=r_o} = 2\left(\rho_A - \rho_{ss}\right)/r_o \tag{3.25c}$$

The analytical solution can be obtained and it is used in the MATHCAD® program. On the edges of the natural convection zone, the concentration becomes the steady-state value given by Equation 26.

The subject of horizontal dispersion on surface waters is very mature. Based on a published review of data and correlations (Thibodeaux 1996), the following sea surface dispersion equation—based on cloud size and reduced by a factor of 10 to remove shear current effects—is used for the embayment DOUs:

$$D = 3.6r^{4/3} \tag{3.26}$$

Where r (m) is the radial distance from the dredge and D (m^2/s) is the lateral turbulent diffusivity on surface waters. Typical of such correlations and as shown by this result, the turbulent dispersion coefficient is proportional to the cloud size raised to the 4/3 power.

Model applications

The focus of this section is to verify whether the model produces reasonable estimates using sample input parameters. It is not designed to provide emission results for the IHC site. However, input values from this site along with other data from similar sites (Sanchez 2002) were used to test the model.

These chemical properties were based on naphthalene with a bedsource concentration of 2.65 mg/kg. Some of the DOU parameters include:

- wind velocity of 9.26 mph
- water flow-through of 0.5 m^3/s
- surface area of 1569 m^2
- 300 hp dredge.

The equilibrium air concentration is assumed to be negligible. Figure 3-6 shows the flux to air profile as a function of flow residence time, τ, from the dredge point ($\tau = 0$) for a curtained-off dredge (case A) and a dredge without a curtain (case B).

Shown in Figure 3-6 is a typical emission profile for Case A (solid line) and B (dashed line) DOU and downstream plume area; see Figure 3-3 for the types. Figure 3-6 shows three sections of emissions as mentioned in the

model discussion in previous sections: forced convection zone of the DOU, natural convection zone of the DOU, and natural convection zone of the downstream section. The forced zone ($\tau \leq 0.8$ hr) contains the highest level of emissions due to the high concentrations in this zone and the enhanced in MTC due to the dredge. The next emission zone ($0.8 \leq \tau \leq 3.0$) is the Case A DOU natural convection area that is lower due to the decrease in mass transfer coefficient and the concentration. The last zone displays the emissions for the downstream plume departing the containment area. Although the flux continues to decrease, it does not go to zero because of the ongoing dissolution from the dredge-produced residual layer on the bottom. Case B flux is lower because the silt curtain is absent and chemical out-flow on the TSS occurs. Case A with the silt curtain keeps concentrations higher in the zone around the dredge.

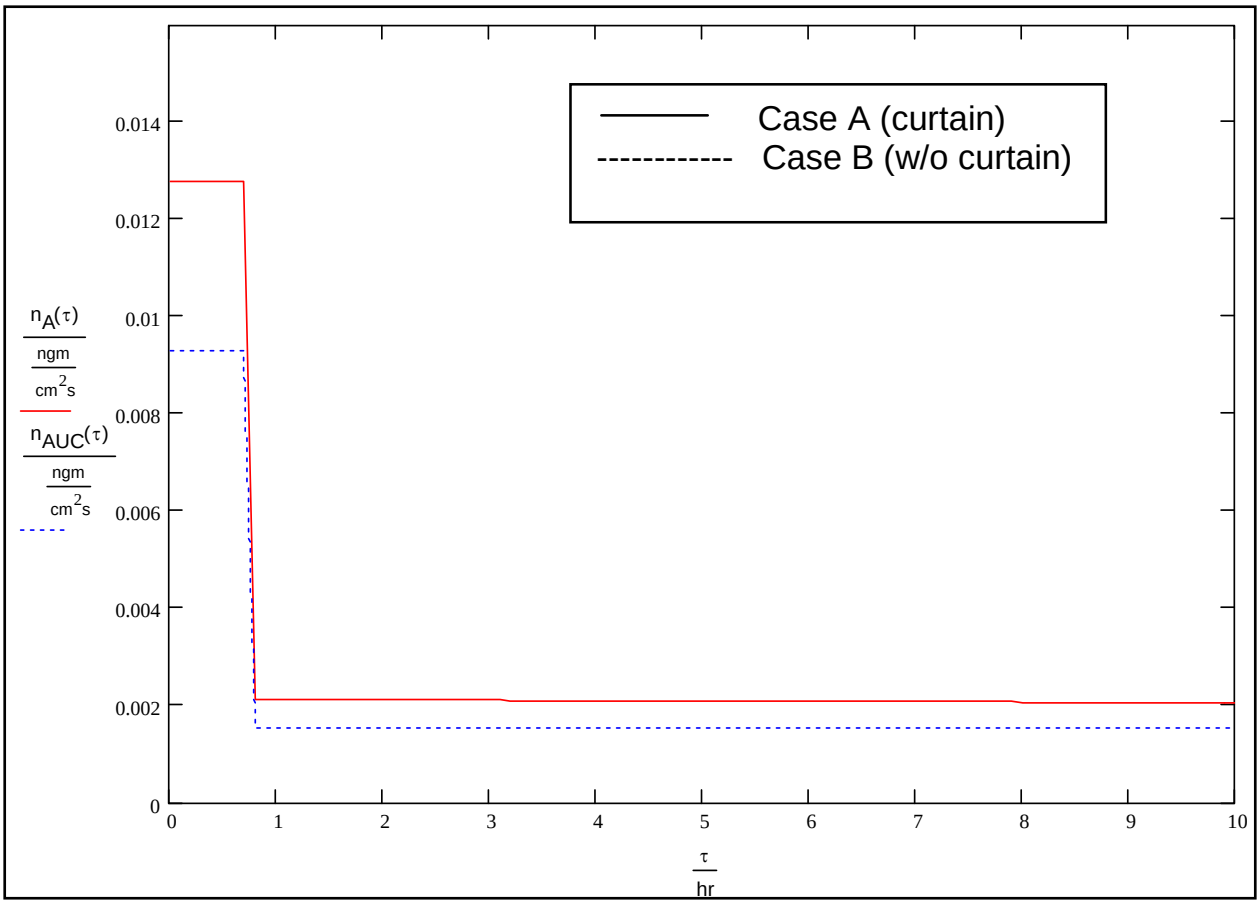

Figure 3-6. Chemical Flux from River DOU and Downstream

Figure 3-7 is an emission flux profile for an impoundment-type DOU; see Figure 3-3 for an illustration of this Case C DOU. Within the forced convection zone of radius 13 m, the flux is uniform and highest. Immediately

beyond this well-mixed and highly turbulent zone receiving chemical input from dredge generated particle resuspension, the flux decreases dramatically. Being beyond the influence of the dredge and its influence on the MTCs, the natural convection mass transfer processes are much less turbulent. A "shoulder" flux occurs for 13 ≤ r ≤ 18 m in the horizontal dispersion zone. Beyond r = 18m, the on-bottom residual layer maintains a non-zero flux.

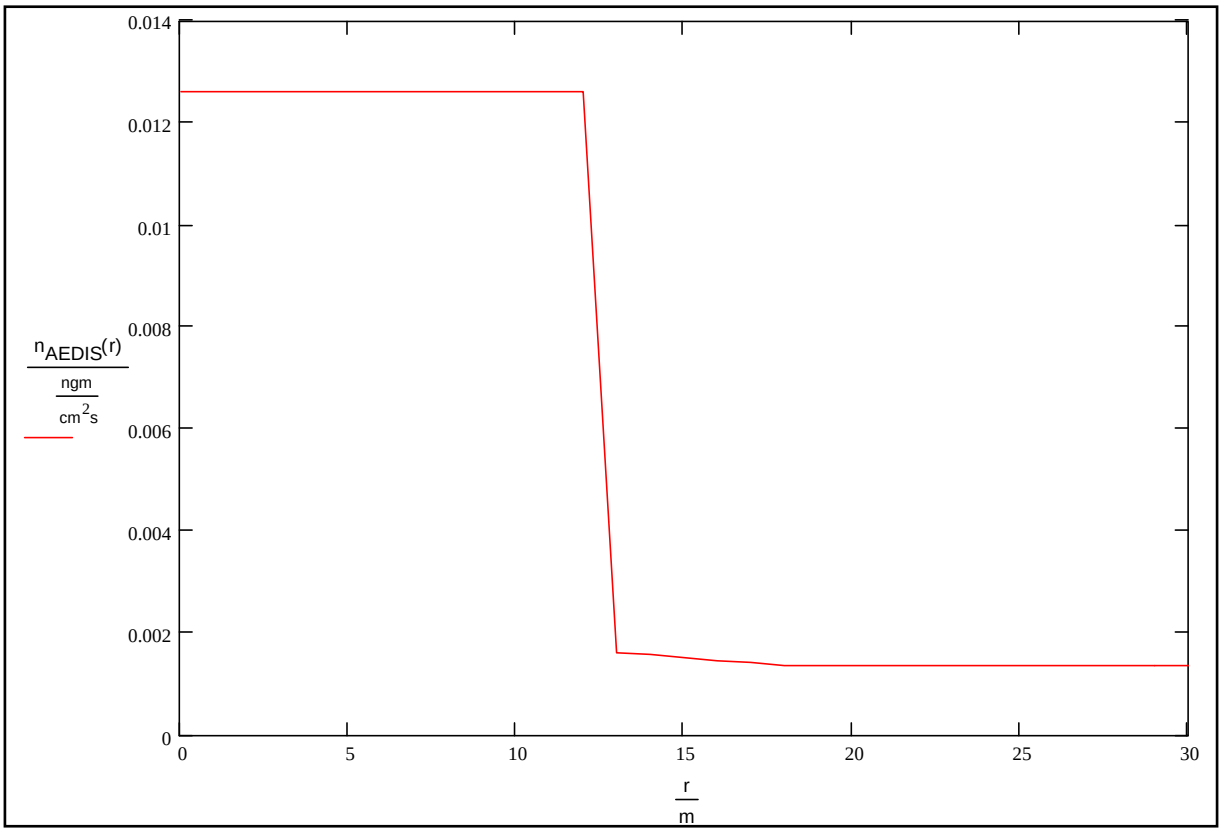

Figure 3-7. Chemical flux from impoundment-type DOU.

Such numerical simulations as depicted in Figures 3-6 and 3-7 were performed with the three DOU vaporization models as a check on their expected computation performance, to gain some insight relative to the magnitude of the emission rates, and to perform a sensitivity analysis on key input parameters. As noted above, the parameters roughly approximate those planned for dredging at the IHC site for naphthalene. Table 3-4 contains the projected naphthalene emission rate in gm/d.

Table 3-4. Projected naphthalene emission (gm/day) originating from 1600 m^2 forced convection zone.

DOU Type	Input Parameter Perturbed†					
	(1) BC*	(2) Conc.	(3) Rate	(4) Dredge	(5) Wind	(6) Flow
Curtained stream	24.1	48.2	43.7	14.3	67.5	25.7
Un-curtained stream	17.0	33.9	24.8	11.3	51.0	21.6
Embayment	9.39	18.9	10.4	8.86	23.6	9.45
*Base case: Conc. 2.65 mg/kg, Rate 250 cu yd/h, Dredge R = 1.0%, Wind 9.3 mi/h, Flow 0.5 m^3/s. †All 2X the base case except Dredge= ½ X the base case.						

The first column of rates reflects the base-case (BC) simulation; the key input values used appear at the bottom of the table. The results indicate that a curtained-off or containment barrier enclosed dredge site produces the highest rates. This is due to the elevated uniform chemical concentration within both the forced plus natural convection containment area. For an uncurtained stream, the concentration decreases downstream upon leaving the forced convection. In the natural convection area, the flux decreases as well. This decrease results in an overall lower rate in comparison.

Similarly in the embayment case, turbulent diffusion in two directions from the forced convection zones produces even lower concentrations in the natural convection zone and a correspondingly lower flux. Generally speaking, the three cases produce rates of similar numerical magnitudes; the rates vary within a factor of approximately 2X.

Five of the BC input parameters were perturbed and the corresponding rates computed. The results appear in columns 2 through 6 in Table 3-4 for each DOU type. In all cases the curtained stream DOU emission rates are highest and embayment is lowest. All perturbed parameters were 2X the base case except the particle generation ratio Dredge, which was reduced by one-half. In reducing Dredge to 0.5% (see column 4), the emissions were reduced but not by the ½X factor. The residual layer bed-sediment source is a significant factor and attenuates the expected reduction. Increasing the naphthalene loading by 2X effectively increases the emission rate by 2X; see column 2. Both the water column particles and bed source loading concentration respond to the doubling in producing a 2X rate increase. Doubling the dredging rate, as shown by the results in

column 3, increases the rates as well. The increase is less than 2X, however, and that for the curtained DOU is largest and the embayment rate lowest, both changed little from the BC.

Hydraulic flow increase by 2X has little effect on the emission rates compared to the BC. Small increases in the MTC may explain these modest increases. The wind speed appears to be the most significant forcing function that influences the magnitude of the naphthalene emission rate (see column 5). Its impact occurs through enhanced MTCs. In low flowing streams, the wind velocity is a major factor in creating enhanced water turbulence. This forced "stirring" of the waters elevates the magnitudes of the individual MTCs both on the air-side and the water-side of the air-water interface as well as at the bottom sediment interface. The three MTCs' relationships with the wind speed variable are given as Equations 3.34, 3.35, and 3.36 later in this chapter.

Exposed dredged material CDF emissions model

Upon performing a literature review and model simulation of the subject, it was found that the chemical vaporization process for drying DM solids was in a poor state of development. Model predictions to air from natural soils and unsaturated sediments for chemicals found in bed sediment were 10X to 100X greater than the reported laboratory and field flux data. In addition, data existed for one field-scale experiment that simulated chemical vaporization from a drying DM. Modeling of the data was problematic (see Appendix 1A). Based on these findings, it was decided to perform a large-scale wind tunnel vaporization experiment with IHC DM in order to better understand the process.

The outcome of the project was judged to be very successful. A consistent set of flux data was obtained for three PAHs that provided the basis for a better understanding of the combined bed drying and chemical vaporization mechanism. Based on this outcome, it was possible to construct a satisfactory emission model for a CDF in receipt of DM solids. The reader is referred to Chapter 2 for details of the emission model (Fountain et al. 2005).

Ponded CDF emission model

Model overview

In the case of hydraulic dredging, the dredge facility (consisting of the extraction machine and the DM slurry operation) is intimately connected to the CDF. These connections are illustrated in Figure 3-8. At the dredge site, the DM is mixed with water to form Q_{ds}, which is the flow of solids and water from the DOU. The solid-to-water ratio is selected so that the slurry can be easily pumped to the CDF through a pipeline. From experience, such ratios are well established. Make-up water, Q_M, from the stream or embayment may be used to create the appropriate ratios. A portion of this stream eventually emerges from the discharge of the CDF and must be treated prior to entering the waterway. Since water treatment is costly, the CDF discharge can be wholly eliminated during steady-state operations by recycle water as shown in Figure 3-8. Ideally, only during dewatering of the CDF at the end of the dredging season is water discharge treatment required.

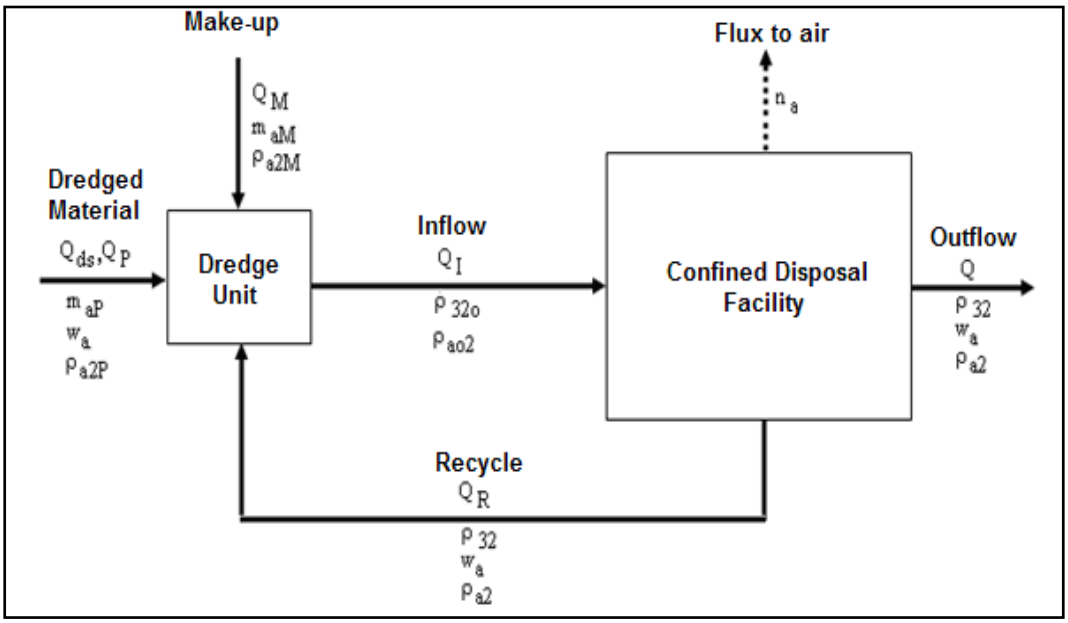

Figure 3-8. Conceptual illustration of dredge-slurry unit and the CDF operations.

During dredging, the slurry exit stream flows into the CDF entrance. Within the CDF, suspended solids are removed from the water column by settling to the bottom. Sand separates first, followed by the silt size particles, and finally the clay fraction settles. Most of the material flows to the bottom of the CDF as a density flow. Only about 10% of the fines are

suspended in the CDF pond. The material then flocculates and settles. The density flow on the bottom densifies and settles as a mass or layers and expels water to the pond. A shallow sloping sediment-water surface (i.e., delta) develops along the length of the CDF from the entrance to discharge. Figure 3-9 illustrates this process. A water column exists within the CDF, and the surface in contact with the air is the source of the volatile chemical emissions. Weirs or other level control devices maintain a fixed water elevation. In most operations this is true but not in the recirculation option for IHC. As time progresses during the dredging season, solid material slowly replaces the water mass and the average water column depth decreases. Upon reaching its design capacity, any remaining water is drained and the DM is allowed to consolidate and stabilize before final closure. From a daily operation perspective and for the seasonal operation as well, many aspects of the CDF operation are transient. Concentrations of chemical and suspended solids are constantly changing with time.

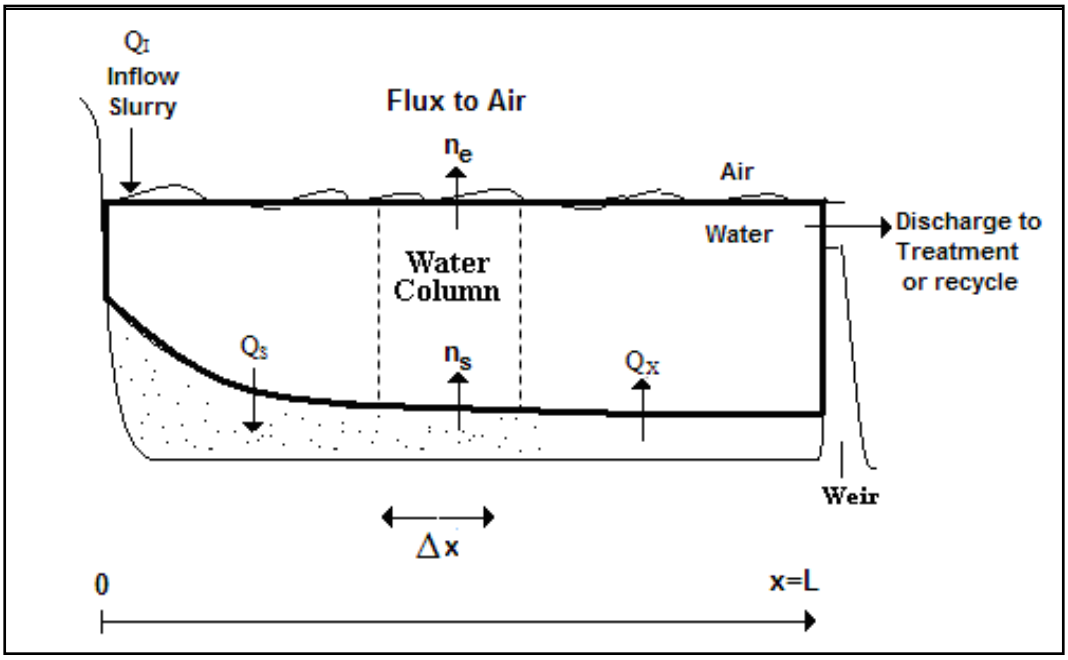

Figure 3-9. Ponded CDF profile view.

Most of these fluctuations are unknowable and therefore unpredictable. The approach in the modeling effort will be to assume a steady-state operation and to accommodate variable changes that capture the most conservative emission predictions. For example, the hydraulic flow model for the water through the CDF will be assumed to be plug flow. This model maximizes the chemical concentrations in the water column, which in turn maximizes the emissions to air. Since the water column depth is known to

change slowly over time, simulations of emissions at least at two depths, one at start and another shallow, operated at steady-state will bracket the hydraulic retention times that are known to affect the emission rates.

The following section contains the details of the model developed for estimating emissions from a ponded CDF. In the development, assumptions will be needed; they have been chosen so as to maximize the model predicted fluxes. The model consists of three simultaneous mass balances; solids, water, and chemical. Once a single final algorithm is produced that represents the chemical flux for a CDF operating with water recycle, however, it can be used for the so-called conventional CDF operation that has a once-through or one-pass water use. This case is simulated by setting the recycle stream flow rate to zero; in Figure 3-8, $Q_R = 0$.

Solids balance

The dredge extracts material (i.e., solids and water) from the bed at a constant volumetric rate of Q_{ds} (m^3/s). A fraction of this volumetric flow consists of pore water that can be defined by Q_P (m^3/s). The remainder is dry solids of rate m_P (kg/s). In order to meet the slurry pumping requirements of solids-in-water concentration ρ_{320} (kg/m^3), the solids mass balance around the dredge slurry unit shown in Figure 3-9 is:

$$m_P + m_M + m_R = Q_I \rho_{320} \tag{3.27}$$

where Q_I is the volumetric water rate entering the CDF (m^3/s). The additional dry solids rates on the left-hand side of Equation 3.27 are, m_M, make-up water solids (kg/s) and, m_R, recycle water solids (kg/s). This result can be solved for Q_I; typically, the solids in the make-up and recycle water are insignificant in comparison to the dredged solids. A typical value for ρ_{320} is 170 kg/m^3.

Water balance

For the dredge slurry-unit facility, the steady-state water volumetric balance is:

$$Q_P + Q_M + Q_R = Q_I \tag{3.28}$$

where, if no recycle is used, $Q_R = 0$. As shown in Figure 3-8, the recycle stream reconnects the dredged slurry unit with the CDF. The water flow from the DOU can be evaluated as follows:

$$Q_P = Q_{ds}\varepsilon_2 \tag{3.29}$$

where ε_2 is the water volume fraction in the DM. The Q_{ds} can be determined for a mechanical dredge by estimating the bucket volume of sediment excavated and the cycle time of the dredge bucket. Other water flows include precipitation inputs such as rain or snow and outputs such as evaporation. It is assumed that these are approximately equal, so they balance each other and do not appear in the Figure 3-8.

The CDF water balance is slightly more complex. Some internal flows are important; see Figure 3-9. As the slurry enters the CDF, the solid particles quickly settle forming a mud layer that moves along the bottom, which consists of a high solids-to-water ratio with initial bed water porosity, ε_I. This ratio results in the temporary capture of much water between the settling particles at a rate of Q_S (m^3/s). This flow is considered an outlet flow. The control volume for the water balance is the dark solid line in Figure 3-9. As shown, it includes the water column above the newly deposited solid surface. As time proceeds, bed consolidation occurs in which the particles pack together by gravity, thus eliminating pore water (a process termed bed consolidation). The final bed water porosity, ε_F, results and produces a return flow of pore water upward as shown in Figure 3-9. This rate of expressed water-flow entering the water column from the bed contraction process is Q_X (m^3/s). The difference between Q_S and Q_X is called the "bulking losses" water rate Q_B, which has a net downward flow into the bed (see Figure 3-9). In effect, this portion of the slurry water accumulates and remains in the CDF bottom sediment as pore water. The CDF water steady-state balance is:

$$Q_I = Q_R + \left(Q_S - Q_X\right) \tag{3.30}$$

where

$$Q_B \equiv Q_S - Q_X = \frac{Q_\Gamma \rho_{32o} \varepsilon_\Gamma \left[1 - \left(\varepsilon_I - \varepsilon_F\right)\right]}{\rho_3 \left(1 - \varepsilon_I\right)} \tag{3.31}$$

and ρ_3(kg/m3) is the particle density of the consolidated bed. The other terms have been defined above.

The consequence of the bulking loss is relevant to the chemical mass balance. They represent a chemical mass accumulation and advection exchanges across the sediment-water interface, which impacts the effective water column chemical concentration and the volatile emission rate. These flows enter the chemical mass balance discussed next.

Chemical mass balance

In Figure 3-9 the CDF includes a control volume (CV) element as a portion of the water column. It has dimensions of length = (Δx), height = water depth (h), and width (w), all in units of meters. Performing a steady-state chemical balance on this CV allows for a quantitative description of the concentration in the water. The hydraulic flow is from left-to-right through the differential volume. Conceptually, the mass balance for volatile chemical A includes the following processes:

1. Advective inflow at position x,
2. Inflow of expressed pore water from the bed,
3. Diffusion-type mass transfer from bed surface into the water column,
4. Advective outflow,
5. Settling solids captured water outflow,
6. Evaporation to air, and
7. Reaction degradation in the water column.

Since the dredge-slurry unit is connected to the CDF by two streams as shown in Figure 3-9, two concentrations, ρa2 and ρ_{a02}, in the recycle and inflow streams, respectively, are unknown. Separate mass balance around each unit yields two equations which, when solved simultaneously, yield simple chemical algorithms for these parameters. A chemical mass balance on the differential CV is integrated from the inlet at x=0 with concentration ρ_{a02} to yield the following result for the concentration profile across the length of the CDF to the discharge point at x=L:

$$\rho_{a2}(x) = f_2(x)\,\rho_{a02} + \left(f_2(x) - 1\right)\cdot \rho_{a2P}\left(\frac{\alpha_2}{\beta_1 - \alpha_1}\right) \qquad (3.32a)$$

where

$$f_2(x) = \left(\frac{\beta_2 L - \beta_1 x}{\beta_2 L} \right)^{\left(\frac{\alpha_1}{\beta_1} - 1 \right)} \quad (3.32b)$$

$$\rho_{a02} = \rho_{a2P} \left(\frac{Q_P + m_p K_{a32}}{dn \cdot Q_I} \right) + \rho_{a2M} \left(\frac{Q_M}{dn \cdot Q_I} \right) + \rho_{a2L} \left(\frac{Q_R}{dn \cdot Q_I} \right) \quad (3.32c)$$

The definitions of parameters are as follows:

$$\alpha_1 = {}^{i}K_{a2} + {}^{iii}K_{a2} + v_S + k_a^{iii} L$$

$$\alpha_2 = {}^{iii}K_{a2} + v_X$$

$$\beta_1 = \frac{Q_B}{L \cdot w}$$

$$\beta_1 = \frac{Q_I}{L \cdot w}$$

$$dn = 1 + \rho_{320} K_{a32}$$

$$\nu = \frac{Q_X}{L \cdot w}$$

$$\nu = \frac{Q_S}{L \cdot w}$$

The $''k_{A3}$ is the sediment-water MTC (m/s) and $^1K_{A2}$ the volatilization MTC (m/s). The other terms have been defined previously.

Conceptually, Equation 3.32 represents the chemical fate in the CDF. Assumptions inherent in the CDF chemical fate model represented by Equation 3.32 will be presented in the following section. Convenient assumptions that maximize the flux are to assume these include no degradation/reaction ($k_a''' = 0$) and no chemical in the atmosphere $\rho_{a2}** = 0$.

The chemical flux to air is obtained by the product of $'K_{a2}$ and ρ_{a2}. Since ρ_{a2} varies from inlet to CDF outlet, the flux must be summed at each point

along the length (i.e., integrated) and multiplied by the CDF area to obtain the mass emission rate:

$$W = {}'K_{a2} Lw\left[\overline{\rho}_a - \rho_{a2}^{**}\right] \tag{3.33}$$

where $\overline{\rho_a}$ is the average concentration, L is the CDF length, and w is the CDF width. The emission rate, W, is in kg/s.

The next section presents the relationships needed to obtain the various MTCs used in Equation 3.32. As noted above, the solid associated chemical was included in the mass balance. However, a solids balance that includes particle settling rates was not performed. Field data based on observed TSS concentrations rather than solid balances estimates were used instead. The concentration of solid particles at the exit of the CDF is assumed to be negligible because of the hydraulic retention time of the liquid generally being quite large, which allows efficient particle settling (personal conversation with P. Schroeder 2005). The focus on the exit waters deals with the chemical in solution, which is the primary mass fraction.

Mass Transfer Coefficient correlations

With these process conditions within the CDF, the chemical concentration in the water column can then be estimated for use in calculating the evaporative flux. Chemical dissolution flux from the bed-sediment surficial layers is an input source to the water column. In chemical dissolution flux the MTC is estimated by the following expression:

$$K_{a32} = \frac{\frac{bC_D\rho_1}{\rho_2} v_1^2 h^{1.25}}{LM_a^{0.5}} \tag{3.34}$$

where b is the empirical constant 18.9 and the wind velocity drag coefficient, C_D, is 0.00166. The velocity of wind v_1 (m/s), density of air ρ_1 (g/cm^3) and water ρ_2 (g/cm^3), water column depth h (m), length of PCDF (L, m), and molecular weight of the chemical (M_a) are used to estimate the MTC in units of m/s (Becker and Thibodeaux 1982).

The individual MTC for the water/air interface is estimated using the local air-side and water-side MTCs (Thibodeaux 1996). These MTCs are then

combined with the well known two-resistance theory. An existing correlation for ethyl ether is used for the liquid-side MTC:

$$^{i}K_{a21ethylether} = 0.094 \cdot v_1^2 \tag{3.35}$$

An existing correlation for water evaporation from reservoirs is used to estimate the air-side MTC:

$$^{i}K_{a21watervapor} = 358 \cdot v_1^i \cdot A_S^{-0.05} \tag{3.36}$$

The MTC for both Equations 3.35 and 3.36 are given in cm/hr for a known wind velocity, υ_1 (m/s) or υ'_1 (mph), and CDF surface area, A_s (acre). Graham's Law may be used to convert both the coefficients to other chemicals.

Model application

A limited number of numerical simulations of naphthalene volatilization to air from a ponded CDF operation were performed. The purpose was to challenge the model with some realistic operational input data in order to obtain a response that could be used to judge the realism of the outputs in light of their expected behavior patterns. The simulations were generally based on data from the proposed CDF for the DM from the IHC in South Chicago, IL. DM is to be extracted at a rate of 250 yd^3/hr. A pumpable slurry with solids-to-water ratio of 170 kg/m^3 is desirable. The naphthalene average chemical loading concentration on the DM is 2.65 mg-A/kg-solid. The CDF is assumed to be 525 m in length, 263 m in width, and 3 m in depth. The water inflow is estimated at 1490 m^3/hr.

The two choices of water source for forming the pumpable slurry are from the waterway or from the CDF. The conventional operation employs once-through water that is taken from the waterway, used in the slurry operation, treated, then discharged back to the waterway. The alternative operation is to use water obtained from within the CDF near the outlet point, thereby eliminating some water treatment costs. Figure 3-10 illustrates the concentration profile for naphthalene in solution across the length of the CDF. For the base case described above at 25°C with a 10 mph wind, the concentration is 10 μg/L at the exit of the slurry discharge pipe. In order to maintain the 3 m water depth, 123 m^3/h water must be obtained from the waterway while recycling 1280 m^3/h from the CDF outlet. So called

"bulking losses" amount to 208 m^3/h, which remains in the CDF bed sediment. The inlet concentration of 10 µg/L gradually decreases in a nonlinear fashion with increasing distance and residence time within the CDF until it is 4.2 µg/L at the exit. The upper line denotes the maximum 10 µg/L entering concentration during dredging. The lower line at 2.9 µg/L is the uniform steady-state concentration in the water column resulting from the naphthalene dissolution from the bed sediment when the dredging operation ceases. The upper and lower lines are shown for reference to the actual profile line.

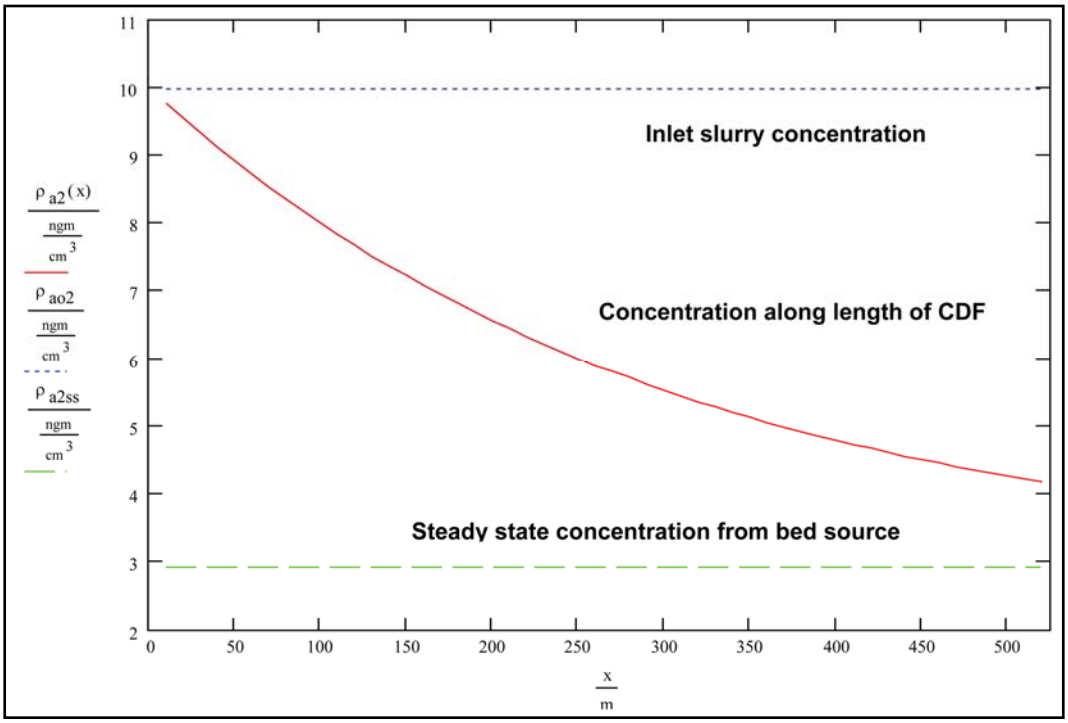

Figure 3-10. Concentration of naphthalene in a ponded CDF.

Numerical results of simulations appear in Table 3-5. The naphthalene emission rate for the recycled water conditions described above is 276 gm/day. The emission rate for the conventional operation, which uses naphthalene-free water rather than the 4.2 µg/L water at the CDF exit, is very similar at 274 gm/day. These two conditions of recycle are repeated for all parameters as no and yes in column 3; the rates appear in column 4 of the table. The model suggests that using recycle water containing quantities of naphthalene will not significantly enhance the emission rate. This lack of enhancement occurs because there is a very significant mass of naphthalene entering with the incoming slurry from the dredge but

insignificant amounts entering with the recycle water of concentration 0.0042 mg/kg. Guidance for interpreting the results in Table 3-5 follows.

Seven parameter perturbations were simulated; they appear in column 2 of Table 3-5. The resulting emission rates appear in column 5. Column 6 is the percentage change in the rate compared to the base cases. As given in case 1 of Table 3-5, doubling the solids-to-water ratio decreases the emissions by 21%. With a higher solids ratio, less water-soluble naphthalene enters because less water enters the CDF; this lowers the emission rate. Due to particle settling, the slurry solids entering form a layer of solids on the bottom of the CDF. Naphthalene dissolves from this bottom layer, and this process contributes to evaporation as well. Turning the bed source off numerically lowers the emission rate to 248 gm/day. Therefore, the bottom bed-sediment source of naphthalene in the CDF accounts for 9.5% of the volatiles released while the CDF is receiving the DM slurry.

Table 3-5. Naphthalene volatilization rate simulations.

Case	Parameter	Recycle	Base Rate gm/day	Rate gm/day	% Change
1	Slurry solids-to water 170 to 340 kg/m^3 Bed Source turned off	No Yes No	274 276 274	216 217 248	-21 -21 -9.5
2	Water column depth 3 to 6 m Bed Source turned off	No Yes No	274 276 274	302 304 249	10 10 -9.5
3	Dredge Extraction rate 250 to 500 yd^3/hr 0 yd^3/ht	No Yes -	274 276 274	334 337 134	22 22 -51
4	Surface area of CDF 34 to 68 acres	No Yes	274 276	404 405	47 47
5	Wind velocity 10 to 20 mph	No Yes	274 276	694 702	153 154
6	Wind and Depth 10 mph/3m to 20mph/6m	No Yes	274 276	959 961	250 250
7	Bed sediment concentrator 2.65 to 5.3 mg/kg	No Yes	274 276	549 550	100 100

Simulation case 2 involves a doubling of the CDF water column depth. A 10% increase in the emission rate occurs; see Table 3-5. This increase occurs because the additional water mass in the CDF increases mass of the soluble naphthalene available for evaporation.

Simulation case 3 involves a doubling of the contaminated sediment extraction rate. This doubling results in only a 22% increase in the evaporation rate. In doubling the dredging rate from 191 to 382 m^3/day (250 to 500 yd^3/day), the rate of water slurry formation is doubled as well. Although twice the mass-rate of naphthalene enters the CDF, the maximum solubility cannot be exceeded. The average level of soluble naphthalene concentration does increase in the CDF waters, which results in the 22% increase in emissions to air.

Simulation case 4 involves doubling the surface area of the CDF from 13.75 to 27.52 hectares (34 to 68 acres) of ponded water. Only a 47% increase in emissions occurs. Doubling the area also doubles the volume. As the volume doubles, the concentration within is lower since the mass of naphthalene entering with the DM remains the same. The net result is only a 47% increase in the mass emission rate of naphthalene to the air.

The remaining three simulation cases reflect environmental factors that affect the emission rate rather than CDF operational factors. Whereas the operators of the CD have a degree of control over the slurry, depth, extraction rate, and pond area, the environmental factors are beyond operator control. These factors include the wind speed and the loading level of naphthalene on the DM. A dramatic increase occurs with increasing wind speed. Doubling the wind speed resulted in a 150% increase in emissions. Wind speed directly affects water column turbulence, which favors higher transport coefficients both at the air-water interface and the sediment-water interface in a highly nonlinear fashion. As shown in simulation case 6, combining increases in both wind and water depth escalates the release rates. An increase of 250% results. Case 7 behaves as expected, however. As the bed-sediment concentration doubles, so do the emission rates.

When dredging ceases, the DM slurry no longer delivers a naphthalene load to the water column. However, the bottom of the CDF is covered with sediment solids with essentially the same chemical loading as is the entering DM. Dissolution of naphthalene from this sediment source continues to contribute a concentration to the water column, which in turn evaporates. At steady-state this concentration is 3.0 μg/L and the rate is 134 gm/day. As shown in case 3 of Table 3-5, this mass release quantity is down 51% of the normal BC emission rate of 274 gm/day. The CDF model contains the steady-state algorithm for obtaining this rate when dredging ceases.

Summary, conclusions, and recommendations

The models provided in this document have been developed to aid in the planning of dredging operations by demonstrating methods used to determine chemical emissions to air. In dredging, sources of significant emissions can be found in two locations; the DOU and the CDF. Significant progress has been made in the modeling of volatile emissions to air since Thibodeaux (1989). This progress is based in large part on laboratory research and field studies performed by the ERDC/Environmental Laboratory, Vicksburg, MS in collaboration with the Department of Chemical Engineering, Louisiana State University, Baton Rouge. The combined work has led to a much better understanding of the processes underlying the chemodynamics of volatilization from operations and activities associated with the dredging and disposal of contaminated sediments. Highlights of this work were studies focused on the thermodynamics of the multiphase chemical partitioning between solid particles, water and air and the need for site-specific experimental data to support and fine tune general predictive algorithms. Follow-on kinetic studies with laboratory-scale simulation and field experiments verified the partitioning role and gave insight into the importance of transport kinetics in the three-step process.

This work provided key information and detailed understanding of the unit operations necessary to conceptualize the appropriate chemodynamic models for developing quantitative descriptions of the various chemical and physical processes. Conventional approaches using completely-mixed and plug flow reactor concepts were employed in model development. In all cases the Lavoisier species mass balance was used to formulate the steady-state models. Although the general model approaches and concepts used in model construction are well established and theoretically sound, some processes and process parameters reflecting key chemical fluxes remain in a crude state of technical understanding and development.

This chapter represents a synthesis of that accumulated knowledge focused onto developing an upgrade of the earlier 1989 models. What follows is a summary of the progress made and the challenges remaining in the development of modeling tools for making design estimates of volatile chemical emissions from dredging and disposal of contaminated sediments. Site conditions at the IHC were adapted and modified, then used to test the proposed calculating algorithms and procedures, thus providing numerical results as a reality check. The status of the models developed for

three emission locales will be presented and include: the DOU emission locale model, the exposed DM confined disposal facility (EDM-CDF) emission local model, and the ponded dredge material confined disposal facility (PDM-CDF) emission model.

The DOU model

The DOU model was partitioned into three main scenarios that include: (1) emissions from dredging enclosed rivers, (2) emissions from rivers without enclosures, and (3) emissions from embayments. In each of these models, the chemical emissions consisted of an area producing a constant source of volatile emissions and another producing a plume of chemical either downstream in the case of the river or radial dispersion of chemical in the case of an embayment. In order to perform these calculations, these areas of chemical release were categorized into two zones: forced and natural convection.

The *forced convection zone* includes the area near to the dredge and its operations for which mass transfer is influenced by the disturbance in the water column and at the benthic layer by the dredge head. This zone is comprised of MTCs for wind, hydraulic flow, and dredge disturbance.

The *natural convection zone* beyond the dredge forced zone consists of the areas of dredging that do not have enhancements due to the dredge disturbances in the water. Techniques and algorithms were provided in order to estimate these MTCs primarily for the dredge interaction with the chemical release. Methods for evaluating the area of the convective zones as well as the area of the DOU were provided for using the equations in calculating the chemical flux.

Some major weaknesses of the DOU model involve the dredge device particle and chemical generation process. Whereas some good quality data exist on the mass of sediment re-suspension produced, little is known about the chemical kinetics of release from particles or the MTCs controlling evaporation. To skirt one of these knowledge gaps, equilibrium chemical partitioning between solid particles and water is assumed. This approach is commonly used but is known to be overly conservative and results in high soluble concentrations in the water column and fluxes to air. In the case of dredge-machine-generated vaporization MTCs, none exists. The analogous process approach adopted in this report for estimating these MTCs provides at best only crude ranges of values. Research

aimed at understanding and quantifying both the particle-to-water release kinetics and the dredge influenced MTCs are needed in order to reduce the large uncertainties inherent in the magnitudes of the emission estimates. Both laboratory simulations and field-scale process studies are needed. Simultaneous studies on particle size distributions and their settling characteristics will be needed to support the kinetics and MTC studies. The focus should be primarily aimed at the forced convection zone near the dredge unit. In addition field-scale vaporization measurements around both mechanical and hydraulic dredges are needed to provide sets of realistic data with which to verify the emission model predictions.

The EDM-CDF model

This type of CDF receives DM approximately at in-situ water content, which is spread to form a drying-mud surface layer. As a generic type, this emission locale has received considerable study over the past 15 or so years. Its status has benefited much from chemical evaporative studies of pesticides applied to agricultural soils and hazardous waste applied to surface soils and landfarms for both treatment and disposal. The theoretical modeling approaches used are nearly identical to those proposed for chemical emissions from drying DM beds. Pilot-scale field and wind tunnel studies have been conducted at ERDC to investigate the unique features of the chemical emission from this source material (Ravikrishna et al. 2001). A key finding was the significant role which co-extracted pore water plays in a drying-consolidation process and its influence on the chemical vaporization flux. Including this key aspect, the basic soil emission model has been modified and was found to work well at the pilot-scale level. Sets of field-scale vaporization measurements using various types of DM are needed to verify predictions of this recently developed model.

The PDM-CDF model

This disposal option consists of a dredge unit producing a DM aqueous slurry connected by pipeline to a settling pond that retains the solids and has a means of recycling pond discharge water back to the dredge unit. Formulated hydraulically as a plug-flow evaporative-settling reactor, the modeling of this combined dredge-pond process followed a conventional approach. Chemical emission models for surface impoundments have been available for general use for more than 25 years and enjoy a high degree of development and numerous verification studies. However, one particular

challenge for the slurry discharge aspect of this ponded emission device was the realistic characterization of the density-driven flow of material that occurs near the bottom of the pond. A dense mud layer "densifies" as it moves along and expels water that mobilizes chemicals to the water column from which volatilization occurs. A better understanding of the water expelling process and the associated dissolution mass-transfer process across the semi-solid water interface would reduce the uncertainties associated with the present model formulation. Laboratory and field studies are needed to isolate and examine the settling-densifying process and the associated chemical mass-transfer. In addition volatilization measurements are needed on several pond types to provide independent checks on the model predictions of emission fluxes.

References

Becker, B., and L. J. Thibodeaux. 1982. Chemical transport rates near the sediment of a wastewater impoundments. *Environmental Progress* 1(4): 296-200.

Cohen, Y., H. Taghavi, and P. A. Ryan. 1988. Chemical Volatilization in Nearby Dry Soils under Non-Isothermal Conditions. *J. Environ. Qual.* 17(2): 198-204.

de Seze, G., K. T. Valsaraj, D. D. Reible, and L. J. Thibodeaux. 2000. Sediment-air equilibrium partitioning of semi-volatile hydrophobic organic compounds. Part 1. Method development and water sorption isotherm. The Science of the Total Environment. 253, 15-26. Part 2. Saturated vapor pressure, and effects of sediment moisture content and temperature on the partitioning of polyaromatic hydrocarbons. *The Science of the Total Environment*. 253: 27-44.

DiGiano, F. A., C. T. Miller, and J. Yoon. 1993. Predicting release of PCBs at point of dredging. *J. Environ. Eng*. 119: 72-89.

Estes, T. J., P. R. Schroeder, W. R. Loikets, E. R. Taylor, V. Agrawal, C. Caine, and R. Gallas. 2003. Indiana Harbor and Canal (IHC) Dredging and Disposal Alternatives Analysis – Evaluation of Relative Requirements, Emissions and Costs for Mechanical and Hydraulic Dredging Alternatives. Vicksburg, MS: U.S. Army Engineer Research and Development Center.

Estes, T. J., P. R. Schroeder, D. Druzbicki, D. C. Scharre, and R. Gallas. 2004. Indiana Harbor and Canal (IHC) Dredging and Disposal Alternatives Analysis – Mechanical Dredging Comparative Analysis. Vicksburg, MS: U.S. Army Engineer Research and Development Center.

Fountain, K. F., L. J. Thibodeaux, K. T. Valsaraj, R. Ravikrishna. 2005. PAH Volatilization From Dredged Material Under IHC/CDF-Like Conditions: Wind Tunnel Flux Measurements and Modeling. 179p

Gulliver, J. 2005. University of Minnesota, Department of Civil Engineering Minneapolis, MN.

Hayes, D. F., and P. Y. Wu. 2001. Toxic Constituent Losses During Dredging of Contaminated Sediments. Paper presented at EPA Superfund Workshop on Contaminated Sediments, Alexandria, VA, May 30-June 1, 2001.

Jury, W. A., R. Grover, W. F. Spencer, and W. J. Farmer. 1980. Modeling Vapor Losses of Soil-Incorporated Triallate, *Soil Sci. Soc. Amer. J.* 44: 445-450.

Jury, W. A., W. F. Spencer, and W. J. Farmer. 1983(I), 1984a(II), 1984b(III), 1984c(IV). Behavior Assessment Model for Trace Organics in Soil. I. Model Description. *J. Environ. Qual.* 12(4): 558. II. Chemical Classification and Parameter sensitivity. *J. Environ. Qual.* 13(4): 567-572. III. Application of Screening Model. *J. Environ. Qual.* 13(5), 573-578. IV. Review of Experimental Evidence. *J. Environ. Qual.* 13(4): 1984-1986.

Malcolm Pirnie/TAMS-Earth Tech. 2003. Engineering Performance Standards Hudson River. Part 1: Dredging Resuspension-Attachment D. Public Draft-May 2003, 1-76.

Mayer, R. J. Letey, and W. J. Farmer. 1974. Models For Predicting Volatilization of Soil-Incorporated Pesticides. *Soil Sci. Soc. Amer. Proc.* 38: 563-568.

Qaisi, K. M., W. D. Constand, and L. J. Thibodeaux. 1997. Impact of Barge Traffic on stream reaeration: Laboratory Experiments. *J. Environ. Engineering* 123(7): 716-719.

Ravikrishna, R., C. Price, S. Yost, K. T. Valsaraj, J. M. Brannon, and L. J. Thibodeaux. 2001. Air emission flux from contaminated dredged materials stored in a pilot-scale confined disposal facility. *J. Air & Waste Management Association*. 51: 361-373.

Reible, D.D., D. Hayes, C. Lue-Hing, J. Patterson, N. Bhowmils, M. Johnson, and J. Teal. 2003. Comparison of long-term risks of removal and in situ management of contaminated sediments in the Fox River. *Soil and Sediment Contamination*, 12(3): 325-344.

Sanchez, F. F. 2001. A multimedia model for assessing chemical fate during dredging of contaminated bed-sediment. MS Thesis. Gordon and Mary Cain Department of Chemical Engineering, Louisiana State University, Baton Rouge, LA.

Sanchez, F. F., L. J. Thibodeaux, K. T. Valsaraj, and D. D. Reible. 2002. Multimedia Chemical Fate Model for Environmental Dredging. Practice Periodical of Hazardous, Toxic, and Redioactive Waste Management. April issue. American Society of Civil Engineering (ASCE) 120-128.

Schroeder, P. R. 2005. Vicksburg, MS: U. S. Army Engineer Research and Development Center.

Springer, C., K. T. Valsaraj, and L. J. Thibodeaux, Emissions of Volatile Organics Chemicals from Landfills and Waste Piles. 1984. Final Report to USEPA Municipal Environmental Research Laboratory Solid and Hazardous Waste Research Division. Cincinnati, OH. Dec. 1984.

Thibodeaux, L. J. 1989. Theoretical Models for Evaluation of Volatile Emissions to Air During Dredged Material Disposal with Applications to New Bedford Harbor, Massachusetts. Miscellaneous Paper EL-89-3, U.S. Army Engineer Waterway Experiment Station, Vicksburg, MS.

Thibodeaux, L. J., M. Poulin, and S. Even. 1994. A model for enhanced aeration of streams by motor vessels with application to the Seine river. *J. of Haz. Mats*. 37: 459-473.

Thibodeaux, L. J. 1996. *Chemodynamics- Environmental Movement of Chemicals in Air, Water, and Soil.* John Wiley, New York 1979. [ISBN 0-471-04720-1]

Thibodeaux, L. J., and K. T. Duckworth. 2001. The effectiveness of environmental dredging: A study of three sites. *Remediation*. Summer issue pp 5–33.

Thibodeaux, L. J., R. Ravikrishna, and K. T. Valsaraj. 2002. Volatilization rates from dredged material and soils-A literature review. Final Report. USACE, Chicago District. Vicksburg, MS: U.S. Army Engineer Research and Development Center.

Thibodeaux, L.J., H. Huls, R. Ravikrishna, K.T. Valsaraj, M. Costello, and D.D. Reible. 2004. “Laboratory Simulation of chemical evaporation from dredge-produced sediment slurries”, Environmental Engineering Science, vol 21, no.6, p. 730-740.

Valsaraj, K. T., R. Ravikrishna, B. Choy, D. D. Reible, L. J. Thibodeaux, C. B. Price, S. Yost, J. M. Brannon, and T. E. Myers. 1999. Air emissions from exposed contaminated sediments and dredged material. *Environmental Science & Technology* 33: 142-149.

Valsaraj, K. T., R. Ravikrishna, J. J. Orlins, J. S. Smith, J. S. Gulliver, D. D. Reible, and L. J. Thibodeaux. 1997. Sediment-to-air Mass Transfer of Semi-volatile Contaminants due to Sediment Resuspension in Water. *Advances in Environmental Research* 1(2): 145-156.

Appendix 3A: Glossary of Symbols

n_A	Mass flux of chemical A, (ng/cm²-hr)
ρ_{A2}	Chemical concentration in water, (ng/cm³)
ρ_{A2i}	Chemical concentration in water at air/water interface, (ng/cm³)
ρ_{A1i}	Chemical concentration in air at air/water interface, (ng/cm³)
ρ_{A1}	Chemical concentration in air, (ng/cm³)
ρ^*_{A2}	Equilibrium chemical concentration in air, (ng/cm³)
ρ^{**}_{A2}	Equilibrium chemical concentration in confined disposal facility (CDF) sediment pore water, (ng/cm³)
$^1k'_{A2}$	Local water-side mass transfer coefficient at air/water interface, (cm/hr)
$^2k'_{A1}$	Local air-side mass transfer coefficient at air/water interface, (cm/hr)
$^1k'_{A2FC}$	Local water-side mass transfer coefficient at air/water interface in the forced convection zone, (cm/hr)
$^1k'_{A2NC}$	Local water-side mass transfer coefficient at air/water interface in the natural convection zone, (cm/hr)
$^1k'_{A2D}$	Local water-side mass transfer coefficient at air/water interface accounting for dredge enhancement, (cm/hr)
$^1K'_{A2}$, $^{'}K_{A2}$	Overall water-side mass transfer coefficient at air/water interface, (cm/hr)
$^1K'_{A2FC}$	Overall water-side mass transfer coefficient at air/water interface in the forced convection zone, (cm/hr)

$^{1}K'_{A2NC}$	Overall water-side mass transfer coefficient at air/water interface in the natural convection zone, (cm/hr)
$^{3}k_{A2}$	Local sediment-side mass transfer coefficient at air/water interface, (cm/hr)
H_x	Equilibrium partitioning coefficient for chemical A at air/solid interface, (dimensionless)
K_{A32}, $^{''}K_{A3}$	Equilibrium partitioning coefficient for chemical A at solid/water interface, (L/kg)
K_{oc}	Partitioning coefficient of chemical A between octanol and water, (L/kg)
f_{oc}	Fraction of organic carbon within a particle, (dimensionless)
K_{A31}, $^{'}K_{A3}$	Equilibrium partitioning coefficient for chemical A at a solid/air interface, (L/kg)
A_F	Area of dredging operable unit (DOU) with enhanced total suspended solids (TSS) from dredging activity, (m^2)
A_N	Area of DOU without enhanced TSS from dredging activity, (m^2)
A_{DOU}	Total DOU area, (m^2)
D_{A2}	Diffusivity of chemical A in water, (cm^2/sec)
s	Surface renewal parameter (cycles/hr)
τ_{bucket}	Cycle time of the bucket
n'_{BO}	Oxygen mass flux (ng/cm^2-hr)
E	Specific power delivery efficiency, (dimensionless)
α	Dirty water to clean ratio, (dimensionless)

P	Nameplate horsepower, (hp)
T	Water temperature, (°C)
ρ_{A2FC}	Chemical concentration in water in forced convection zone, (ng/cm^3)
ρ_{A2NC}	Chemical concentration in water in natural convection zone, (ng/cm^3)
ρ_{32FC}	Suspended solid concentration in forced convection zone, (ng/cm^3)
ρ_{32NC}	Suspended solid concentration in natural convection zone, (ng/cm^3)
w_a	Chemical loading concentration for bed sediment, (mg/kg)
ρ_{32}	Suspended solid concentration in water, (ng/cm^3)
ρ_b	Bulk density of sediment (gm/cm^3)
n_{ADOUNC}	Chemical flux from natural convection area of DOU, (ng/cm^3-hr)
n_{ADOUFC}	Chemical flux from forced convection area of DOU, (ng/cm^3-hr)
ρ'_{A2NC}	Downstream chemical concentration, (ng/cm^3)
τ	Retention time, (1/hr)
h	Height of water column, (m)
n_{ADS}	Chemical flux from downstream area of DOU, (ng/cm^3-hr)
r_o	Radius of forced convection zone, (m)
ρ^o_{A2}	Chemical concentration in solution in forced convective zone of radial plume dispersion, (ng/cm^3)

D_{A2y}	Horizontal diffusivity of the chemical, (ft^2/s)
r	Radial distance of plume/embayment from forced zone, (m)
$\rho_{A2}(r)$	Chemical concentration in water in natural convection zone at distance r from forced convective zone, (ng/cm3)
ρ_{A2SS}	Steady-state chemical concentration in water in natural convection zone at outer boundary distance from forced convection zone, (ng/cm3)
K_o	Modified Bessel function of the second kind, (dimensionless)
P	Delivered mechanical power, (hp)
ε_1	Sediment air filled porosity, (dimensionless)
D_e	Effective diffusivity of chemical A, (cm^2/hr)
C_A	Chemical concentrations in air exiting wind tunnel, (ng/m^3)
Q_1	Air volumetric flowrate, (m^3/s)
N_A	The chemical flux to air, (ng/m^2-h)
C_S	Chemical concentration at surface of sediment, (mg/kg)
t_b	Time when the water layer is effectively absent from DM surface, (hr)
t_D	Time when surface is dry of water and pore spaces are primarily air-filled, (hr)
t'_d	Surface drying time, (hr)
n	Number of patches, (patches)
C_f	Flux calibration factor to exposed DM, (dimensionless)
Q_P	Water flowrate from dredge site, (ft^3/s)

ρ_{aP2}	Chemical concentration in water in pore water at DOU site, (ng/cm^3)
Q_B	Flowrate of bulking losses to confined disposal facility (CDF) sediment, (ft^3/s)
Q_X	Flowrate of pore water from CDF sediment, (ft^3/s)
Q_S	Flowrate of water to CDF sediment, (ft^3/s)
Q_R	Flowrate of recycle from CDF, (ft^3/s)
Q	Total flow of dredged material (DM) from sediment to the barge, (ft^3/s)
ε_2	Water porosity in sediment at the DOU site, (dimensionless)
ε_I	Initial water porosity of sediment/mud at CDF site, (dimensionless)
ε_F	Water porosity in sediment/mud at CDF site after consolidation, (dimensionless)
v_s	Velocity of inlet water flowing into sediment bed from particle settling process, (m/s)
v_x	Velocity of CDF pore water flowing into water column from consolidation process, (m/s)
A_s	Surface area of CDF, (m^2)
b	An empirical constant, (dimensionless)
C_D	Drag coefficient, (dimensionless)
ρ_2	Density of water at design conditions, (g/cm^3)
l	Length of ponded CDF (PCDF), (m)
M_a	Molecular weight of chemical, (gm/mol)

v_1	Wind velocity, (m/s)
v'_1	Wind velocity, (mph)
Q_{ds}	DM volumetric flowrate from DOU bottom, (ft^3/s)
m_M	Solids in water used to create slurry, (mg/kg)
m_P	Solids in water of stream from dredge site, (mg/kg)
m_R	Solids in water of recycle stream, (mg/kg)
ρ_3	Particle density, (gm/cm^3)
Q	Water volumetric flowrate, (ft^3/s)
ρ_{ao2}	Chemical concentration at x=o entrance to CDF, (ng/cm^3)
ρ_{32o}	Suspended solid concentration at entrance to CDF, x=o, (ng/cm^3)
A_{stot}	PCDF surface area, (m^2)

Appendix 3B: Input to DOU Model Sample Calculations

Chemical Properties

$w_A := 3380 \cdot \frac{mg}{kg}$ "Sediment loading concentration in DOU (mg/kg)"

$\rho_{Astar} := 0 \frac{kg}{L}$ "Chemical concentration in air above DOU (mg/L)"

$K_{A32} := 260 \frac{L}{kg}$ "Sediment/Water partition coefficient for chemical A (L/kg)"

$D_{A2} := 7.5 \cdot 10^{-6} \frac{cm^2}{s}$ "Diffusivity of chemical A in water (cm^2/s)"

$H_x := 0.01980$ "Henry's constant for chemical A (unitless)"

Mass Transfer Coefficients

$k_{A1} := 3.476 \times 10^{3} \frac{cm}{hr}$ "Air-side at air/water interface MTC of chemical A (cm/hr)"

$k_{dredge} := 3 \frac{cm}{hr}$ "Liquid-side at air/water interface MTC of chemical A from dredge (cm/hr)"

$k_{flow} := 0.046 \cdot \frac{cm}{hr}$ "Liquid-side at air/water interface MTC of chemical A from water flow (cm/hr)"

$k_{wind} := 1.611 \cdot \frac{cm}{hr}$ "Liquid-side at air/water interface MTC of chemical A from wind flow (cm/hr)"

$'K'_{A2} := 1.618 \frac{cm}{hr}$ "Overall natural surface liquid-side at air water interface MTC of chemical A (cm/h

$'K_{A2} := 4.362 \frac{cm}{hr}$ "Overall forced surface liquid-side at air water interface MTC of chemical A (cm/hr

DOU Specification

$\rho_{32NC} := 50\frac{gm}{L}$ "TSS in natural zone of DOU (gm/L)"

$\rho_{32FC} := 500\frac{gm}{L}$ "TSS in forced zone of DOU (gm/L)"

$Q_w := 0.5\frac{m^3}{s}$ "Total river water volumetric flowrate (m^3/s)"

$v_{wind} := 9.261mph$ "Wind velocity (mph-no units for input)"

$w := 100m$ "Width of DOU (m)"

$h := 15m$ "Height of water column in DOU (m)"

$v_{water} := 7.456 \times 10^{-4} \cdot mph$ "Velocity of water into DOU (m/s)"

$A_{DOU} := 1569m^2$ "Area of DOU (m^2)"

$\tau_{DOU} := 13.075hr$ "Residence time for flow in DOU (hr)"

$P_D := 300hp$ "Power of dredge (hp)"

$A_{FDOU} := 473.8m^2$ "Area of forced convective zone in DOU (m^2)"

$A_{NDOU} := 1095.2m^2$ "Area of natural convective zone in DOU (m^2)"

$\tau_{FDOU} := 3.948hr$ "Residence time for flow in foced zone of DOU (hr)"

$\tau_{NDOU} := 9.127hr$ "Residence time for flow in natural zone of DOU (hr)"

Appendix 3C: Input to PCDF Model Sample Calculations

Chemical Properties

$K'_{a32} := 260\frac{L}{kg}$ "Chemical partition coefficient from sediment to water (L/kg)"

$H_\rho := 0.0198$ "Henry's constant for chemical (dimensionless)"

$w_a := 2.65\cdot\frac{mg}{kg}$ "Dredge area sediment loading concentration (mg/kg)"

Mass Transfer Coefficient

$'k_{a21ee} := 1.878\frac{cm}{hr}$ "Liquid-side local mass transfer coefficient for ethyl ether (cm/hr)"

$'k_{a21} := 1.395\frac{cm}{hr}$ "Liquid-side local mass transfer coefficient for chemical A (cm/hr)"

$"k_{a12wv} := 2996.5\frac{cm}{hr}$ "Gas-side local mass transfer coefficient for water vapor (cm/hr)"

$"k_{a12} := 1.341\times 10^3\frac{cm}{hr}$ "Gas-side local mass transfer coefficient for chemical A (cm/hr)"

$'K_{a2} := 1.325\frac{cm}{hr}$ "Mass transfer coefficient from water to air (cm/hr)"

$"K_{a3} := 3.095\frac{cm}{hr}$ "Mass transfer coefficient from sediment to water (cm/hr)"

DOU Specification

$\rho_3 := 2.41\frac{gm}{cm^3}$ "Particle density of dredged material (gm/ml)"

$\rho_b := 1.1\frac{gm}{cm^3}$ "Bulk density of dredged material (gm/ml)"

$Q_{ds} := 250\frac{yd^3}{hr}$ "Dredge rate (yd^3/hr)"

$\varepsilon_2 := 0.7$ "DOU water porosity of dredged sediment (dimensionless)"

$\varepsilon_I := 0.7$ "Initial CDF water porosity of dredged sediment (dimensionless)"

$\varepsilon_F := 0.3$ "Final CDF water porosity of dredged sediment (dimensionless)"

$A_{stot} := 35.1acre$ "CDF total surface area (acre)"

$A_s := 1acre, 2acre .. A_{stot}$ "CDF surface area interval and range for final mass evaporation rate (acre)"

$v_1 := 10mph$ "Wind velocity in the x-direction (mph)"

$Q_P := 1.312\frac{ft^3}{s}$ "Dredge site pore water volumetric flowrate (ft^3/s)"

$m_P := 38421.1\frac{gm}{s}$ "Dredge site solid mass flowrate (gm/s)"

$\rho_{32o} := 170\frac{gm}{L}$ "Suspended solids concentration in influent (gm/L)"

$Q_I := 7.981\frac{ft^3}{s}$ "CDF water volumetric flowrate (ft^3/s)"

$Q_S := 2.878\frac{ft^3}{s}$ "Water volumetric flowrate to CDF sediment (ft^3/s)"

$Q_X := 1.151\frac{ft^3}{s}$ "Water volumetric flowrate to water column from consolidation (ft^3/s)"

$Q_B := 1.727\frac{ft^3}{s}$ "Water volumetric flowrate to water column from consolidation (ft^3/s)"

$Q_R := 6.254\frac{ft^3}{s}$ "Recycle water volumetric flowrate (gm/s)"

$Q_M := 0.415\frac{ft^3}{s}$ "Makeup water volumetric flowrate (ft^3/s)"

$m_M := 0\frac{gm}{s}$ "Makeup water solid mass flowrate (gm/s)"

$m_D := 38.421\frac{kg}{s}$ "Total dredge solids flowrate (gm/s)"

$v_x := 0.083\frac{cm}{hr}$ "Water velocity in the x-direction (m/s)"

$v_s := 0.207\frac{cm}{hr}$ "Water velocity in the x-direction (m/s)"

$\rho"_{a2} := 0\frac{mg}{L}$ "Chemical concentration in air above CDF (mg/L)"

$\rho_{a2P} := 10.192\frac{ngm}{cm^3}$ "Chemical concentration in sediment pore water at dredge site (ngm/cm^3)"

$\rho_{32} := 8.764\times 10^3.\frac{ngm}{cm^3}$ "Suspended solids concentration in basin (mg/L)"

REPORT DOCUMENTATION PAGE

Form Approved
OMB No. 0704-0188

1. REPORT DATE *(DD-MM-YYYY)*	2. REPORT TYPE	3. DATES COVERED *(From - To)*
April 2008	Final report	

4. TITLE AND SUBTITLE
Investigations of the Controlling Factors for Air Emissions Associated with the Dredging of Indiana Harbor and Canal and CDF Operations

5a. CONTRACT NUMBER

5b. GRANT NUMBER

5c. PROGRAM ELEMENT NUMBER

6. AUTHOR(S)
Louis J. Thibodeaux, Kalliat T. Valsaraj, Raghunathan Ravikrishna, Kenneth Fountain, and Cynthia L. Price

5d. PROJECT NUMBER

5e. TASK NUMBER

5f. WORK UNIT NUMBER

7. PERFORMING ORGANIZATION NAME(S) AND ADDRESS(ES)
Environmental Laboratory, U.S. Army Engineer Research and Development Center, 3909 Halls Ferry Road, Vicksburg, MS 39180-6199;
Louisiana State University, Department of Chemical Engineering, Baton Rouge, LA 70803

8. PERFORMING ORGANIZATION REPORT NUMBER
ERDC/EL TR-08-17

9. SPONSORING / MONITORING AGENCY NAME(S) AND ADDRESS(ES)
U.S. Army Engineer District, Chicago
Chicago, IL

10. SPONSOR/MONITOR'S ACRONYM(S)

11. SPONSOR/MONITOR'S REPORT NUMBER(S)

12. DISTRIBUTION / AVAILABILITY STATEMENT
Approved for public release; distribution is unlimited.

13. SUPPLEMENTARY NOTES

14. ABSTRACT

This report describes a series of investigations conducted examining a number of specific factors that control air emissions associated with the dredging of Indiana Harbor and Canal (IHC) and associated IHC Confined Disposal Facility (CDF) operations. Three primary objectives were addressed: (1) measurement of Henry's Law constants and sediment-water desorption constants for various chemicals in the IHC sediment, (2) measurement of volatile emissions from IHC sediments exposed to air, and (3) reformulation of models for air emissions from dredging of contaminated sediment and handling of dredged materials.

Equilibrium sediment-water partition constants for PAHs and PCBs in IHC sediments were measured in laboratory investigations. These values are presented and compared to literature values. Laboratory experiments measuring the water-air partition constant (Henry's Law constant) were conducted using IHC pore water. Experimentally determined Henry's constants for PAHs and PCBs are presented and compared to literature values. Investigations from wind tunnel studies measuring semi-volatile emissions from IHC sediments are summarized. A model for estimating emissions from mechanical or hydraulic delivery of dredged IHC sediments is presented. Chemical volatilization models for emissions from dredging operations associated with IHC sediment and site conditions are discussed.

15. SUBJECT TERMS
Volatile emissions
Polyaromatic hydrocarbons
Dredged material
Confined disposal facility (CDF)
Henry's Law constant
K_d
Volatile emissions modeling
Dredging operations
Ponded CDF

16. SECURITY CLASSIFICATION OF:			17. LIMITATION OF ABSTRACT	18. NUMBER OF PAGES	19a. NAME OF RESPONSIBLE PERSON
a. REPORT	b. ABSTRACT	c. THIS PAGE			19b. TELEPHONE NUMBER *(include area code)*
UNCLASSIFIED	UNCLASSIFIED	UNCLASSIFIED		144	